Disclinations, dislocations, and continuous defects: A reappraisal

M. Kleman*

Institut de Minéralogie et de Physique des Milieux Condensés (UMR CNRS 7590), Université Pierre-et-Marie-Curie, Campus Boucicaut, 140 rue de Lourmel, 75015 Paris, France

J. Friedel

Laboratoire de Physique des Solides (UMR CNRS 8502), Université de Paris-Sud, Bâtiment 510, 91405 Orsay cédex, France

(Published 2 January 2008)

Disclinations were first observed in mesomorphic phases. They were later found relevant to a number of ill-ordered condensed-matter media involving continuous symmetries or frustrated order. Disclinations also appear in polycrystals at the edges of grain boundaries; but they are of limited interest in solid single crystals, where they can move only by diffusion climb and, owing to their large elastic stresses, mostly appear in close pairs of opposite signs. The relaxation mechanisms associated with a disclination in its creation, motion, and change of shape involve an interplay with continuous or quantized dislocations and/or continuous disclinations. These are attached to the disclinations or are akin to Nye's dislocation densities, which are particularly well suited for consideration here. The notion of an extended Volterra process is introduced, which takes these relaxation processes into account and covers different situations where this interplay takes place. These concepts are illustrated by a variety of applications in amorphous solids, mesomorphic phases, and frustrated media in their curved habit space. These often involve disclination networks with specific node conditions. The powerful topological theory of line defects considers only defects stable against any change of boundary conditions or relaxation processes compatible with the structure considered. It can be seen as a simplified case of the approach considered here, particularly suited for media of high plasticity or/and complex structures. It cannot analyze the dynamical properties of defects nor the elastic constants involved in their static properties; topological stability cannot guarantee energetic stability, and sometimes cannot distinguish finer details of the structure of defects.

DOI: 10.1103/RevModPhys.80.61 PACS number(s): 61.72.Bb, 61.30.Mp, 61.43.−j, 61.46.Hk

CONTENTS

*maurice.kleman@mines.org

I. INTRODUCTION

A. Gereral considerations: Dislocations, disclinations, dispirations, and disvections

Defects in mesomorphic phases (or liquid crystals) have been the subject of numerous investigations in the last 30 years. This research has emphasized the importance of *disclinations*, line defects first defined by Volterra (1907), and the main specific defects of liquid crystals (Friedel, 1922). As a consequence, the role of defects of a similar nature has also been recognized in other media, most of them (though not all) with non-solid-crystalline symmetries. This article is devoted to the geometrical and topological concepts relevant to this field of research, in various media where disclinations act in interplay with other defects, mostly other types of line defects (dislocations).

We compare two different theoretical approaches to the classification of line defects, the Volterra process and the topological stability theory. They are not equivalent, but rather complementary. The topological theory has attracted attention because it can be used to classify not only line defects, but also defects of any dimensionality, in a very general manner, on the basis of the topological properties of the order parameter. The Volterra process applies only to line defects, which it classifies by the elements of the symmetry group within the ordered medium. This approach allows us to deal with the (static and dynamical) interplay between disclinations and other line defects. Continuous defects (which relate to continuous symmetries) thus control the shape of quantized disclinations with which they are associated, either attached to them or accompanying them at a small distance. These specific defects of the Volterra process have been little studied in recent years. Yet the sustained interest in mesomorphic and frustrated phases, and in other media whose structural properties are remote from those of three-dimensional (3D) crystalline media, justifies a reappraisal of the subject.

The Volterra process yields the same main conclusions as the topological stability theory, but at a finer level, by properly handling boundary conditions and all plastic relaxations, including those related to line-attached defects. This approach can be particularly useful when dealing with nanostructures or with dynamical properties, when the viscosity is large.

We do not approach the subject of mesomorphic phases immediately. The final situation depends of course on the symmetries of the media under consideration, a topic that is not considered in the first part (Sec. II) of our article, and on the physical nature of the relaxation processes that bring the defects toward their final, stable or metastable, state. We consider several structures characteristic of ill-condensed media. But we first make a detour through isotropic uniform solid media, with the sole purpose of understanding the generic geometrical relations between disclinations and dislocations, and their interplay. A number of new results are presented, which has forced us to limit the review of some topics (the foundations of the topological theory, geometrical frustration), especially when excellent reviews already exist. On the other hand, the basic ingredients of the theory of continuous defects, in the perspective we want to place it, are rather scattered in the literature, and in any case deserve some deeper analysis; the distinction between constitutive and relaxation line-attached dislocations is new and structures this topic.

As a major application, the concept of disclination in smectic-A (SmA) and other mesomorphic phases will be considered at some length. Other topics of some importance will also be tackled: (i) the role of disclinations in polycrystal structure and deformation, of importance for polynanocrystals; (ii) the structure of an undercooled liquid, which features a curved-space crystal mapped into flat physical space. This is a typical example, along with liquid-crystalline blue phases (BPs), of geometrical frustration. Our analysis of defects in a 3D amorphous curved space S^3 is new and generalizes the results for the usual E^3 amorphous phase.

We find it useful to recall the main features of the description of defects in ordered media in terms of the Volterra process and its extension, the topological classification, and the theory of continuous defects, all involved in our description of disclinations.

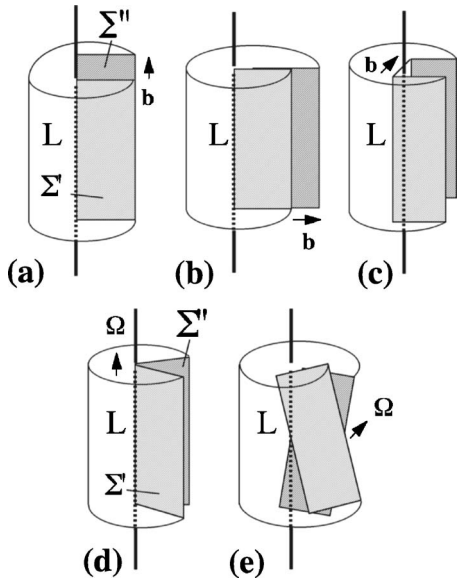

FIG. 1. The Volterra process for elementary types of dislocations: (a) screw dislocation, (b) and (c) two constructions of the same edge dislocation; and disclinations: (d) wedge disclination, (e) twist disclination. The original cut surface Σ is a vertical half plane bounded by the axis of a cylinder of matter. View (c) and (d) before the void is filled and the medium relaxed (all). From Kleman and Lavrentovich, 2003, Fig. 8.2., p. 265, with kind permission of Springer Science and Business Media.

B. The Volterra process and its plastic extension

Recall the main characteristics of the Volterra process for defect lines in a solid body (Volterra, 1907); cf. Friedel (1964). Cut the matter along a surface Σ (the cut surface) bound by a line L (a loop or an infinite line), displace the two lips Σ' and Σ'' of the cut surface by a relative rigid displacement that can be analyzed as the sum of a translation $\mathbf{b}$ and a rotation $\mathbf{\Omega}$, introduce matter in its perfect state (i.e., elastically undeformed) in order to fill the void left by the rigid displacement, or remove matter in the regions of double covering, glue back together the new matter and primitive matter along the lips Σ' and Σ'', and let the medium relax elastically. Figure 1 represents the Volterra process for different orientations of $\mathbf{b}$ and $\mathbf{\Omega}$ with respect to a straight dislocation line. This process is certainly ill defined along the line L itself (an elastic singularity remains along L, the defect) and generates a singularity of the order parameter on the cut surface; however, this latter difficulty disappears if $\mathbf{b}$ and $\mathbf{\Omega}$ are translational and rotational symmetries of the medium (quantized, perfect defects). The strain field is small if the rigid displacement is restricted to a translation of small amplitude, comparable to the atomic distance, say; L is then a dislocation, and $\mathbf{b}$ is its Burgers vector. There are always large-amplitude displacements if the Volterra process applies to a rotation $\mathbf{\Omega}=\Omega\mathbf{t}$, except on the axis of rotation $\mathbf{t}$ itself; L is then a disclination. This is the reason why research in the field of defects presents such complexity and, thereby, such an accumulation of riches.

When the Volterra process involves at the same time a translation and a rotation, one has a dispiration (Harris, 1970, 1977).[1]

In a curved space, as discussed in this paper, the lines produced by a Volterra process are disclinations or disvections, the latter being the nearest equivalent to (translation) dislocations.

1. Quantized perfect disclinations

The situation is particularly simple if the line is straight, along the rotation vector (wedge disclination); it is more complex in the Volterra process sense when the rotation vector is perpendicular to the line (twist disclination), in which case it generally involves the simultaneous presence of perfect dislocations attached to the twist line. Research in this domain is very lively: the approach in terms of the Volterra process is supplemented here by the theory of topological stability (see Sec. I.C below).

Stemming from the Volterra process picture of a defect, line and surface geometry theory is specifically employed for columnar and lamellar media (Kleman *et al.*, 2004) and, more generally, for liquid media with quantized translations (Achard *et al.*, 2005). Riemannian geometry is the main mathematical tool used to treat perfect quantized disclinations in geometrically frustrated media (Kleman, 1989).

2. Three important concepts in the development of the Volterra process

(i) *Imperfect line singularities*. If the relative displacement $(\mathbf{\Omega},\mathbf{b})$ is not a symmetry of the medium, the defect line is bordering a surface of misfit along the cut surface of the Volterra process. One then speaks of imperfect dislocation, disclination, or dispiration. This is for instance the case, in a crystal, of partial dislocations bordering a stacking fault or of disclinations bordering grain boundaries.

(ii) *Continuous distributions of defect lines of infinitesimal strength* $(\mathbf{\Omega},\mathbf{b})$, already considered by Volterra (1907). Such planar distributions were introduced by Frank (1950b) for describing pure flexion and rotation grain boundaries, which can be attached to straight wedge and twist disclinations, respectively ($\mathbf{\Omega}$, respectively, parallel and perpendicular to the line). Three-dimensional distributions were introduced by Nye (1953)

[1]Dispirations have been studied only in some smectic phases where symmetry elements include simultaneously a translation and a rotation. Tanakashi *et al.* (1992) have observed dispirations in an antiferroelectric smectic phase ($\mathrm{Sm}C_A$): the layer thickness d_0 is half the repeat distance of the polarization $\mathbf{P}$, which changes sign from one layer to the next. Hence a d_0 translation and a π rotation of $\mathbf{P}$ together constitute a helical symmetry. See also Kuczinski *et al.* (1999) for observations in a chiral antiferroelectric smectic phase ($\mathrm{Sm}C_A^*$), and Lejček (2002) for theoretical considerations, and references therein.

and others to describe plastic distortions of minimal energy.

(iii) *Plastic relaxation*, leading to an extended Volterra process. In a medium such as a liquid crystal, where some of the stresses can be released plastically in a viscous way, this relaxation plays a large role in reducing the energy and increasing the mobility and flexibility of disclinations. The classical Volterra process, which refers to a solid (frozen) medium, has then to be completed by a stress relaxation that can be analyzed in terms of a three-dimensional continuous distribution of dislocations of infinitesimal strength. This is usually obtained by replacing the elastic stress field of a solid medium by the elastic stresses referring to the liquid crystal considered [see, e.g., Frank and Oseen equations (Frank, 1958) replacing Hooke's elasticity]. We talk in this case of an extended Volterra process.

Somewhat similar plastic stress relaxations are possible in solids at the tips of slip lines or cracks, considered as dislocations or disclinations; the end of a subboundary produced by slip can also relax plastically by developing a localized crack. One can also talk in those cases of extended Volterra processes, but remember that the plastic relaxation can now have a finite elastic limit, or at least strongly viscous friction (Friedel, 1959b).

The motion and bending of disclinations involve the production of two-dimensional continuous distributions of infinitesimal dislocations that can often disperse in a liquid crystal, or be plastically relaxed in a solid, or again be absorbed by another defect, as we show by some examples.

C. The topological classification

1. Why do we use a topological classification?

We outline the general principles of this theory and illustrate them using examples of liquid-crystal phases, in order to bring out the concept of topological stability (the essential contribution of this theory to the physics of defects), and to comment on the effects of noncommutativity of the symmetries, which are taken into account in a systematic way in this theory.

The topological theory started with the papers of Rogula (1976), Volovik and Mineev (1976), and Toulouse and Kleman (1976); for recent reviews, with emphasis on mesomorphic phases, see Mermin (1979), Michel (1980), and Trebin (1982). The topological classification remedies a number of difficulties in the Volterra process when applied to ill-condensed matter, mostly liquid crystals. Liquid-crystal defect features have no equivalent in the usual solid crystals: disclinations whose core singularity vanishes, point singularities, and 3D knotted nonsingular configurations. (i) The Volterra process correctly describes straight wedge disclinations of strength $|k|=1/2$ (i.e., rotational symmetries of angle $\omega=\pm\pi$), but cannot be extended to $|k|>1/2$ [i.e., angles $\omega=(2n\pm1)\pi$, $n\neq0, n\in Z$], in its naive version. (ii) Twist disclinations cannot be constructed, except locally [for an illustration, see Harris (1977)]. (iii) Escape in the third dimension (Meyer, 1973) does not result from the Volterra process.

However, these difficulties can also be dealt with successfully by introducing the concept of the extended Volterra process.

2. The order-parameter space

The topological classification of defects relies on the application to ordered media of the methods and concepts of algebraic topology; standard references are Steenrod (1957) and Massey (1967). The manifold V of internal states, also called the vacuum or the order-parameter space, is the space of all possible different positions and orientations of the perfect crystal in (flat) Euclidean space. Let H be the symmetry group of the ordered structure $G=E^3=R^3\square O(3)$ the group of Euclidean isometries of E^3. The symbol $\square$ indicates the semidirect product of groups. R^3 is the 3D group of continuous translations $O(3)=SO(3)\times Z^2$; the full group of rotations, with center of symmetry included. The symbol $\times$ indicates the direct product of groups; H is a subgroup of G. V is then the quotient space G/H. Observe that V is not a group, generically, except if H is a normal subgroup of G.

Examples of order-parameter spaces have been given by Kleman and Lavrentovich (2003); the order-parameter space of a uniaxial nematic $V(N)=P^2$ is the projective plane; the order-parameter space of a 3D crystal, regarding only the translations, is $V(\text{Crystal})=T^3$, the 3D torus.

These concepts extend in a natural way when G is the group of a space M of constant but nonzero curvature, and H a subgroup of G, i.e., the group of symmetry of an ordered structure of habit space M. We make use of this extension in the investigation of defects in frustrated media; see Sec. VII.

3. The first homotopy group (the fundamental group) of the order-parameter space

Now consider how the order-parameter space V enters into the issue of the topological classification of defects. We start from a distorted ordered medium, in which the order parameter is broken along a line L. In order to test the topological nature of the breaking, surround L by a closed loop γ entirely located in a well-ordered structure, well ordered in the sense of the usual theory of dislocations in solids. It is possible to attach to each point $\mathbf{r}$ belonging to γ a tangent perfectly ordered structure, which maps in a unique way onto some point $R\in V$. When $\mathbf{r}$ traverses the closed loop γ, R traverses a closed loop Γ on V. Call this well-defined continuous mapping ϕ:

$$\phi:\gamma\rightarrow\Gamma.$$

The function ϕ can be extended continuously to the whole continuous domain D of the ordered medium in which the order parameter is well defined, since the order parameter is expected to vary continuously in D.

Therefore, any continuous displacement of γ in D maps onto a continuous displacement of Γ. There is, consequently, a relation of equivalence between the different images Γ; it is this equivalence that is described by the notion of homotopy (Steenrod, 1957). All the Γ's belonging to the same class of equivalence are represented by an element $[\Gamma]$ of a group, the so-called fundamental group (or first homotopy group) $\Pi_1(V)$. More precisely, $\Pi_1(V)$ is the group of classes of oriented loops belonging to V, equivalent under homotopy, and all having the same base point. This latter technicality has no effect on the classification of defects. It is more important that, in most cases, the fundamental group is not commutative, a property related to the fact that the topological charge of a defect, i.e., the corresponding element in $\Pi_1(V)$, is modified when the defect $[\Gamma]$ circumnavigates about a defect $[\Gamma']$; it is changed to $[\Gamma'][\Gamma][\Gamma']^{-1}$, an element of the same conjugacy class. It is therefore usual to consider that all elements of a given class of conjugacy represent the same defect. Examples are provided later.

D. The theory of continuous defects

This theory flourished in the early 1960s [see Nye (1953), Bilby *et al.* (1955), Kondo (1955-1967), Kröner (1981)]; it was at that time applied to solid crystals only. The theory concentrates mostly on the study of sets of line defects, whether these defects, of the quantized type, are considered at such a scale that the concept of defect density makes sense, or whether the characteristic invariants carried by the defects (in the sense of Volterra, i.e., translations, rotations) are continuous, with the result that the notion of infinitesimal defects—with vanishing Burgers vector dislocation or vanishing rotation vector disclination—is significant. Indeed, most results of the theory of continuous defects relates to continuous distributions of dislocations of infinitesimal strength, to intrinsic point defects (interstitials, vacancies, etc.), and, to a lesser extent, to disclinations of infinitesimal strength. The main geometrical ingredients of the continuous theory of dislocation line defects and intrinsic point defects are the concepts of torsion and curvature on a manifold; the points of contact with Einstein's theory of generalized relativity are therefore numerous, and have been stated a number of times (Hehl *et al.*, 1976; Kröner, 1981): cosmic strings are spacetime topological defects that may be described in delta-function-valued torsion and curvature components, carried, respectively, by translation- and rotation-symmetry-breaking defects in a Minkowskian manifold (Vilenkin and Shellard, 1994). For recent spacetime defect calculations, see, e.g., Letelier (1995), Puntigam and Soleng (1997), and references therein. Defects such as disclinations whose characteristic invariants belong to noncommutative groups cannot so easily be turned into density sets. Methods borrowed from the field theory in high-energy physics have also been applied; this is the so-called gauge field theory of defects; cf. Julia and Toulouse (1979), Dzyaloshinskii and Volovik (1980), and Dzyaloshinskii (1981).

It was expected that these continuous approaches would open the way to solutions of a certain number of problems that are difficult to attack using the physics of quantized defects when these defects are numerous. Thus the dynamical theory of dislocations in solids, defect melting theory, and the defect content of deformed frustrated phases [see, e.g., Frank and Kasper phases, quasicrystals, even amorphous media and glasses, and mesomorphic blue phases or twist grain boundary (TGB) phases] would also provide a suitable definition of other defect densities: of disclinations, point defects, and so on. The rich and interesting courses given at the Les Houches Summer School on Defects held in 1980 (Dzyaloshinskii, 1981; Kröner, 1981) took stock of the various advances in continuous and gauge field theory made at the time.

However, although the continuous theory of defects is of rare mathematical elegance, applications have been scarce, one of the most convincing being perhaps the analysis of magnetostrictive effects in ferromagnets (Kleman, 1967). At the discussion meeting organized in Stuttgart (Kröner, 1982), Kröner made the following remark:

> Although the field theory of defects [by field theory he obviously meant the traditional theory of continuous defects as well as its gauge field extension] has found many applications, the early hope that it could become the basis of a general theory of plasticity has not been fulfilled. Among various reasons we mention, first of all, that the defects, namely, the dislocations, that above all are responsible for plastic flow, do not form smooth line densities that can well be described by a dislocation density tensor field. Direct observation of dislocations in crystals, for instance, by means of electron microscopy, shows that dislocations rather form *three dimensional networks* [our emphasis] that are interconnected in practically immobile nodes and other often complex local arrangements…. These networks have a strong statistical component, a fact that shows that a real physical understanding of plasticity requires also considerations in the frame of statistical physics. However, a statistical theory of interacting deformable lines that can be created, annihilated, and change their length has never been worked out.

To these remarks it can be added that the material-science physicists, who certainly know best the problems and traps of the physics of defects, are in general not fully aware of the mathematical tools (non-Riemannian manifolds, exterior calculus, Grassmann algebra, differentiation on manifolds, and fiber bundles) that are at the very basis of continuous gauge theory. This language problem has little chance of being resolved in the near future, inasmuch as the gap between material scientists and field theorists keeps widening. We here avoid as much as possible complex mathematical tools.

In any case, we are led to conclude that field theory is not a panacea. On the other hand, the fundamentals of plastic deformation and fracture of crystalline materials have recently undergone a revival through the development of new experimental methods that now explore nanometric scales, and through the improvement of computer power and computing methods.

Dislocations (whose set of characteristic invariants is isomorphic to an infinite Abelian group) and intrinsic point defects are the dominant defects in solid crystals; there is therefore no real necessity to introduce in the theory the group-theoretic description of other types of defects that would require finite Abelian groups or non-Abelian groups, making the theory unmanageable. Notwithstanding this simplification, Kröner's criticism remains valid; even if one restricts consideration to static situations, the continuous theory neglects real dislocation networks—in the sense of Frank (1950b)—and the frictional effects due to them. This is probably the true reason why the theory of continuous dislocations has found so little use yet.

E. Disclinations

1. Disclinations and continuous dislocations

There is, however, a situation where dislocation densities retrieve their true importance and where continuous theory plays a role; it is with disclinations considered as singularities of dislocation and disclination densities. This is the point of view taken here, and it has some relevance to mesomorphic phases, and perhaps also to quasicrystals, Frank and Kasper phases, undercooled liquids, polynanocrystals, and, more generally, frustrated phases.

Disclinations can exist in solid crystals, whose building blocks are atomic and pointlike; but the continuous theory has not been applied much to disclinations in solid crystals, where such objects have a large energy. On the other hand, disclinations are the rule in mesomorphic phases, whose building blocks are anisometric molecules (rodlike, disklike, etc.). These disclinations quite often appear as the singularity set of a dislocation density. This explains the interest in reconsidering the continuous theory of defects, although new concepts have to emerge. The case of mesomorphic phases requires an extension of the theory of continuous defects for solids to situations when there is locally only one physical direction (the director), i.e., no local trihedron of directions, as in the uniaxial nematic N, the SmA, and the columnar D cases;[2] see also a related remark in Sec. IV.A.2. The role of stress relaxation is especially important and complex in such mesomorphic phases.

[2]The continuous theory of defects makes use of lattice manifolds, whose points carry local trihedra.

2. Three-dimensional networks

The question also arises whether disclinations form 3D networks in amorphous systems, liquid crystals such as cholesteric blue phases, and undercooled liquids—it has been hypothesized that glass disorder can be described in terms of disclinations in an icosahedral curved crystal (Kleman and Sadoc, 1979)—or in nanocrystals, clusters (Friedel, 1984), quasicrystals and Frank and Kasper phases, where they are documented (Frank and Kasper, 1958, 1959; Nelson, 1983a). In such 3D networks, disclinations have to be somewhat flexible, which is possible (whether these disclinations are quantized or not) only if other defects, dislocations, or disclinations (continuous or not) are attached to them. Thus consideration of the interplay between dislocations and disclinations goes beyond mesomorphic phases. This question will be presented and discussed in this article.

F. Outline

To summarize, the continuous theory of defects in its primitive form considers only dislocation densities, which are singularities of continuous fields. It does not consider finite defects like disclinations, neither grain boundaries nor Frank networks. This article, contrariwise, assumes the coexistence of finite and infinitesimal defects. Grain boundaries are introduced. Field-theory instruments are not employed; but this is possible [see Kleman (1982b) in a similar context, but because of the advances presented here, results have to be reconsidered]. An important aspect of disclinations in mesomorphic phases is the relation of their flexibility and mobility to the relaxation of stresses imposed by the boundary conditions (static or dynamic). We suggest that both dislocation and disclination densities play leading roles in such relaxation processes.

Section II concerns the description, in geometrical terms, of the defect structure of disclinations, without taking into account constraints due to the symmetries of the medium. Section II applies to amorphous media and isotropic liquids, but it does not provide more than the geometrical tools needed to study the role of stress relaxation mediated by continuous defects in various media and how it affects disclination line flexibility and mobility, and the geometrical rules for building disclination networks. It is therefore directly applicable to solid media only.

The results of Sec. II are employed in Sec. III to shed new light on the properties of nanocrystals, and are extended in Sec. IV to quantized disclinations, examples being found in mesomorphic phases. This is where we discuss the relationship between topological stability and the kind of stability that stems from the Volterra process. Sections IV and V (devoted to focal conics in SmA liquid crystals considered as quantized disclinations) discuss the nature of disclinations in partly ordered materials, and their interplay with continuous and/or quantized dislocations.

TABLE I. The different types of line defects (first column) viewed in the Volterra perspective. Second column: the symmetries they break. Third column: systems in which the defect type of the corresponding row is present. Fourth column: interplays between disclinations and the other types of line defects, described by the extended Volterra process. As a general rule, quantized line defects correspond to some nontrivial class of homotopy belonging to $\Pi_1(V)$, continuous line defects belong to the zero class. V is the order-parameter space.

Defect type	Broken symmetry	Volterra process	Extended Volterra process
Dislocation	Translation	*Quantized*: solid crystals, smectics, TGB phases,[a] cholesterics *Continuous*: amorphous solids, nematics, and other liquid crystals	Grain boundaries, nanocrystals Nye dislocation densities, dislocations attached to disclinations Disclinations (N, N_B, N^*,SmA, amorphous systems)
Disclination	Rotation	*Quantized*: solid crystals,[b] liquid crystals, frustrated media (amorphous solids, glasses, blue phases) *Continuous*: liquid crystals	Disclination networks
Dispiration	Rotatory translation	*Quantized*: SmC*[c] *Continuous*: cholesterics	Dispirations attached to disclinations
Disvection	Noncommutative translation[d]	Crystals in spaces of constant nonvanishing curvature, e.g., S^3	Disvections attached to disclinations

[a]Considered in footnotes only.
[b]Isolated disclinations are not present usually in crystals, due to their long-range stresses.
[c]Not considered in this article.
[d]Such translations, also named *transvections* after Cartan (1963), are present in crystals with nonvanishing constant curvature.

Defects in frustrated phases are discussed in Sec. VI. Taking into account the frustrated local order, this section extends to three-dimensional spherical amorphous media the results obtained in Sec. II for three-dimensional Euclidean amorphous media, making full use of the quaternion representation of the geometry of S^3. Important results are (i) that dislocations, like the translational symmetries they break, are noncommutative—we call them *disvections*; (ii) that infinitesimal disclinations (rather than dislocations) are attached to twist finite disclinations. This result emphasizes the role of disclination networks in frustrated media. A part of Sec. VI is devoted to the classification of defects in the spherical {3,3,5} polytope, which has been used as a template for amorphous media with local icosahedral order. Section VI.B discusses some characteristics of the decurving process of curved media just mentioned.

The discussion in Sec. VIII bears on a comparison between the extended Volterra process and the topological theory—a question that runs as a thread through the entire article—and expatiates on the question of plastic relaxation, i.e., the role in various media of continuous mostly and quantized defects in stress relaxation.

Table I summarizes the different types of line defect, related in one way or another to the Volterra concept of the defect, investigated in this article.

II. CONTINUOUS DEFECTS IN ISOTROPIC UNIFORM MEDIA: GEOMETRICAL INTERPLAY BETWEEN DISCLINATIONS AND DISLOCATIONS

An amorphous metal, considered at a scale larger than the atomic size, is an example of an isotropic uniform solid medium. The Volterra process allows the consideration of continuous, nonquantized dislocations and disclinations that carry stresses. On the other hand, a result of the topological theory of defects is that these are not topologically stable. The objects to which this section is devoted are therefore, at best, metastable. In Secs. II.A–II.D, we investigate disclinations of finite strength whose rotation vector $\boldsymbol{\Omega}$ is constant in modulus and direction. Such objects are attended by two types of attached infinitesimal dislocation (constitutive and relaxation dislocations), from which the concept of an extended Volterra process emerges. We comment on the equivalence between these infinitesimal dislocation sets and grain boundaries in Sec II.E. In Secs. II.F and II.G, we investigate the case when the rotation vector varies along the line in direction and in modulus. The ensuing considerations directly yield an expression for the fundamental invariant of a disclination, which we call the Frank vector. The Frank vector is for disclinations what the Burgers vector is for dislocations; in particular, it satisfies a Kirchhoff relation at disclination nodes. Detailed study of quantized disclinations is postponed to Secs. IV and V.

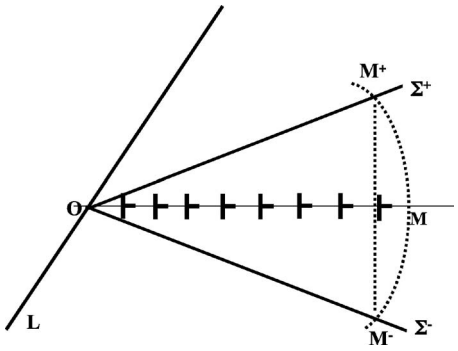

FIG. 2. Wedge disclination L and its edge dislocation content. $OM=OM^-=OM^+$; $M^+M^-=2OM\sin\frac{\Omega}{2}$.

This case of an isotropic uniform medium is chosen for the simplicity of relaxations in the extended Volterra process. As mentioned, it is somewhat artificial to distinguish relaxations of stresses involved in the motions of a given (nonquantized) disclination from those for the dispersion of the disclination itself: the same plastic properties are involved in both, and should occur in similar lengths of time in nonviscous liquids. It is only for very viscous liquids or, better, for amorphous solids with slow atomic diffusion that one can assume that short-range relaxation of stresses due to the motion of the dislocations is more rapid than their dispersion lifetime, which we consider here as infinite.[3] The dynamical competition of the two processes in viscous liquids has so far not been much studied.

The models developed and applied in Secs. II and III are extended in Secs. IV and V to quantized and topologically stable disclinations.

A. Dislocation content of a straight wedge disclination

We consider an infinitely long wedge disclination line L, of rotation angle $\mathbf{\Omega}=\Omega\mathbf{t}$, the rotation axis $\mathbf{t}$ being along L (Fig. 2).

The Volterra process consists in opening a dihedral void of matter (for simplicity we consider a disclination of negative strength). The relative displacement of the lips of the cut surface Σ, which we take to be a half-plane, at a point $\mathbf{M}$ of Σ, is written as $\sin\frac{\Omega}{2}\mathbf{t}\times\mathbf{OM}$, $\mathbf{O}$ being any origin on L; this displacement can also be the result of a set of edge dislocations [Friedel (1964), Chap. 1] located uniformly in Σ, and whose total Burgers vector $\mathbf{b_M}$ is precisely $2\sin\frac{\Omega}{2}\mathbf{t}\times\mathbf{OM}$, for those dislocations lying between the edge of the dihedron and $\mathbf{M}$, i.e., with density

$$d\mathbf{b_M}=2\sin\frac{\Omega}{2}\mathbf{t}\times d\mathbf{M}, \tag{1}$$

thus producing a tilt boundary of rotation $\mathbf{\Omega}$ along Σ.

We give some examples.

(i) In an amorphous solid or a glass the angle Ω can take any value; a continuous distribution of dislocations thereby yields a continuous wedge disclination. This tilt boundary introduces a mismatch of short-range atomic order, which can be suppressed if some local atomic diffusion is allowed at short range.

(ii) In a ferromagnetic solid, the meeting line of several magnetic walls is a continuous wedge disclination whose angle Ω relates directly to the magnetoelastic constants (Kleman, 1974). Again, this disclination can be analyzed in terms of continuous dislocations.

(iii) Nonquantized wedge disclinations in a crystalline solid are the limits of tilt boundaries, which are split into finite dislocations parallel to that limit; this is the type considered up to now. The angle Ω can take any value; it is tuned by the density of edge dislocations. For small values of Ω, the continuous distribution of infinitesimal dislocations can also regroup into parallel dislocations of finite strength allowed by the crystal structure (see Sec. III.C for a more detailed discussion). In the general case, this is an imperfect disclination with a stacking fault that is a tilt boundary. Such disclinations have very large energies, as long as Ω is finite, in the absence of any plastic relaxation. They can nevertheless be produced, for instance, when a slip line crosses a low-angle grain boundary, during plastic deformation of polygonized crystals; they can also be associated in parallel pairs of equal rotation strength and opposite signs. The stress concentrations produced at the cores of the disclinations are often relaxed by the development of cracks (Friedel, 1964).

Remark. The Volterra process is properly defined for $|\Omega|\leqslant\pi$. Observe that Eq. (1) does not distinguish (i) between $\Omega=2\pi$ and $\Omega=0$, and (ii) between $\Omega=2\pi-\alpha$ and $\Omega=\alpha$. This equation puts limits on the application of the Volterra process and on the use of Eq. (1). Notice also that it is inconsistent to consider a unique Volterra process with an angle $|\Omega|\geqslant 2\pi$, since this requires removing matter (for $\Omega>0$) or adding matter (for $\Omega<0$) in at least a full space. Hence, for any angle $\Omega=(2n+1)\pi+\alpha$, $|\alpha|<\pi$, one has to consider $2n+1$ successive applications of the Volterra process, followed by a Volterra process of angle α.

We now deepen the relationship of a wedge disclination with its accompanying dislocations by first considering the displacement of the entire line parallel to itself (Sec. II.B), and second displacing a part of the line only (Sec. II.C).

B. Emitted and absorbed dislocations: Constitutive and relaxation dislocations

It is clear that the energy of the disclination becomes prohibitive if the rotation axis $\mathbf{t}$ stays in place when the

[3]Such dynamical considerations also apply to quantized disclinations, whose dispersion lifetime is in essence infinite. For example, the stress relaxation of quantized disclinations in nematics and other liquid crystals, where translation and rotation symmetries are partly or totally continuous, can be assigned to continuous dislocations and disclinations.

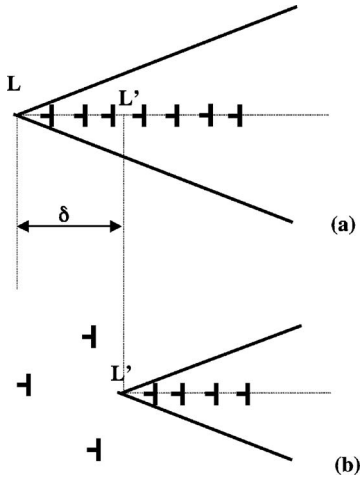

FIG. 3. Displacement of a wedge disclination from (a) L to (b) L' by emission of dislocations that disperse away.

disclination is displaced; if some plastic relaxation is allowed, $\mathbf{t}$ moves to a new position by the emission or absorption of a certain number of dislocations. We have to specify the direction of this motion, as the stress about L depends on the position of the cut surface Σ in space, even if the medium is isotropic.

1. Motion in the cut surface

If L is moved in the plane of Σ by a displacement vector $\boldsymbol{\delta}$, the total Burgers vector $\mathbf{b}_{\boldsymbol{\delta}}$ of emitted or absorbed dislocations is $\pm 2\sin(\Omega/2)\mathbf{t}\times\boldsymbol{\delta}$: these are edge dislocations; $\mathbf{b}_{\boldsymbol{\delta}}$ is the sum total $\mathbf{b}_{\boldsymbol{\delta}}=\Sigma\mathbf{b}_e$ of elementary dislocations $\mathbf{b}_e$ allowed by the symmetries of the medium (Fig. 3).

In an amorphous solid or a glass, the $\mathbf{b}_e$'s may have any modulus. In an ordered solid, the $\mathbf{b}_e$'s have to be equal to translation symmetries of the medium. Notice that in both cases emitted and/or absorbed dislocations contribute to the relaxation of the sample that has suffered the displacement of the disclination. To illustrate this point in the amorphous solid case, observe that it would make no sense if emitted dislocations remained in place in the continuation of the cut surface, because this would not modify the strains and stresses previously carried by the medium, before the line moved. In other words, one is led to recognize the existence of two types of dislocation density: those belonging to the actual cut surface of the disclination, which we call constitutive dislocations, and those left in the wake of the moving disclination, which we call relaxation dislocations. In principle, since the stress field attached to a wedge line L, measured in a frame of reference attached to L, is independent of the position of L, relaxation dislocations should carry no stress at all at complete relaxation; they are dispersed in the entire space with vanishing Burgers vectors if they are continuous, or vanish at the boundaries of the sample if they are quantized.

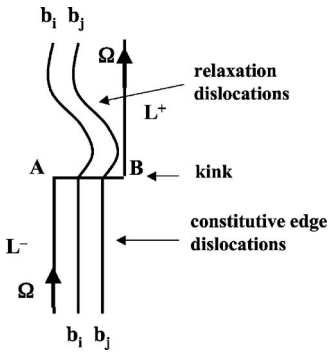

FIG. 4. Kink AB linking the two wedge half lines L^- and L^+. The cut surface Σ is supposed to be on the right of the disclination L^-, AB, L^+. The upper segments of the dislocations that traverse AB tend to disperse away (plastic relaxation), while keeping attached to the constitutive segments on the kink.

2. Motion off the cut surface

If L is translated off the plane of Σ by $\boldsymbol{\delta}$, the total Burgers vector of the absorbed dislocations is also $\pm 2\sin(\Omega/2)\boldsymbol{\nu}\times\boldsymbol{\delta}$, where $\boldsymbol{\nu}$ is the new axis of rotation. A new piece of cut surface, parallel to the $\{\boldsymbol{\nu},\boldsymbol{\delta}\}$ plane, is created.

C. Twist component of a disclination

We now turn our attention to a line L made of three segments, namely, two parallel semi-infinite wedge segments L^- and L^+ joined by a third perpendicular segment **AB** of small length, called a kink (Fig. 4). We assume that the cut surface Σ is a plane that contains the three segments.

The L^+ segment is the result of a displacement of a part of the entire line parallel to itself by a translation $\boldsymbol{\delta}=\mathbf{AB}$, by emitting or absorbing dislocations. In this process, $\boldsymbol{\Omega}$ stays parallel to itself. According to the results above, we have, on the Σ side of **AB**, constitutive dislocations of total Burgers vector

$$\mathbf{b}_e(\mathbf{AB}) = \pm 2\sin\frac{\Omega}{2}\mathbf{t}\times\mathbf{AB}, \tag{2}$$

and on the other side of **AB**, relaxation dislocations of total Burgers vector

$$\mathbf{b}_d(\mathbf{AB}) = \pm 2\sin\frac{\Omega}{2}\mathbf{t}\times\boldsymbol{\delta}. \tag{3}$$

These two quantities being equal, we see that dislocations cross the segment **AB**, but behave quite differently on either side.

A classical Volterra process, acting once for all on the cut surface of the disclination line, is not relevant to the present geometry, because such a Volterra process can be performed only if the rotation vector $\boldsymbol{\Omega}$ is fixed in space.

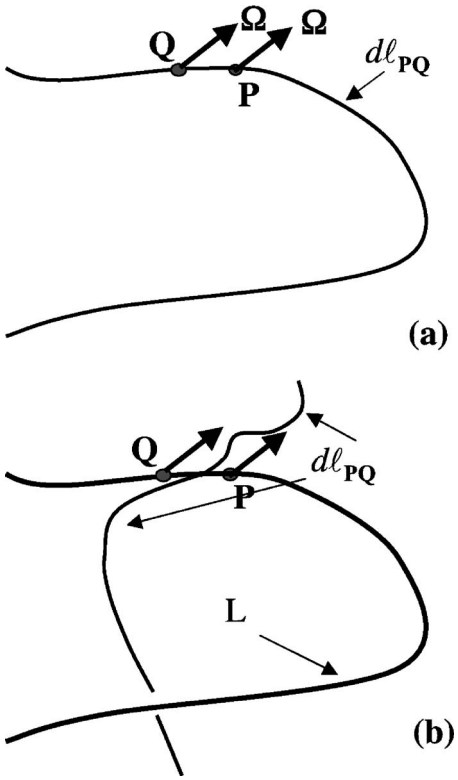

FIG. 5. Constitutive and relaxation dislocations attached to a disclination. Generic case. (a) The infinitesimal dislocations $d\ell_{PQ}$ are constructed assuming first that the cut surface bound by L is common to all $d\ell$'s attached along L. (b) Then each $d\ell_{PQ}$ is deformed at fixed P, Q; the two parts of $d\ell_{PQ}$ on both sides of the infinitesimal arc PQ do not have the same elastic distribution. L is the limit between the two distribution types.

D. Ω constant: Generic disclination line

Again, we restrict our attention to the isotropic case. Consider a curved disclination line: Fig. 5 shows a disclination with $\mathbf{\Omega}$ constant in length and in direction from point to point along L. The angle between L and $\mathbf{\Omega}$ varies from point to point. Let $\mathbf{P}$ and $\mathbf{Q}=\mathbf{P}+\frac{d\mathbf{P}}{ds}\,ds$ be two points infinitesimally close together on L. The Burgers vector of the infinitesimal dislocation introduced by the variation of position of $\mathbf{\Omega}$ from $\mathbf{P}$ to $\mathbf{Q}$ is, by reasoning on the cut surface Σ as above, equal to $d\mathbf{b}_{PQ}=\mathbf{d}_Q(\mathbf{M})-\mathbf{d}_P(\mathbf{M})$, where

$$\mathbf{d}_P(\mathbf{M}) = 2\sin\frac{\Omega}{2}\mathbf{t}\times\mathbf{PM},$$

$$\mathbf{d}_Q(\mathbf{M}) = 2\sin\frac{\Omega}{2}\mathbf{t}\times\mathbf{QM}$$

are the displacements of the cut surface at $\mathbf{M}$, any point on Σ, seen, respectively, from $\mathbf{P}$ and $\mathbf{Q}$. Hence

$$\mathbf{d}_Q(\mathbf{M})-\mathbf{d}_P(\mathbf{M}) = -2\sin\frac{\Omega}{2}\mathbf{t}\times\frac{d\mathbf{P}}{ds}\,ds. \tag{4}$$

This dislocation, which we denote $d\ell_{PQ}$, can be thought of as attached to the line at the infinitesimal arc $\mathbf{PQ}$. Of course $d\mathbf{b}_{PQ}$ has to be a translation allowed by the symmetry of the phase. The shape taken by $d\ell_{PQ}$ resulting from plastic relaxation optimizes the energy carried by the disclination.

1. Two types of continuous distribution of dislocations

The question arises whether any infinitesimal relaxation dislocation $d\ell_{PQ}$, attached to L at the arc $\mathbf{PQ}$, crosses the line L, and transforms on the other side of L into a constitutive infinitesimal dislocation with the same Burgers vector, as it does in the simple case investigated in Sec. II.C. The answer is positive, and the demonstration is as follows. Since $\mathbf{M}$ is on the cut surface Σ of L, Eq. (4) is, as a result, valid on the full area of Σ. In other words, the infinitesimal dislocation line $d\ell_{PQ}$ with Burgers vector db_{PQ} has the same cut surface as L, and consequently meets L, is fixed between P and Q, and is closed in the manner of L [Fig. 5(a)]. In fact, with the local rotation vector defined as above, the disclination L is the result of creating a density of infinitesimal $d\ell_{PQ}$ by infinitesimal Volterra processes on the same cut surface.

Now we deform these $d\ell_{PQ}$ dislocation lines (this is an allowed operation), opening them into infinite lines (or line segments ending on the boundaries of the sample) in such a way that now they cross the imaginary line L, which divides each of them into two semi-infinite arcs. This process traces out the bounds of the cut surface Σ along L if one imposes different types of distribution for the line arcs on both sides of L, yielding different elastic distributions. In the spirit of Fig. 4, one can imagine on one side a 2D surface tiled with constitutive dislocations, a kind of generalized misorientation boundary, and, on the other side, relaxation dislocation segments dispersed in space [see Fig. 5(b)].

Of course, some stresses carried by the disclination can also be relaxed by defects that are not attached to the line, e.g., infinitesimal dislocations nucleated in the bulk; these are Nye dislocations, which we discuss later when we come to layered media (smectics) (Sec. IV.B.2), and in Appendix A. But we shall not consider nonattached defect densities in the present section. The final result depends on the material properties of the medium, whether it has solid elasticity (amorphous) or viscous behavior (liquid). In this latter case the relaxation can be complete.

2. Line tension of twist vs wedge segments

Notice that we have realized a dislocation geometry that displays two metastable configurations with a set of infinitesimal dislocations, namely, those of the misorientation boundary and those fully dispersed. Therefore the core region of a twist disclination line, where these two configurations merge, has a contribution to the total energy that scales as its length. The other contribution is the energy of the dislocation lines, essentially that of the constitutive dislocations, which scales as the area of the cut surface, i.e., the square of the length of the line. One expects this contribution to be larger than the first one.

Therefore the line energy per unit length of line is proportional to the length of the line. The latter contribution is worth comparing with the energy per unit length of a wedge line, which scales as the square of the transverse size: the line tension of a disclination is thus a linear function of their length that reduces to a proportionality for wedge disclinations, whereas, for twist disclinations, one must add a small constant term due to their relaxed dislocations.

E. Disclinations and grain boundaries

As in crystalline solids (see Sec. II.A), wedge lines in solid amorphous materials carry a large energy, except in the same circumstances as indicated above. The existence of twist lines or mixed twist-wedge lines is even less probable, and their mobility and change of curvature are certainly negligible, since mobility would require the climb of the attached dislocations, which requires plastic deformation. Hence a caveat: Except in the case of polycrystals (considered later), the discussion that follows assumes implicitly that there is no restriction on reaching low-energy states by plastic relaxation; it therefore applies to an amorphous material endowed with a finite viscosity, which operates through the existence and mobility of infinitesimal relaxation dislocation densities. One does not expect such processes to be possible in a solid crystal. But the comparison between crystals and amorphous media is worth carrying out, especially through the parallel concepts of the grain boundary and cut surface.

1. Comparison of Frank's grain boundary and Friedel's disclination

Equation (1), integrated along a segment **MN** of the disclination line L, gives the total Burgers vector of the dislocations that are attached to any segment **MN** of L (and lie along its cut surface Σ_L),

$$\Delta \mathbf{b}_{\mathbf{MN}} = 2 \sin \frac{\Omega}{2} \mathbf{t} \times \mathbf{MN}. \tag{5}$$

Equation (5) is similar to Frank's formula (Frank, 1950b) for a crystal grain boundary Σ_{GB} of angle of misorientation $\boldsymbol{\omega} = \omega \mathbf{s}$, $|\mathbf{s}| = 1$. Frank's formula yields the total Burgers vector of the (quantized) dislocations that cross any segment **PQ** belonging to Σ_{GB},

$$\Delta \boldsymbol{\beta}_{\mathbf{PQ}} = 2 \sin \frac{\omega}{2} \mathbf{s} \times \mathbf{PQ}. \tag{6}$$

This similarity does not come as a surprise, after the foregoing discussion. In particular, one can deduce from Frank's approach that any closed line in a grain boundary can be chosen as a disclination line, provided the exterior dislocation segments are allowed to relax. Identifying Eqs. (5) and (6) and assuming $\mathbf{M} = \mathbf{P}$, $\mathbf{N} = \mathbf{Q}$, we have

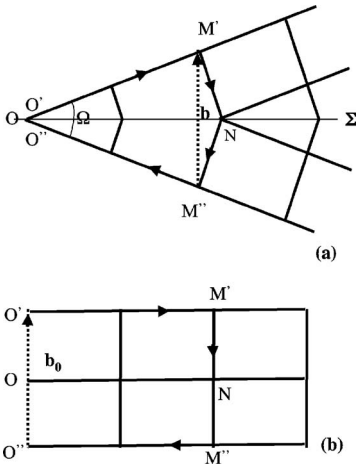

FIG. 6. Burgers vector. A crystal structure has been superimposed to show more clearly the Burgers circuit $O'M'NM''O''OO'$—in (a) the final state and in (b) the initial state—and the rotation $\boldsymbol{\Omega}$ of the Volterra process.

$$\sin \frac{\Omega}{2} \mathbf{t} \times \mathbf{MN} = \sin \frac{\omega}{2} \mathbf{s} \times \mathbf{MN}, \tag{7}$$

which yields either

$$\sin \frac{\Omega}{2} \mathbf{t} - \sin \frac{\omega}{2} \mathbf{s} = 0 \tag{8}$$

or

$$\sin \frac{\Omega}{2} \mathbf{t} - \sin \frac{\omega}{2} \mathbf{s} \propto \mathbf{MN}. \tag{9}$$

We assume that $\boldsymbol{\omega}$ is a constant vector, i.e., that the cut surface of the disclination line belongs to a unique grain boundary. Equation (8), which yields $\Omega = \omega$, $\mathbf{t} = \mathbf{s}$, applies when $\boldsymbol{\Omega}$ is a constant vector, which is what we have assumed up to now. Equation (9), on the other hand, expresses that other possibilities exist, with $\Omega \neq \omega$, $\mathbf{t} \neq \mathbf{s}$, where the tangent $\mathbf{t}$ to the disclination ($\mathbf{MN} = \boldsymbol{\tau}\, ds$) belongs to the plane $\{\mathbf{t}, \mathbf{s}\}$. Although $\boldsymbol{\omega}$ is a constant vector, Eq. (9) applies to a variable $\boldsymbol{\Omega}$, a situation discussed in Secs. II.F and II.G. We present later an example obeying Eq. (9) (see Appendix C).

Remark. The $2 \sin \frac{\Omega}{2}$ (or $2 \sin \frac{\omega}{2}$) factor in Eqs. (1), (5), or (6) deserves some comments.

The integral Burgers vector $\mathbf{b}$ of the cut Σ is considered as a lack of closure of a Burgers circuit in the final state [more properly in the final state of the Volterra process before elastic relaxation of the sector $M'OM''$ here introduced; Fig. 6(a)].

It is usual for dislocations to consider the Burgers vector $\mathbf{b}_0$ as a lack of closure in the initial state; one would then have (Fig. 6)

$$|\mathbf{b}| = M'M'' = 2OM' \sin \frac{\Omega}{2}$$

and

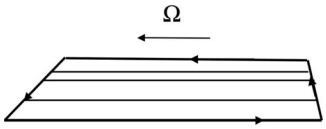

FIG. 7. An elementary disclination of mixed character. The constitutive dislocations (inside) are drawn, but not the relaxation dislocations (outside).

$$|\mathbf{b}_0| = OO' = 2OM' \tan\frac{\Omega}{2}.$$

Such a difference originates from the noncommutativity of the Burgers circuit and the rotation of the disclination. Obviously, the formula in $2\sin\frac{\Omega}{2}$ is to be preferred, as it correctly describes the final state, the only one of interest here. The difference is noticeable only for large Ω's, where the Burgers vector $\mathbf{b}$ of the constitutive dislocation is smaller by a factor $\cos\Omega/2$ than $\mathbf{b}_0$ of a crystal dislocation. In the following, we use the Burgers vector formula $\mathbf{b}$; it appears as follows in the Frank vector introduced in Sec. II.F.2:

$$\mathbf{f}(\boldsymbol{\Omega}) = 2\sin\frac{\Omega}{2}\mathbf{t}. \tag{10}$$

2. Isolated twist segments

Equation (6) has been derived by Frank for a finite segment **PQ**, independently of any loop to which **PQ** could pertain; dislocations that cross this segment (the crossing set) in the grain boundary have two parts (relaxation on one side of **PQ**, constitutive on the other), with no violation of any conservation law on Burgers vectors. Such a segment and its set of attached dislocations constitute a sort of stripe in the grain boundary, geometrically and topologically independent of it (certainly not energetically, but we pay no attention to this question).

Therefore, proceeding with our analysis, we conclude that a continuous disclination line can be made of a sequence of independent segments $\mathbf{M}_i\mathbf{M}_{i+1}$, possibly infinitesimal, each of them carrying a different rotation vector $\boldsymbol{\Omega}_{i,i+1}$. Each stripe $\mathbf{M}_i\mathbf{M}_{i+1}$ defines a grain boundary of finite width. Therefore any isolated, finite segment MN can divide each of the dislocations (continuous or quantized) belonging to the crossing set into constitutive (on one side) and relaxation (on the other side) dislocation segments. Each stripe has two edges parallel to $\boldsymbol{\Omega}$ and two edges of mixed character (see Fig. 7).

A stripe is an elementary disclination, with a twist (or mixed, but not pure wedge) segment transverse to the stripe. The longitudinal boundaries of the stripe, along the dislocations that construct the stripe, can be considered as wedge segments. Thus a stripe, considered as a disclination loop, is necessarily of mixed character.

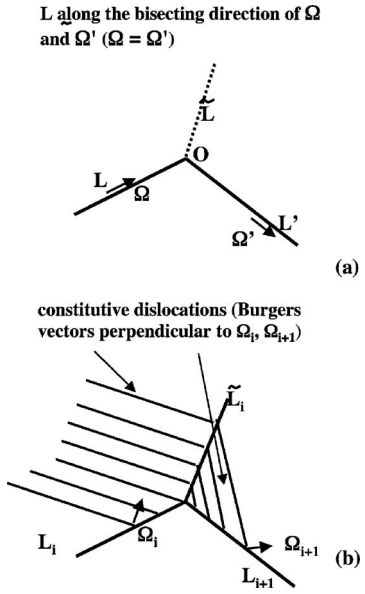

FIG. 8. A polygonal disclination: (a) two semi-infinite wedge lines L and L' meeting at **O**; (b) polygonal disclination made of segments L_i of mixed character (twist wedge). The Burgers vectors are continuous across the line parallel to $\tilde{\boldsymbol{\tau}}_i$.

F. Polygonal disclination lines: Attached disclinations

Disclinations with a rotation vector varying in length and direction are possible; they require attached disclinations (or attached disclination densities). For clarity, we do not introduce disclination densities immediately, and develop the theory for attached disclinations of finite strength. A disclination can be thought of as the sum of infinitesimal stripes that tile its cut surface and partition it into long stripes, elongated along the constitutive dislocations; the situation is reminiscent of the tiling of the cut surface of a dislocation into elementary dislocation loops.

1. Wedge polygonal loops and bisecting disclination lines

Consider, for instance, Fig. 8(a), which represents a disclination line made of two semi-infinite wedge segments L and L'. The stripes are divided into two sets parallel to the disclination segments; the continuity of the constitutive dislocations is ensured, when $\boldsymbol{\Omega}' = \boldsymbol{\Omega}$, if the twist edges of the stripes are along the line that bisects L and L'. It is easy to show that the Burgers vectors of the constitutive dislocation segments parallel to L and L' are continuous across this line.

A wedge loop is nothing other than a continuous generalization of Fig. 8(a), applied to a closed polygonal disclination; $\boldsymbol{\Omega}$ is constant in length and everywhere tangent to the loop, the constitutive dislocations close into loops entirely located in the cut surface.

The bisecting line has a special stability because it has no relaxation dislocations attached to it. It is indeed a wedge disclination, as established by the analysis that follows.

2. Disclinations meeting at a node: Kirchhoff relation, Frank vector

The foregoing considerations generalize to a polygonal disclination made of segments L_i of mixed character (twist wedge), with $\mathbf{\Omega}_i$ varying in direction but also in modulus ($\mathbf{\Omega}_i \neq \mathbf{\Omega}_j$) [Fig. 8(b)]. The considerations that follow apply when there are no restrictions on $\mathbf{\Omega}_i$, $\mathbf{\Omega}_j$, and the directions of the segments L_i and L_j; they are not necessarily in the same plane. Let $L_i(\mathbf{\Omega}_i)$ and $L_{i+1}(\mathbf{\Omega}_{i+1})$ be two consecutive disclination segments. The constitutive dislocation segments meet without discontinuity of the Burgers vector on the half line parallel to the direction

$$\tilde{\boldsymbol{\tau}}_i = 2\sin\frac{\Omega_i}{2}\mathbf{t}_i - 2\sin\frac{\Omega_{i+1}}{2}\mathbf{t}_{i+1}, \tag{11}$$

as, following Eq. (10), the density of dislocations must be counted along the common edge $\tilde{L}_i$ of the two boundaries.

In effect, if $\mathbf{O}_i\mathbf{P}$ is parallel to $\tilde{\boldsymbol{\tau}}_i$, we have

$$2\sin\frac{\Omega_i}{2}\mathbf{t}_i \times \mathbf{O}_i\mathbf{P} = 2\sin\frac{\Omega_{i+1}}{2}\mathbf{t}_{i+1} \times \mathbf{O}_i\mathbf{P}. \tag{12}$$

Equation (12) means, according to Frank's formula, that the Burgers vector is continuous across any segment parallel to $\tilde{\boldsymbol{\tau}}_i$. The half line $\tilde{L}_i$ is a generalization of the bisecting line. Notice that, in general, the planes $\{\tilde{L}_i, \tilde{\boldsymbol{\tau}}_i\}$ and $\{\tilde{L}_{i+1}, \tilde{\boldsymbol{\tau}}_{i+1}\}$ are not tilt planes for the constitutive dislocations; this happens only if $\mathbf{\Omega}_i$ and $\mathbf{\Omega}_{i+1}$ and the directions of the segments L_i and L_{i+1} are four coplanar directions.

a. Kirchhoff relation

We introduce, instead of the rotation vector $\tilde{\mathbf{\Omega}}_i = \tilde{\Omega}_i\tilde{\mathbf{t}}_i$,

$$\tilde{\boldsymbol{\tau}}_i = 2\sin\frac{\tilde{\Omega}_i}{2}\tilde{\mathbf{t}}_i. \tag{13}$$

Equation (11) then takes the form

$$2\sin\frac{\Omega_i}{2}\mathbf{t}_i = 2\sin\frac{\tilde{\Omega}_i}{2}\tilde{\mathbf{t}}_i + 2\sin\frac{\Omega_{i+1}}{2}\mathbf{t}_{i+1}, \tag{14}$$

which can be written

$$\mathbf{\Omega}_i = \tilde{\mathbf{\Omega}}_i + \mathbf{\Omega}_{i+1} \tag{15}$$

if the rotation angles are small. In these expressions, the signs are such that the line L_i is oriented inward (toward $\mathbf{O}_i$), whereas L_{i+1} and $\tilde{L}_i$ are oriented outward. If the orientations are so chosen that they all are outward or all inward, one gets

$$\sum_P 2\sin\frac{\Omega_P}{2}\mathbf{t}_P = 0. \tag{16}$$

Equation (16) is valid for any number of disclination segments meeting at the same point **O** (see below).

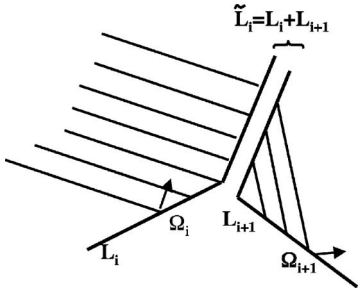

FIG. 9. Polygonal disclination as in Fig. 8: splitting of $\tilde{L}_i$.

Equation (16) does not contain any reference to the directions of the disclination segments meeting in **O**; it is akin to a Kirchhoff relation for the vectors $2\sin(\Omega_P/2)\mathbf{t}_P$. Notice in particular that Eq. (15), which is valid for small angles, is obtained straightforwardly by considering Frank circuits about the lines L_i, L_{i+1}, and $\tilde{L}_i$. We call the vector $\mathbf{f}=2\sin(\Omega/2)\mathbf{t}$, which plays for a disclination line the same role as the Burgers vector **b** plays for a dislocation line, the Frank vector. This vector is oriented in the same direction as the rotation vector $\Omega\mathbf{t}$.

By ensuring that line $\tilde{L}_i$ has no attached relaxed dislocations, Eq. (12) expresses the fact that $\tilde{L}$ has wedge character. Such a choice of $\tilde{L}$ assumes that the twist lines have a larger line tension than the wedge ones because of their core energy, as discussed in Sec. II.E.

b. Lines meeting at a node

We now deepen the disclination nature of $\tilde{L}_i$ in the case considered above when three disclinations meet in $\mathbf{O}_i$. As defined above, it is a wedge line—the Frank vector $\tilde{\mathbf{f}}_i = 2\sin\frac{\tilde{\Omega}_i}{2}\tilde{\mathbf{t}}_i$ is along the line—that is split into two mixed lines, with $\tilde{\mathbf{f}}_i = 2\sin\frac{\tilde{\Omega}_i}{2}\tilde{\mathbf{t}}_i$ Frank vectors and $\tilde{\mathbf{f}}_{i+1} = 2\sin\frac{\tilde{\Omega}_{i+1}}{2}\tilde{\mathbf{t}}_{i+1}$ (Fig. 9). Again, there are no relaxation dislocations along $\tilde{L}_i$ and is therefore a very special wedge line.

Now, line fluctuations $\delta\tilde{L}_i$ would break the continuity of the Burgers vector on $\tilde{L}_i$ and generate relaxation dislocations with Burgers vector

$$\delta\mathbf{b} = 2\sin\frac{\tilde{\Omega}_i}{2}\tilde{\mathbf{t}}_i \times \delta\tilde{L}_i - 2\sin\frac{\tilde{\Omega}_{i+1}}{2}\tilde{\mathbf{t}}_{i+1} \times \delta\tilde{L}_i,$$

according to Eq. (1) ($\delta\mathbf{b} = \delta\mathbf{b}_i - \delta\mathbf{b}_{i+1}$), by adding the effects of the two lines involved in the splitting, i.e., from Eq. (11),

$$\delta\mathbf{b} = 2\sin\frac{\tilde{\Omega}_i}{2}\tilde{\mathbf{t}}_i \times \delta\tilde{L}_i - 2\sin\frac{\tilde{\Omega}_{i+1}}{2}\tilde{\mathbf{t}}_{i+1} \times \delta\tilde{L}_i = \tilde{\boldsymbol{\tau}}_i \times \delta\tilde{L}_i. \tag{17}$$

From Eq. (17) it emerges that $\tilde{\boldsymbol{\tau}}_i$ is the Frank vector of the $\tilde{L}_i$ disclination. These considerations also confirm

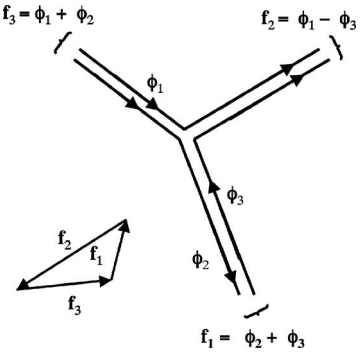

FIG. 10. Three broken disclinations of Frank vectors ϕ_1, ϕ_2, ϕ_3, meeting at a point and composing three disclinations obeying Kirchhoff relation $\mathbf{f}_1+\mathbf{f}_2+\mathbf{f}_3=0$ (inset).

that Eq. (16) is a Kirchhoff relation at a node where three disclinations meet.

Notice that our reasoning has given a specific role to one of the three disclinations $\tilde{L}$, but this restriction can be easily removed. Consider three Frank vectors ϕ_1, ϕ_2, and ϕ_3, and construct three disclination segments meeting at a common point **O**, such that

$$\mathbf{f}_1 = \phi_2 + \phi_3, \quad \mathbf{f}_2 = -\phi_3 + \phi_1, \quad \mathbf{f}_3 = -\phi_1 - \phi_2. \tag{18}$$

This can be done by giving a sharp corner to the three disclinations $\boldsymbol{\phi}_i$ at **O** and joining their straight segments two by two, as in Fig. 10. If all segments L_i are along $\mathbf{f}_i$, the L_i's are all of wedge character, and there are no relaxation dislocations attached to them. The appearance of relaxation dislocations attached with the L_i's would make them change direction. The final geometry depends on the energy balance between the grain boundaries (the constitutive dislocations), the relaxation dislocations, and the core energy of disclinations. Notice that the three L_i's are coplanar if they are of wedge character.

The extension to any number of disclinations is obvious, which justifies our claim concerning Eq. (16). Notice, however, that whereas Fig. 10 represents three grain boundaries merging two by two along three disclinations, the case of four disclinations (say) meeting at a node requires, in the most general case, four grain boundaries merging three by three along the four disclinations; each of them is then split into three subdisclinations. Such a geometry occurs by nature in ideal polynanocrystals (see Sec. III.C.2).

Remark. In accordance with the remark at the end of Sec. II.A, Eq. (16) does not apply properly if one of the angles $|\Omega_p| > \pi$.

3. Disclinations merging along a line

The situation where three lines L_1, L_2, and L_3 merge along a unique line L is also worth considering. One expects that the Kirchhoff relation

$$\mathbf{f}_1 + \mathbf{f}_2 + \mathbf{f}_3 = \mathbf{0} \tag{19}$$

is satisfied. This case is physically represented in a ferromagnet by three Bloch walls merging along a Bloch line, dislocations being the sources of the magnetoelastic stresses (Kleman, 1974). More generally, one expects that in an amorphous medium n disclinations $\cdots\mathbf{f}_i\cdots$ merging along a line yield a unique disclination of the Frank vector $\mathbf{f}=\Sigma_i\mathbf{f}_i$.

G. Generic disclination lines: Disclination densities

We now come to the generic case when a disclination line L is smoothly curved and its Frank vector varies smoothly. Consider two infinitesimally close points **P** and **Q** on L, with Frank vectors $\mathbf{f}_P$ and $\mathbf{f}_Q$; we write

$$Q = P + \mathbf{s}\delta s,$$

$$\mathbf{f}_Q - \mathbf{f}_P = 2\sin\frac{\Omega_Q}{2}\mathbf{t}_Q - 2\sin\frac{\Omega_P}{2}\mathbf{t}_P,$$

$$\mathbf{s}_Q - \mathbf{s}_P = \frac{d\mathbf{s}}{ds}\delta s = \frac{\mathbf{n}}{R}\delta s. \tag{20}$$

Here $\mathbf{s}_P$ and $\mathbf{s}_Q$ are the unit tangents to L in **P** and **Q**, **s** is a unit vector pointing from **P** to **Q**, which can be chosen to leading order equal to $\mathbf{s}_P$, and likewise **n** is the principal normal in P. R is the radius of curvature of L in P. The variation between **P** and **Q** of the displacement on the cut surface of L in **M** can be written

$$\delta\mathbf{b} = \mathbf{f}_Q \times \mathbf{QM} - \mathbf{f}_P \times \mathbf{PM}$$
$$= -\mathbf{f}_P \times \mathbf{s}\delta s + (\mathbf{f}_Q - \mathbf{f}_P) \times \mathbf{PM}. \tag{21}$$

The first term $(-\mathbf{f}_P\times\mathbf{s}\delta s)$ measures the relaxation dislocation densities attached to the line between **P** and **Q**. We now focus on the second one, which measures the relaxation disclination densities. According to Kirchhoff's relation, we have $-\delta\mathbf{f}=\mathbf{f}_Q-\mathbf{f}_P$, the sign chosen such that the attached disclination densities $\frac{d\mathbf{f}}{ds}$ are oriented outward (as $\mathbf{f}_Q$), and $\mathbf{f}_P$ is inward.

If we assume that L is a wedge disclination, i.e., $\mathbf{t}_P = \mathbf{s}_P$, $\mathbf{t}_Q=\mathbf{s}_Q$, we have

$$\delta\mathbf{f} = \delta\Omega_P\mathbf{t}_P + \frac{2}{R}\sin\frac{\Omega_P}{2}\mathbf{n}\delta s. \tag{22}$$

The first term of the right member $(\delta\Omega_P\mathbf{t}_P)$ measures the effect of the variation in modulus of the rotation vector. In its absence, the rotation vector of the attached disclinations is along the principal normal. This is obviously reminiscent of the bisecting disclination line. If the attached disclinations have a wedge character, i.e., are along the principal normals, again as above, there are no supplementary dislocations accompanying them, apart from those constituting L, and we might expect that the energy is minimized. Another result, not visible in the previous analysis (Sec. II.F.2), is that the curvature of the disclination line L is directly related to the presence of the attached disclinations.

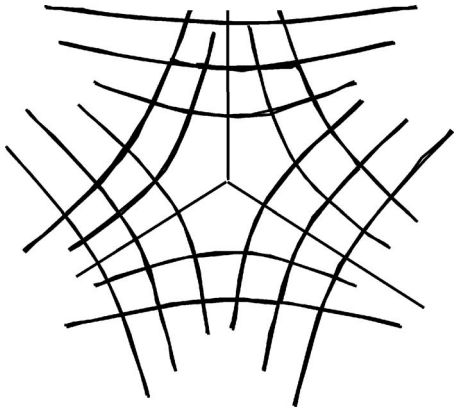

FIG. 11. Quantized wedge disclination in a crystal, $\Omega=-\pi$.

In the generic case ($\mathbf{t}_P \neq \mathbf{s}_P$, $\mathbf{t}_Q \neq \mathbf{s}_Q$, $\delta\Omega_P \neq 0$), the Frank vectors of the attached disclinations are no longer along $\mathbf{n}$, but, as shown in the previous analysis, there is still a choice for the direction of the attached disclinations for which the supplementary dislocations are canceled; and the conclusion on the relation between curvature and attached disclinations is still valid.

III. COARSE-GRAINED CRYSTALLINE SOLIDS, GRAIN BOUNDARIES, POLYNANOCRYSTALS

A. Coarse-grained crystalline solids

Nonquantized wedge disclinations in a crystalline solid have been mentioned previously; they are akin to the limited tilt boundaries discussed in Sec. II.

Grain boundaries of small misorientation angle (subgrain boundaries) are well documented; they are limited by wedge, twist, or mixed disclinations, according to the geometrical interactions between Burgers and Frank vectors discussed previously. These interactions are restricted to those that imply Burgers vectors equal to translation symmetries of the medium.

Large misorientation angle grain boundaries are especially important in polynanocrystals.

A quantized disclination in a crystalline solid carries an angle $\mathbf{\Omega}$ of rotational symmetry of the crystal; in the wedge case, the line is itself the axis of this symmetry (see Fig. 11). As emphasized, the related energy is extremely large and so their existence is improbable. A related imperfect disclination occurs when the grain boundary is a plane of geometry of large atomic density for the two grains. If this imperfect disclination is rejected outside the sample, one has a low-energy twin.

Quantized disclinations in mesomorphic media are discussed in Secs. IV and V.

B. Grain boundaries

1. Classification of grain boundaries and of continuous disclinations

Grain boundaries in solids are classified according to the orientation of the rotation vector $\boldsymbol{\omega}$ with respect to the plane of the boundary Σ_{GB}: a tilt grain boundary occurs when $\boldsymbol{\omega}$ is in Σ_{GB}, and a twist grain boundary when $\boldsymbol{\omega}$ is perpendicular to Σ_{GB}. This classification makes sense: a tilt grain boundary can be split into a set of parallel identical edge dislocations whose Burgers vectors are perpendicular to the boundary; a twist grain boundary can be split into two sets of parallel identical screw dislocations whose Burgers vectors belong to the boundary. Such splittings are currently observed in small-misorientation grain boundaries (also called subboundaries). Each set of screw lines of a twist grain boundary carries nonvanishing stresses, but the long-distance stresses of the two sets cancel.[4]

We have classified disclination lines according to the orientation of the rotation vector $\boldsymbol{\omega}$ with respect to the line direction L: a wedge line when $\boldsymbol{\omega}$ is along L, and a twist line when $\boldsymbol{\omega}$ is perpendicular to L. This classification is perfectly adequate when no account is taken of the presence of a grain boundary attached to the line, e.g., quantized disclinations (no grain boundaries), but is not consistent with the grain boundary classification. For instance, a tilt grain boundary can be limited by either a wedge disclination or a twist disclination.

A finer classification of continuous disclinations (i.e., carrying a grain boundary) seems therefore appropriate.

(i) *Wedge* disclination line, Fig. 12(a): L is parallel to the constitutive dislocations of a tilt boundary; $\boldsymbol{\omega}$ is parallel to L.

(ii) *Normal tilt* disclination line, Fig. 12(b): L is perpendicular to the constitutive dislocations of a tilt boundary; $\boldsymbol{\omega}$ is perpendicular to L.

(iii) *Pure twist* disclination line, Fig. 12(c): L belongs to a twist boundary; $\boldsymbol{\omega}$ is perpendicular to the boundary, thus to L. We have taken $|\mathbf{b_1}|=|\mathbf{b_2}|$; hence $\mathbf{b}=\mathbf{b_1}+\mathbf{b_2}$ perpendicular to L, as required.

2. Polycrystals as compact assemblies of polyhedral crystals

Nearly perfect polycrystals, as possibly created by annealing, can be viewed as compact assemblies of polyhedral grains. Their common facets are commonly triangu-

[4]The boundary conditions (vanishing strains at infinity) of a set of parallel screw dislocations in a twist grain boundary can be satisfied in two different ways: either by a purely (nonplastic) strain field or by a second set of parallel screw dislocations, perpendicular to the first set, forming another twist boundary parallel to the first one (Nabarro, 1967). It is well known that this latter situation is achieved in real solid crystals, the two parallel twist boundaries being located in the same plane. On the other hand, it is believed that there is only one set of screw lines in the "twist grain boundary" liquid crystalline phase (denoted TGBA phase) [see Renn and Lubensky (1988), Kamien and Lubensky (1999)]; in that case also, the long-distance cancellation of the stresses carried by each grain boundary can be achieved either by a purely (nonplastic) strain field or by the presence of a family of parallel grain boundaries at periodic distances. We favor this second possibility, in similarity with the case of solid crystals; but a detailed calculation is still lacking.

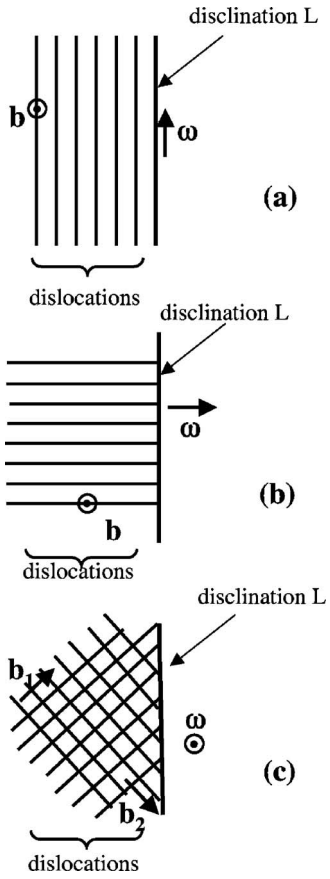

FIG. 12. Classification of continuous disclinations in a solid: (a) wedge disclination, (b) normal tilt disclination, and (c) pure twist disclination.

lar and fairly flat grain boundaries Σ, each surrounded by a disclination line L of strength equal to the rotation $\boldsymbol{\omega}$ of the grain boundary.

Three grains meet along a fairly straight edge E bordering such a facet, where the three parallel disclinations combine along the edge (Fig. 13). In such a stress-free annealed polycrystal, each such triplet of parallel disclinations must compensate their long-range stresses.

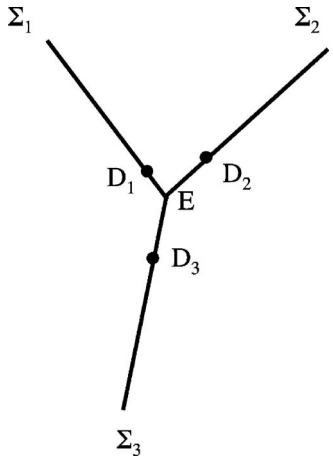

FIG. 13. The three parallel disclinations D_i, with rotations $\boldsymbol{\omega}_i$, along an edge E between three grain boundaries $\Sigma_{,i}$.

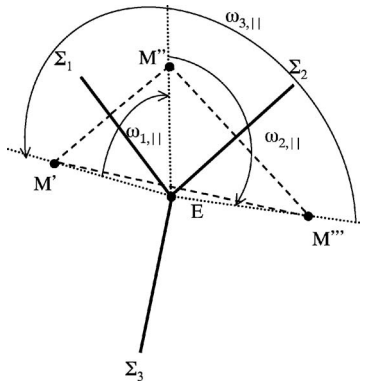

FIG. 14. Composition of the three edge disclinations of parallel rotations $\boldsymbol{\omega}_{i,\|}$.

a. Kirchhoff relations

To analyze the stresses due to the three disclinations D_i of an edge E, we have again to distinguish the contributions of the wedge components $\boldsymbol{\omega}_{i,\|}$ [parallel to E; cf. Fig. 12(a)] from those of the normal tilt and pure twist components $\boldsymbol{\omega}_{i,\perp}$, with attached dislocations, Figs. 12(b) and 12(c).

For this second part $\boldsymbol{\omega}_{i,\perp}$, the compensation of the three families of relaxation dislocations leads to the same condition as above for a node:

$$\sum_i \mathbf{f}(\boldsymbol{\omega}_{i,\perp}) = \mathbf{0}, \tag{23}$$

with $\mathbf{f}(\boldsymbol{\omega}) = 2 \sin \frac{\omega}{2}\mathbf{t}$.

To have a completely stress-free edge, the wedge components $\boldsymbol{\omega}_{i,\|}$ must also add up to zero:

$$\sum_i \boldsymbol{\omega}_{i,\|} = \mathbf{0}. \tag{24}$$

It is clear from Fig. 14 that the Volterra process which produces $\boldsymbol{\omega}_{1,\|}$ and $\boldsymbol{\omega}_{2,\|}$ by moving M' to M'' and M'' to M''' sums up to an effect opposite to that which $\boldsymbol{\omega}_{3,\|}$ produces by moving M''' to M'. Thus, using Eq. (1) and the fact that M', M'', and M''' are on a circle centered at E, one gets

$$M'M'' \cos \angle (M''M'M''') + M''M''' \cos \angle (M''M'''M') - M'M'' = 0$$

because

$$\sin \frac{\omega_{1,\|}}{2} \cos \frac{\omega_{2,\|}}{2} + \sin \frac{\omega_{2,\|}}{2} \cos \frac{\omega_{1,\|}}{2} = \sin \frac{\omega_{1,\|} + \omega_{2,\|}}{2} = -\sin \frac{\omega_{3,\|}}{2}.$$

b. Subboundaries

For small misorientation boundaries, and also for boundaries whose orientation does not differ much from a small energy twin, all or part of the continuous dislocations cluster into a periodic distribution of quantized dislocations (Burgers, 1939a, 1939b; Read and Shockley,

1950). This polygonization was first observed by x rays and described in these physical terms by Crussard (1944a, 1944b), after annealing of fcc single crystals strained in multislips (stages II and III). Later observations after etching of low-angle boundaries (Lacombe and Beaujard, 1948) provided the first experimental proof of the decomposition of these boundaries into rows of dislocations, and various techniques such as electron microscopy for metals and semiconductors and pinning of dislocations by precipitates in transparent ionic solids analyzed the details of the dislocation networks on the subboundaries and the way these dislocations connect at the edges of the grains [cf. Friedel (1964, 1985)]. These dislocations can slip under stress, especially after annealing of crystals strained in single slip (stage I), which produces especially simple networks as pictured in Fig. 12 (Washburn and Parker, 1952); in the more general case, the bowing under stress of the dislocations of the various sub-boundaries decreases the effective elastic moduli by a large fraction (Friedel *et al.* 1955).

c. Large misorientation boundaries

Following Friedel (1926), who calls them "macles par mériédrie," Bollmann (1970) has established similar dislocation arrangements for large misorientation boundaries, in terms of a crystallographic network common to both grains in contact along the boundary. A common crystallographic network has also been put forward by Friedel (1926) for what he calls "macles générales." But generally it is believed that the boundary is an amorphous contact on an atomic thickness, with possible ledges along which one of the grains can overlap into the other. These configurations, as a whole, obey the same conditions of stability as small-angle boundaries, but allow more stressed states than the former, like roughness, glide, lateral motions of the grains, and so on.

d. Specific complications that arise from the crystal structure

The coalescence of continuous distributions of infinitesimal dislocations, considered in this paper, into quantized crystal dislocations can introduce some complications that should be stressed, as they have no equivalents in liquid crystals or magnetic structures. Some of the following complications have been presented by Friedel (1964).

(i) In the simplest cases, the infinitesimal dislocations coalesce into quantized dislocations, all with the same directions of line and Burgers vector. This condition optimizes the energy of contact between grains at the expense of an elastic distortion of the crystal, over a distance from the grain boundary of the order of the distance $l=ON$ between dislocations (Fig. 6). This is the case for three grain boundaries meeting along wedge disclinations, as in Figs. 12(a) and 14, when one set of edge dislocations rearrange after straining in stage I of a single-slip system; another example is given by two (or three) systems of screw dislocations building a network of increasing density into a twist boundary, as in Fig. 12(c), this can be obtained by torsion of a hexagonal lattice along the hexagonal axis of symmetry, e.g., in graphite (de Gennes and Friedel, 2007) and in hcp metals (Fivel, 2006).

(ii) In most cases, however, where dislocations of a number of slip systems have been developed by straining, the subboundaries of the polygonal structures obtained by recovery are each composed of a distribution of two or more systems of dislocations, so as to produce subboundaries of mixed nature and more or less random orientation. Such subboundaries are somewhat less stable, as their elastic distortions average out at a larger distance from the subboundaries for a given rotation, owing to the mixing of dislocations of several slip systems.

(iii) Even in the simpler case first considered, Fig. 6 shows that the possible positions of the crystal dislocations can occur only at specific positions such as O and N along the subboundary. The periodic distribution of such dislocations must be coherent with the crystal structure along the boundary; it must correspond to a discrete series of angles ω_i, with intervals increasing with the angle at least for small angles ω_i. A subgrain boundary with an angle between ω_i and ω_{i+1} can be built only of successive segments corresponding to ω_i and ω_{i+1}, and the distance of elastic relaxation away from the boundary is of the order of two such successive domains.

(iv) Figure 6 shows schematically the structure of such a symmetric tilt boundary, in its initial state, with a continuous distribution of infinitesimal dislocations. Their regrouping into quantized crystal dislocations can occur only at distances l_i, where l_i are integer multiples of the lattice period along the boundary ($n=2$ in Fig. 6); l_i is related to ω_i by

$$f_i = b/l_i = \sin \omega_i. \tag{25}$$

For increasing ω_i, this special Frank vector is increasingly smaller than Eq. (10) for the general case.

(v) These ω_i's correspond to coherent structures of lower energy. In fact, in crystal structures with a center of symmetry, they are twins; and Eq. (25) then leads for $\omega_i=\pi$ to a perfect coherence of the two crystals, with vanishing boundary tension. In the absence of a center of symmetry, $\omega_i=\pi$ leads to a twin with especially low boundary tension and again no crystal dislocations. In both cases, the increase of f_i when ω_i decreases from π can be described in terms of an increasing density of crystal dislocations. More generally, perfect matching without crystal dislocations and vanishing grain boundary tension occurs when ω_i is an allowed rotational symmetry of the crystal, such as $\omega_i=\pi/2$ for the case of Fig. 6 with a cubic crystal symmetry. The same occurs, of course, in all cases for $\omega_i=\pm 2n\pi$.

(vi) In cubic structures, such as the twins considered by Friedel (1926) and Bollmann (1970), they can be built on a common superlattice of the two crystals. Such twins, with not too large l_i's so ω_i is not too far from $\pi/2$, can present ledges as sketched in Fig. 15, which introduce supplementary dislocations such as D_2'.

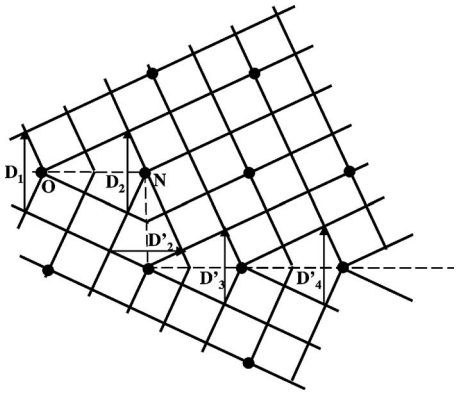

FIG. 15. Ledge in a merihedric twin [cf. Friedel (1926), Bollmann (1970)]. The superlattice is underlined by black dots.

C. Polynanocrystals

Polynanocrystalline materials are assemblies of small polyhedral grains. The grain size ranges from a few nanometers to 1 μm. Their plastic properties, in pure metals, pure semiconductors, and ceramics, show several features. One example is the presence of large internal stresses, which distinguish them from the classic picture of dislocation-driven phenomena in the usual coarse-grained crystalline materials [see, e.g., Weertman *et al.* (1999); Kumar *et al.* (2003); Ovid'ko (2005); Wolf *et al.* (2005); Van Swygenhoven and Weertman *et al.* (2006)]. Polynanocrystals provide a remarkable physical example for discussion of the notions just introduced. We are interested in the relation between the polynanocrystal plastic properties and the disclination and grain-boundary structure.

1. Data on the plastic deformation of polynanocrystalline materials

A dominant mechanism of coarse-grained crystal plastic deformation (work hardening) at low temperature is the slip of dislocation pileups; this mechanism obeys the well-known Hall-Petch relation $\sigma_Y=\sigma_{Y_0}+kl^{-1/2}$, where σ_{Y_0} is the single-crystal yield stress (the friction contribution), k is a material-dependent constant, and l is the grain size [see, e.g., Friedel (1959a)].

But the yield stress does not increase without limit when l approaches atomic sizes. After reaching considerable values in the nanoscopic range, it decreases somewhat below some crossover size l_c—often referred to as the strongest size (Yip, 1998); the material becomes ductile and even "superplastic." This latter property does not occur in all samples, and depends crucially on the absence of porosity (high density) and of nanocracks. It has been observed, e.g., in an iron alloy (Branagan *et al.*, 2003), in nickel (MacFadden *et al.*, 1999; Schuh *et al.*, 2002), and in copper (Lu *et al.*, 2000; Wang *et al.*, 2002; Champion *et al.*, 2003; Koch, 2003; Zhu and Liao, 2004). Nanocrystalline nickel, for instance, exhibits a Hall-Petch strengthening as the grain size decreases down to $l_c\approx 14$ nm, thus reaching internal stresses of order at least ten times those observed in the usual coarse-grained samples.

High ductility requires suppression of plastic flow localization, i.e., strain hardening that stabilizes the tensile deformation, see Ovid'ko (2005). Several mechanisms at the origin of this strain hardening are currently under discussion in the literature.

(i) *Partial dislocations emitted by grain boundaries.* The size range just below l_c is characterized in fcc metals by the appearance of Shockley partials with $(1/6)\langle 112\rangle$ Burgers vectors bordering $\{11\bar{1}\}$ stacking faults and the (correlated) formation of twin lamellae, during which process the yield stress is still increasing; [see, e.g., for Al, Chen *et al.* (2003)]. In effect, one can imagine that the formation of partials on some glide system impedes the motion of partials on another one. A large number of atomistic calculations, reviewed by Van Swygenhoven *et al.* (2006), supports a few experimental results pointing in this direction.

We keep in mind that this type of dislocation-biased plastic deformation must put into play glides and probably lateral displacements or growth or shrinking processes of grain boundaries; the published data do not clearly show whether these glides are analogous to low-temperature glide or employ diffusion mechanisms, at the emission and/or absorption of dislocations.

(ii) *Hardening by annealing and softening by deformation*. Huang *et al.* (2006) have recently reported on the necessity of extremely high stresses in order to nucleate partials in well-annealed, equilibrated, ultrafine nanocrystalline grains of Cu with no intragranular isolated dislocations or twins; on the other hand, the appearance of these grain-boundary or/and disclination (probably) nucleated dislocations softens the material. This is reminiscent of the plastic behavior of whiskers (Ma *et al.*, 2006), and suggests that grain-boundary perfection is an important factor. Indeed, the computer simulations noted above employ grain boundaries that are not totally relaxed and show up ledges that act as sources of partials.

(iii) *Grain-boundary sliding and grain rotation.* It seems that this is the dominant mechanism at high temperatures and/or grain size below l_c, with Coble (1963) diffusion inside the grain boundaries; see Schiøtz *et al.* (1998); Ovid'ko (2002); Van Swygenhoven (2002); Ma (2004); Shan *et al.* (2004).

We distinguish in the following an ideal polynanocrystal configuration, with continuous disclinations and their constitutive dislocations, from actual configurations, with their defects and unusually large internal stresses.

2. Structure of the ideal polynanocrystal

The picture developed above for annealed coarse-grained polycrystals should apply to polynanocrystals. Thus the computer simulations of Van Swygenhoven *et al.* (2000) indicate that there is no difference between boundaries in polynanocrystals and those in coarse-grained materials, and that the degree of organization is often rather high.

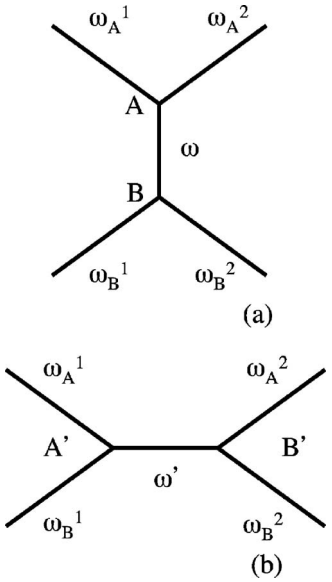

FIG. 16. A modification process frequent in foams and possible in polynanocrystalline media.

Two main differences arise from the conditions of preparation.

(i) Sintering can produce large internal stresses or intergranular cavities. These large stresses should displace possible low-angle boundaries, which are fairly common in coarse-grained polycrystals Friedel *et al.* (1953): such subboundaries should be mobile enough to glide toward large-angle boundaries, with which they should be integrated.

(ii) The usual size of the mosaic structure of crystals, whether in the form of a simple Frank network or of a finely polygonized structure, should not be present in polynanocrystals near their maximum elastic limit, because of their destruction by the high internal stresses, and because annealing conditions should destroy mosaic structures of sizes less than typically 10 μm (Friedel, 1964, p. 240). With these provisos, the conditions of stability of a polynanocrystal should follow the same Kirchhoff relations for coarse-grained materials.

The surface tension E of a subboundary depends on the misorientation ω: $E \approx E_0\omega$, where $E_0 = \mu b/4\pi(1-\nu)$; on the other hand, for large misorientations, above some value $\omega > \omega_{\max} \approx 20°$, E can be taken independent of the direction of the grain boundary with respect to the two grain orientations ($E \approx E_0\omega_{\max}$)—see Friedel *et al.* (1953), Friedel (1964), Chap. 10—as long as the grain boundary is not along or close to a lattice direction common to the two grains.

Most of the grain boundaries in polynanocrystalline materials are large-angle ones; as a consequence, they have an energy fairly independent of the angle of misorientation. If submitted to this sole constant surface tension, the grain boundaries should form angles of $\approx 120°$ at triple junctions. Other forces originate from the wedge disclination segments. Equilibrium can be reached, in principle, by processes of the form described Fig. 16, proposed by Friedel (1985) for solids and well known in foams (Weaire and Hutzler, 2000), which consist, first, in the vanishing of the boundary segment AB, and, subsequently, after a passage through an unstable quadruple junction, the appearance of the boundary segment $A'B'$. In this figure A, B, A', B' are triple junctions seen end on, and $\omega_A^{(1)}$, $\omega_A^{(2)}$, $\omega_B^{(1)}$, $\omega_B^{(2)}$, $\omega_{A'}^{(1)}$, ω, ω' are the wedge component misorientations of the grain boundaries (GBs) whose sections with the plane are drawn; these rotation vectors are all directed along the normal to the figure.

The triple junction Kirchhoff relations can be written

$$\omega + \omega_A^{(1)} + \omega_A^{(2)} = \delta\omega_A \quad \text{along } A,$$

$$-\omega + \omega_B^{(1)} + \omega_B^{(2)} = \delta\omega_B \quad \text{along } B,$$

$$\omega' + \omega_A^{(1)} + \omega_B^{(1)} = \delta\omega_{A'} \quad \text{along } A',$$

$$-\omega' + \omega_A^{(2)} + \omega_B^{(2)} = \delta\omega_{B'} \quad \text{along } B'.$$

They yield

$$\delta\omega_A + \delta\omega_B = \delta\omega_{A'} + \delta\omega_{B'} (= 2\delta\omega).$$

Hence we can write

$$\delta\omega_A = \delta\omega + \delta\varpi, \quad \delta\omega_B = \delta\omega - \delta\varpi,$$

$$\delta\omega_{A'} = \delta\omega + \delta\varpi', \quad \delta\omega_{B'} = \delta\omega - \delta\varpi',$$

where

$$2\delta\varpi = \delta\omega_A + \delta\omega_B, \quad 2\delta\varpi' = \delta\omega_{A'} + \delta\omega_{B'}.$$

$\delta\omega$ measures the repulsive terms between A and B, and between A' and B'; they are equal. The attractive terms $\delta\varpi$ and $\delta\varpi'$ are different; thus modification is favored if $|\delta\varpi'| < |\delta\varpi|$. In the case when $\delta\omega = \delta\varpi = \delta\varpi' = 0$, modification is ruled by the surface tension.

There is probably no chance, although it is in principle possible, that a polynanocrystal reaches the same structural configuration as foreseen for a foam, and even less that this structure coarsens, as 2D foams do (von Neumann, 1952), a result extended recently to 3D foams (Hilgenfeldt *et al.*, 2001).

3. Plastic deformation of a polynanocrystal

The lack of a mosaic structure in fine polynanocrystals prevents the presence of internal Frank-Read sources in the grains. This is well recognized by most. We consider two possible processes: production of partials, and grain-boundary sliding, grain rotation and, more generally, grain boundaries as sources and sinks of dislocations.

a. Production of partials

There are probably several mechanisms possible for the production of partials, some relating to the grain boundaries, others to the disclination lines (triple junctions).

(i) *Constitutive edge dislocations*. The role of the applied stress in a possible bowing of dislocations of the boundary has already been suggested. This is probably a

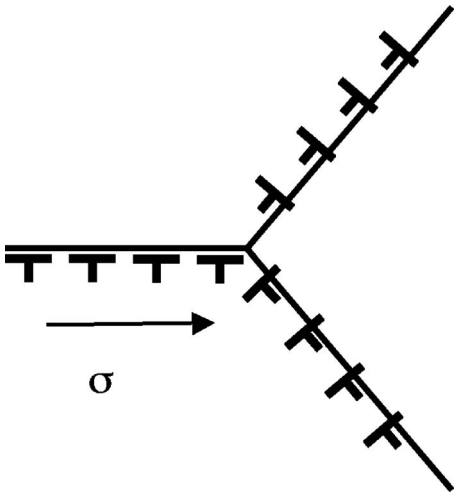

FIG. 17. Slip of a pileup, left half plane, against a normal tilt disclination.

low-temperature mechanism, by glide, but a number of computer simulations [see Van Swygenhoven *et al.* (2006)] as well as experimental works indicate that the process is thermally activated (Van Petegem *et al.*, 2006), and displays a small activation volume. The same dislocations are free, given suitable stresses, to climb in the plane of the boundary, and thus to displace the bordering disclination, thereby displacing the two other boundaries that merge along the common edge along which the disclination is located.

(ii) *Slip of dislocation in the boundary*, whose Burgers vectors are in the plane (Fig. 17).

Such dislocations can pile up along the edges and be at the origin of stress concentrations large enough to nucleate new dislocations and/or move the other grains, as proposed by Ovid'ko (2005). Notice that dislocations considered here are not constitutive or relaxation dislocations of the boundary to which they belong [they do not obey Eq. (1)]. In fact, they pile up classically.

(iii) *Grain boundaries and triple junctions as sources and sinks for dislocations*. The emitted or absorbed dislocations are not constitutive dislocations of the grain boundaries, nor are pairs of dislocations of opposite signs (dipoles). Assume the presence of a ledge on a grain boundary bordered by a triple junction. If this ledge affects only one (possibly two) of the three grain boundaries merging at the triple junction, there is necessarily some kind of splitting of the triple junction into its constitutive disclinations, in the region of the ledge. Consider one of these stripped disclination segments; on it, the ledge determines a double kink AB, $A'B'$ (Fig. 18). According to Eq. (2), the Burgers vector of the dislocation that necessarily joins the two kinks is perpendicular to the kinks and to the rotation vector $\boldsymbol{\omega}$ of the kinked disclination; $\boldsymbol{\omega}$ is certainly close in direction, if not parallel, to the disclination line, according to the analysis of Sec. III.C.2. Thus a large component of the Burgers vector of the dislocation is in the plane of the grain boundary; this might favor slip in this plane. Also, the smaller the kink lengths AB, $A'B'$ (Fig. 18), the

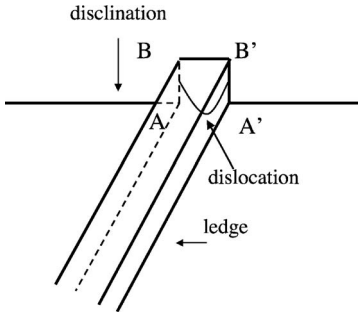

FIG. 18. Double kink on a disclination. The dislocation Burgers vector is in the plane of the grain boundary or close to it; see text.

smaller the Burgers vector of the dislocation attached to them, and the smaller the energy needed to nucleate the double kink. One can therefore speculate that this is the origin of partials (rather than perfect dislocations) and of the related small activation energy and volume (smaller by two orders of magnitude as compared to the values observed in coarse-grained metals).

b. Grain-boundary sliding and grain rotation

These mechanisms of deformation have been mentioned in Sec III.C.1. Notice that a relative rotation $\delta\omega$ of two grains with a common grain boundary requires that the constitutive dislocation densities be modified accordingly, i.e., that an exchange of grain-boundary dislocations with the intergranular medium takes place. Huang *et al.* (2006) have observed that the number of subboundaries decreases under high-T annealing, so that the grains necessarily "roll" (Shan *et al.*, 2004), the trend being seemingly toward a polynanocrystal with large misorientation grain boundaries only.

IV. QUANTIZED DISCLINATIONS IN MESOMORPHIC PHASES

There is no conceptual difficulty in constructing, in the manner of the Volterra process, a quantized wedge disclination in a medium endowed with finite rotational symmetries; e.g., a nematic phase $\Omega=\pm\pi$, a smectic phase ($\Omega=\pm\pi$), liquid crystals in general, a solid crystal ($\Omega=\pm 2\pi/n$, $n=1$, 2, 3, 4, or 6), a quasicrystal (Bohsung and Trebin, 1987) ($n=5,8,10,12$, etc.) or a 3D spherical or hyperbolic curved crystal (Kleman, 1989). In 3D solid crystals, the line energies are so large that disclinations are observed in special conditions only; see Secs. II.A (3D solid crystal wedge lines) and II.E (continuous twist lines) for comments.

Disclinations that are observed in various liquid crystals usually differ widely from those expected to result from a pure (not extended) Volterra process. These differences originate in various liquid-crystal symmetries, and thus in various types of relaxation defect. As in the previous section, one can consider the interplay of quantized wedge disclinations, either with attached dislocations, which transform them into twist or mixed disclina-

tion with the same rotation vector $\mathbf{\Omega}$, or with attached disclinations, which yield a $\mathbf{\Omega}$ variable in a direction that illustrates the large rotation deformations that a liquid crystal can suffer, or again with unattached dislocations that result from their motion. Quantized disclinations constructed by such extended Volterra processes can be described in terms of twist, wedge, or mixed segments, in addition to their physical property of topological stability.

Two questions therefore arise: (i) How are the Volterra characteristics of wedge, twist, or mixed character (i.e., different types of extended Volterra processes) reflected in the topological classification? (ii) Can any quantized disclination, empirically given, be constructed in a systematic way by an extended Volterra process? To point (i) we have a partial answer, namely, that disclinations, when differing only by constitutive dislocations, belong to the same conjugacy class of $\Pi_1(V)$. Point (ii) is considered in the final discussion (Sec. VIII).

A. Quantized wedge disclinations and their transformations

This subsection is devoted to the molecular configurations carried by quantized disclinations, when the limitations that are imposed in the Volterra process by the specific symmetries of the medium are taken into account. Examples given in this subsection relate to nematics (N) and cholesterics (N^*), and in the next subsection to SmA phases. It appears that important disclination properties (shape, flexibility, interplay between them and with other defects, etc.) escape an analysis based solely on the topological classification.

1. N phase

The order-parameter space of the nematic phase is the projective plane P^2, whose first homotopy group $\Pi_1(P^2)$ is Z_2, the group with two elements $\{e,a\}$, $a^2=e$, e being the identity. All topologically classified defects belong to a unique class of homotopy, namely, a; all Volterra defects of strength $|k|=n+\frac{1}{2}$, $|\Omega|=(2n+1)\pi$, $n\in Z^+\cup\{0\}$, can be mapped on a. Most experimental observations yield $n=0$, i.e., two different Volterra disclination types, $k=+\frac{1}{2}$ and $-\frac{1}{2}$, which the topological theory classifies under the same heading; indeed, the topological theory predicts that it is possible to transform smoothly a $k=+\frac{1}{2}$ into a $k=-\frac{1}{2}$ (Bouligand, 1981). In fact, since the Volterra process predicts also $k=n$ (these lines, again, are not topologically stable), the cases $k=+\frac{1}{2}$ and $k=-\frac{1}{2}$ differ by the not topologically stable but Volterra line $k=1$. The Volterra classification thereby proves useful when analyzing experimental results.

Consider a wedge line. Any axis orthogonal to the director is a twofold symmetry axis. The wedge line has to be along such an axis. As a consequence, there is a director that is orthogonal to the line in its close vicinity.

The deformation of a wedge straight line implies a translation and/or a rotation of $\mathbf{\Omega}$ along the line. We apply the considerations of Sec. II.G, Eqs. (21) and (22). The translation and rotation of $\mathbf{\Omega}$ along the line bring (i) a nonvanishing density of attached dislocations

$$\delta\mathbf{b}_{Tr}=-2\mathbf{t}_P\times\mathbf{s}_P\delta s \tag{26}$$

that vanishes if the Frank vector is along the tangent $\mathbf{s}_P$ in $\mathbf{P}$, along the disclination line, i.e., if the deformed disclination is still of wedge character, and (ii) a nonvanishing density of attached disclinations

$$\delta\mathbf{f}_P=\frac{2}{R}\mathbf{n}_P\delta s \tag{27}$$

(this expression is valid in the pure wedge case only), whose infinitesimal Frank vectors $\delta\mathbf{f}_P$ are along the principal normal $\mathbf{n}_P$ to the line in $\mathbf{P}$. Such a defect configuration is allowed if the direction of $\mathbf{n}_P$ is along an actual director, because any director is an axis of continuous rotation symmetry for the N phase. This is in agreement with our remark above, according to which there is a director that is orthogonal to a wedge line in its close vicinity. The density of attached disclinations is vanishing if $\mathbf{\Omega}$ suffers a pure translation along the disclination line.

Continuous defects belong to the identity element of the first homotopy group; this is why their distribution, which is a function of the shape of the line and of the $\mathbf{\Omega}$ field, does not influence the topological invariant, always a for any $|k|=\frac{1}{2}$ disclination line.

A $|k|=1$ disclination line does not require special configuration rules for the director in the near vicinity of the line, because any axis is a 2π rotational symmetry axis. It is then possible to align the director along the line, at the expense of special densities of defects (Kleman, 1973).

Remark. The above description of the curvature of a disclination line in a N phase in terms of defect densities might look overdone; but, at least in what concerns dislocation densities, it is no more so than the description of the strains and stresses in an amorphous medium in terms of defects. There is no difference in nature between the nonvanishing density of dislocations in a nematic and that of an amorphous medium, except that in the first case the dislocations originate on disclinations, and the rules of elastic relaxation differ. In both cases the 3D continuous translational symmetries render the dislocation densities trivial (this is not so in most liquid-crystalline phases, the biaxial nematic N_B being an exception; see below). The disclination densities (continuous rotational symmetries about the directors) are superimposed on the dislocation densities but are independent; it would be interesting, knowing the field of distortions of a N phase, to separate what is due to dislocation densities from what is due to disclination densities.

2. N^* phase

The interplay between continuous dislocations and quantized disclinations in cholesterics has been discussed (Friedel and Kleman, 1969) where this concept was first introduced. There are three types of quantized

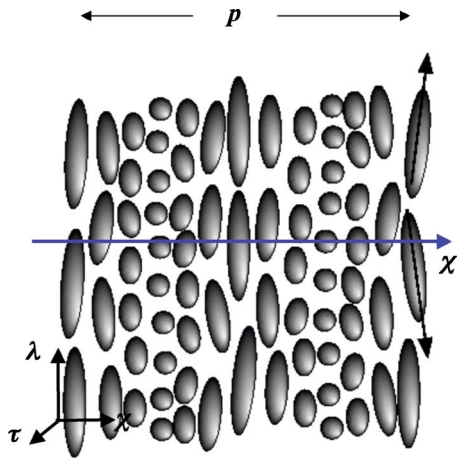

FIG. 19. (Color online) Cholesteric phase N^*. The $\boldsymbol{\lambda}$ and $\boldsymbol{\tau}$ directors indicated on the left side belong to the extreme left molecules. The $\boldsymbol{\chi}$ director is constant throughout. From Kleman and Lavrentovich, 2003, Fig. 2.22, p. 63, with kind permission of Springer Science and Business Media.

rotational symmetries $\boldsymbol{\Omega}$ in a N^* phase, all multiples of the angle π: (i) along the molecular axis, which we denote $\boldsymbol{\lambda}$; (ii) along the helicity axis $\boldsymbol{\chi}$; (iii) along the transverse axis $\boldsymbol{\tau}$ (see Fig. 19). The related Volterra processes yield similar results (similar limitations) to those above for the N phase, since $\boldsymbol{\lambda}$, $\boldsymbol{\chi}$, and $\boldsymbol{\tau}$ are directors; since $\boldsymbol{\lambda}$ is a twofold axis, any direction orthogonal to it, e.g., $\boldsymbol{\chi}$ and $\boldsymbol{\tau}$, is necessarily singular on the core of a Volterra-constructed related disclination, except if the rotation vector is an integer multiple of 4π, as shown by Anderson and Toulouse (1977). Hence, Volterra processes are perfectly defined for $k_\lambda = 2n + \frac{m}{2}$, $n, m \in Z$ (and by an obvious extension for $k_\tau = 2n + \frac{m}{2}$ and $k_\chi = 2n + \frac{m}{2}$). Topologically stable disclinations are classified by the elements of the non-Abelian quaternion group Q_8, whose elements are usually denoted $\{\pm 1, \pm i, \pm j, \pm k\}$ in quaternion notation, or $\{\pm e, \pm i\sigma_1, \pm i\sigma_2, \pm i\sigma_3\}$ in a 2×2 matrix representation, where σ_i's are the Pauli matrices and e is the unit 2×2 matrix. We employ the quaternion notation, which is more appropriate to crystals in curved spaces of constant positive curvature (Coxeter, 1991); see Sec. VI. $\{+1\}$ corresponds to k_λ, k_χ, $k_\tau = 2n$, $\{-1\}$ to k_λ, k_χ, $k_\tau = n$ odd, and $\{\pm i\}$, $\{\pm j\}$, $\{\pm k\}$ to k_λ, k_χ, k_τ half integers, respectively (Mermin, 1979; Kleman *et al.*, 2004).

Employing the Volterra method, we now look for possible attached continuous defects and their role in the flexibility of quantized disclination lines.

a. Attached defects: Continuous dislocations; k_λ, k_χ, and $k_\tau = \pm\frac{1}{2}$ lines

The only possible continuous dislocation Burgers vectors are parallel to the cholesteric planes (orthogonal to the helicity axis $\boldsymbol{\chi}$), which are invariant under any in-plane translation. Consider then a disclination line L, with tangent vector $\mathbf{t}$ at some point $\mathbf{P}$ of L. The associated attached Burgers vectors are along the direction $\boldsymbol{\Omega}\times\mathbf{t}$, according to Eq. (1). Therefore there is no topological obstruction to the flexibility of a line L in a plane perpendicular to $\boldsymbol{\tau}$ if L is a λ disclination, or in a plane perpendicular to $\boldsymbol{\lambda}$ if L is a τ disclination, but no other types of flexibility are allowed for these lines. On the other hand, a χ line could curve in any plane; another way to state this latter result is to notice that a χ disclination line of strength k is also a dislocation of Burgers vector $\mathbf{b} = -kp\boldsymbol{\chi}$, because of the equivalence of a π rotation along the $\boldsymbol{\chi}$ axis with a $\frac{1}{2}p$ translation along the same axis (p is the pitch) [see Friedel and Kleman (1969) and Bouligand and Kleman (1970)].

b. Attached defects: Continuous dispirations; k_χ and $k_\tau = \pm\frac{1}{2}$ twist lines

The other continuous symmetries in a N^* phase are helical rotations $\{\delta\boldsymbol{\Omega}, -p\frac{\delta\Omega}{2\pi}\}$, $\delta\boldsymbol{\Omega} = \delta\Omega\boldsymbol{\chi}$ along the $\boldsymbol{\chi}$ axis, i.e., the combination of a translation and a rotation. The corresponding Volterra defect is a continuous dispiration that combines a dislocation and a disclination. Applying Eq. (1) to the translational part $-p\frac{\delta\Omega}{2\pi}$, the tangent $\mathbf{t}_P$ to the line at $\mathbf{P}$ has to be in the $\{\boldsymbol{\lambda}, \boldsymbol{\tau}\}$ plane (perpendicular to $\boldsymbol{\chi}$). The rotation vector direction $\boldsymbol{\Omega}_P$, which we write $\boldsymbol{\Omega}_P = \Omega\boldsymbol{\varpi}_P$, $|\boldsymbol{\varpi}_P| = 1$, is along $\boldsymbol{\lambda}$ or $\boldsymbol{\tau}$. The vector $\delta\boldsymbol{\varpi} = \boldsymbol{\varpi}_Q - \boldsymbol{\varpi}_P$ [which appears in Eq. (21), where it is denoted $\delta\mathbf{t}$] has to be along $\boldsymbol{\chi}$. We have, after Eq. (21) and assuming that the disclination line strength is $k = \frac{1}{2}$,

$$2\boldsymbol{\varpi}\times\mathbf{t}\,\delta s = -p\frac{\delta\boldsymbol{\Omega}}{2\pi} \quad \text{(dislocation component)},$$

$$2\delta\boldsymbol{\varpi} = \delta\boldsymbol{\Omega} \quad \text{(disclination component)}, \tag{28}$$

and, by elimination of $\delta\boldsymbol{\Omega}$,

$$\frac{d\boldsymbol{\varpi}}{ds} = \frac{2\pi}{p}\mathbf{t}\times\boldsymbol{\varpi}. \tag{29}$$

Equation (29) means that the rotation rate of $\boldsymbol{\Omega}_P$ is $\frac{2\pi}{p}\mathbf{t}_P$. Therefore the rotation rate of the Frenet trihedron attached to the disclination line at $\mathbf{P}$ is

$$\boldsymbol{\omega}_P = \frac{2\pi}{p}\mathbf{t}_P + \frac{1}{\rho(s)}\boldsymbol{\varpi}_P. \tag{30}$$

Because, according to Frenet's formulas, we have $\boldsymbol{\omega} = \tau^{-1}\mathbf{t}_P + \rho^{-1}\mathbf{b}_P$, we infer that the disclination line has a constant torsion $\left(\tau = \frac{p}{2\pi}\right)$, the same for all lines of this type, and that $\boldsymbol{\varpi}_P = \mathbf{b}_P$ is along the binormal of the disclination line. The rotation vector $\boldsymbol{\Omega}_P$ is therefore along the binormal, which is either a $\boldsymbol{\lambda}$ or a $\boldsymbol{\tau}$ direction. Because of Eq. (28) and $\delta\boldsymbol{\Omega}_\mathbf{P} \propto \boldsymbol{\chi}$, it follows that the local $\boldsymbol{\chi}$ axis is along the principal normal $\mathbf{n}_P$, that the rotation vector ($\boldsymbol{\lambda}$ or $\boldsymbol{\tau}$) is along the binormal, and that the tangent to the line is a $\boldsymbol{\tau}$ or $\boldsymbol{\lambda}$ direction. The disclination is of pure twist character. The search for constant torsion curves started with Darboux (1894) and has been the subject of recent investigations, related to the Bäcklund transformation and the classification of surfaces of constant negative curvature [see, e.g., Calini and Ivey (1998)]. Among the solutions, the simplest ones are

those for which $\rho(s)$ is a constant; the curve is then a circular helix with pitch $P=\frac{4\pi^2}{p}\left(\frac{1}{\rho^2}+\frac{4\pi^2}{p^2}\right)^{-1}$ and radius $R=\frac{1}{\rho}\left(\frac{1}{\rho^2}+\frac{4\pi^2}{p^2}\right)^{-1}$. The $\rho=\infty$ limit case is simple and interesting. The disclination line is straight and orthogonal to the $\boldsymbol{\chi}$ axis. Such an object is highly energetic, but can be stabilized by the presence of another straight disclination of opposite sign, parallel to the first one and at a short distance. Continuous dispirations link the two lines in a ribbon. Now, because the set of two disclination lines of opposite signs is equivalent to a dislocation, the ribbon can take any shape, which is comparable to the case discussed by Friedel and Kleman (1969).

As reviewed by Calini and Ivey (1998), there is a considerable variety of closed constant torsion curves with different knot classes. The search for disclinations affecting such shapes in N^* phases remains to be done.

The foregoing analysis of the flexibility of disclinations does not allow for curved lines in the $(\boldsymbol{\lambda},\boldsymbol{\tau})$ plane orthogonal to the $\boldsymbol{\chi}$ axis. But such lines are known to exist, e.g. ellipses belonging to focal conic domains (FCDs), much akin to focal conic domains in Sm*A* liquid crystals (Bouligand, 1972, 1973, 1974). In the limit where the pitch is small compared to the size of the sample, and the size of the FCD is large compared to the pitch that the inner helicity of the N^* layers is a negligible phenomenon, the analysis of these ellipses (and of their conjugate hyperbolas) can be conducted similarly to FCDs in Sm*A* liquid crystals (see below). But in most experimental cases the situation is more delicate, and a thorough investigation is lacking.

Remark 1. The above discussion relates to disclinations of strength $|k|=\frac{1}{2}$, of homotopy classes $\{\pm i\}$, $\{\pm j\}$, or $\{\pm k\}$. The case of $|k|=1$ defects (homotopy class $\{-1\}$) requires a different approach, since Eq. (1) is no longer valid, and we have to treat the $|k|=1$ defect as a sum of two $|k|=\frac{1}{2}$ defects. There is no objection in principle to uniting two disclinations of the same strength $\frac{1}{2}$ along the same line, making then a disclination of unit strength. For instance, in the constant torsion case, such a process of adding two $|k|=\frac{1}{2}$ defects is a way of canceling the singularity at the core, if the rotation vector is along the $\boldsymbol{\tau}$ director (the $\boldsymbol{\lambda}$ director is then along the line); however, the singularity of the order parameter itself, which consists of the three-director trihedron, is not canceled. One can infer that, in the set of defects investigated (Sec. IV.A.2), the twist line $|k|=1$ is favored.

A situation where a nonsingular defect of seemingly $|k|=1$ strength cannot be split into two $|k|=\frac{1}{2}$ defects has been discussed by Bouligand *et al.* (1978), but in fact it relates to nonsingular topological configurations, in the sense of Michel (1980), classified by the Hopf index for the director field, not line defects.

Remark 2. The biaxial nematic phase ($N_{\mathbf{B}}$) has the same topological classification of disclinations as the N^* phase (Toulouse, 1977a; Volovik and Mineev, 1977) but the symmetry group is different. $N_{\mathbf{B}}$ is invariant under any translation (i.e., belonging to E^3) but there are no continuous rotation symmetries. Hence, the only possible way to curve a $N_{\mathbf{B}}$ line is by attaching continuous dislocations, in strong contrast with N. This is an example where the Volterra process appears to give a more detailed view of the defect conformation than the topological theory.

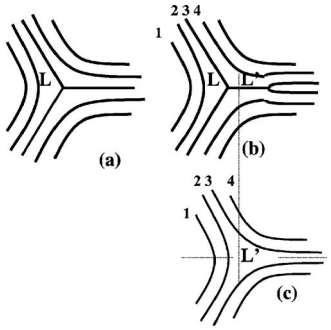

FIG. 20. The disclination located at (a), (b) L is displaced to (c) L' by the absorption of a dislocation of Burgers vector unity ($b=1$, $LL'=1/2$). The dislocation visible in (b) has disappeared in (c) the process.

B. Sm*A* phase

1. Wedge disclinations

Figure 20 shows a $k=-\frac{1}{2}$ wedge line in a Sm phase,[5] displaced from L to L' by the absorption of an edge dislocation $|\mathbf{b}|=d_0$ whose Burgers vector is twice as large as this displacement, $\frac{1}{2}d_0$. The nature of the core has changed. The absorption of a second dislocation equal to the first one, along the same route, would displace the line by the same amount, the total effect of the two displacements being equal to the repeat distance d_0 of the layers, and L being moved to a position L'' (not drawn in Fig. 20), where the original core is retrieved. The analogy with the displacement of a wedge continuous line described in Sec. II.B is striking; the configuration of L'', compared to L, displays a full new layer equivalent to a dislocation of Burgers vector $|\mathbf{b}|=2d_0$ for a displacement $\mathbf{d}_0$ of the disclination line, as obtained by applying Eq. (1). The inverse displacement requires the appearance of a dislocation line on the core, which relaxes and eventually disappears far away from the line.[6]

Frank (1969) was the first to point out that the displacement of a disclination in a liquid crystal (he used a cholesteric phase N^*) involves the emission or absorption of dislocations, which are quantized in the case he considered.

[5]The same picture is valid for a 3D crystal; see the 2D cut along a lattice plane (Fig. 11).

[6]It is often taken for granted that dislocations always nucleate by pairs of opposite signs. Here we have a situation where a dislocation line is nucleated with no partner of the opposite sign. We believe that this possibility is relevant in some important cases. For example, one might in this way nucleate screw dislocations all of the same sign at the Sm*A*→TGBA transition.

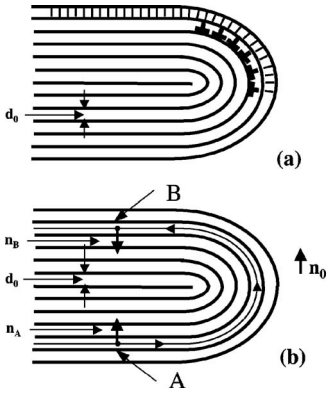

FIG. 21. The $k=1/2$ wedge SmA disclination: (a) Nye's infinitesimal dislocations as agents of layer curvature; (b) calculating the sum total of the infinitesimal dislocations belonging to one layer.

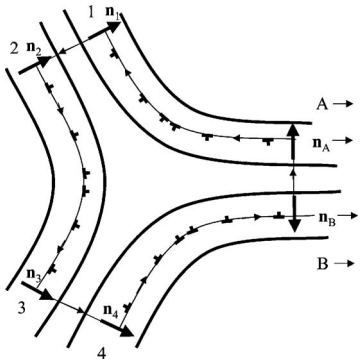

FIG. 22. The $k=-1/2$ wedge SmA disclination; A, $\mathbf{n_A}$ and B, $\mathbf{n_B}$ are at infinity along the asymptotic directions of the disclination configuration. The edge dislocation density vanishes at infinity.

2. Nye's relaxation dislocations

There is a feature not apparent in the analysis of constitutive and relaxation dislocations carried out in Sec. II, namely, the possibility of continuous relaxation dislocations that are directly related to the curvature of the layers, and not attached to the line. Figure 21(a) shows the case $k=\frac{1}{2}$. We now turn our attention to one of the layers inside the disclination wedge. As a liquid layer, its inner group of symmetry is E^2; it thereby admits continuous dislocations whose Burgers vectors are parallel to the layer. Those dislocations determine the curvature $1/\rho$ of the layers, with the relation between the dislocation density and curvature given by $db/ds=d_0/\rho$, where d_0 is the layer thickness. This relation was first established by Nye (1953) for solid crystals (the curvature of the lattice planes is a function of the dislocation densities); see Appendix A.

Let $\mathbf{t}$ be a unit vector along the tangent to the layer in a section perpendicular to the wedge line, and we traverse a path AB in this section, everywhere tangent to the layer along $\mathbf{t}$, in the part of the layer which is curved [see Fig. 21(b)]. The total Burgers vector measured along the path from $\mathbf{A}$ to $\mathbf{B}$ ($\mathbf{A}$, $\mathbf{B}$ are any points on the upper and lower horizontal parts of the path) is

$$\mathbf{b_{AB}} = \int_{\mathbf{A}}^{\mathbf{B}} \mathbf{t}\frac{db}{ds}ds = d_0\int_{\mathbf{A}}^{\mathbf{B}} \frac{\mathbf{t}}{\rho}ds$$
$$= -d_0\int_{\mathbf{A}}^{\mathbf{B}} \frac{d\mathbf{n}}{ds}ds = d_0(\mathbf{n_A}-\mathbf{n_B}), \quad (31)$$

i.e., $\mathbf{b_{AB}}=2d_0\mathbf{n}_0$, where $\mathbf{n}_0$ is the normal to the layers far from the disclination [we have employed one of Frenet's formulas to transform the second integral into the third, namely, $d\mathbf{n}/ds=\mathbf{b}/\tau-\mathbf{t}/\rho$, where $\tau(s)$ is the torsion and $\mathbf{b}(s)$ is the binormal at a point s on the path].

Observe that $\mathbf{b_{AB}}$ is of a sign opposite to that of the Burgers vector of the constitutive dislocations of the disclination line; observe further that the result does not depend on the precise shape of the layer, whose possible strain at finite distance does not invalidate the result of Eq. (31), as long as the layers are parallel and planar far away from the disclination.

Equation (31) establishes that the set of infinitesimal dislocations attending a $k=\frac{1}{2}$ line relaxes the elastic stresses due to the constitutive dislocations, in the geometry considered. This is also true for a $k=-\frac{1}{2}$ line; application of the method of Eq. (31) to Fig. 22 shows that the equivalent Burgers vector is $\mathbf{b_{AB}}=2d_0\mathbf{n}_0$ ($=2d_0\mathbf{n_A}$).

Any layer curvature can be analyzed in terms of Nye's dislocations (see Sec. V for the case of focal conic domains in SmA phases).

The example just developed evidences the main features of the relaxation processes relating to Nye's dislocations: (i) the relaxation of the elastic stresses carried by a disclination that results from a pure (nonextended) Volterra process is obtained by the glide of the Sm layers past each other, which accumulates infinitesimal dislocations; (ii) the accumulation of these dislocations along the layers is equivalent to a set of infinitesimal disclinations attached to the master disclination, analogous to those discussed in Sec. II.G (see a similar discussion relating to focal conics, which are special types of disclinations, in Sec. V)—it is also equivalent to a piling up of subboundaries; (iii) the stresses resulting from the fact that the molecules inside the layers are compressed at one end and stretched at the other introduce an elastic constant at the origin of the Frank-Oseen splay constant for smectics; (iv) finally, the Nye dislocation geometry screens the long-distance stresses carried by the master disclination, which considerably reduces its line tension.

In all cases, the plastic relaxation at the end of a generalized Volterra process can be obtained by the production of generalized Nye dislocations compatible with the structure of the matter under consideration.

3. Topological stability and Volterra process compared in SmA phases: Twist disclinations

How do the topological stability approach and the Volterra process approach compare in SmA phases? The

elements of the first homotopy group $\Pi_1(V)$ classify line defects (dislocations and disclinations). For a SmA phase, $\Pi_1(V_{SmA}) \sim Z \square Z_2$. Let (n,α) denote an element of $Z \square Z_2$, with $n \in Z$ and $\alpha \in Z_2 (=\{e,a\})$. With these notations, the identity (null) defect is denoted $(0,e)$, a dislocation is denoted (n,e), where n stands for the Burgers vector, and a $|\Omega| = \pi$ disclination is denoted $(0,a)$, irrespective of the sign of Ω; $a^2 = e$.

Clearly enough, (n,a) is a $|\Omega| = \pi$ disclination that has absorbed a dislocation (n,e), i.e., that has suffered a translation nd_0. Therefore in Fig. 20, if L is represented by the homotopy class $(0,a)$ [which we write $L \mapsto (0,a)$], then $L' \mapsto (1,e)(0,a) = (1,a)$. Notice that the nature of the core has changed. The absorption of another dislocation of the same sign yields a disclination $L'' \mapsto (2,e) \times (0,a) = (2,a)$ (not represented Fig. 20), with the same core as L. The product of two disclinations yield the identity $(0,e)$. All these operations are summarized in the multiplication rules

$$(n,\alpha)(m,\beta) = (n + \alpha(m), \alpha\beta),$$

$$e(m) = m, a(m) = -m. \tag{32}$$

Observe that any disclination, whatever the nature of its core, can be chosen arbitrarily as the origin disclination $(0,a)$.

With the above analysis, L, L', and L'' are given three different topological invariants. But L and L'' can also be gathered under the same heading in the frame of the topological theory; they belong indeed to the same conjugacy class of $\Pi_1(V_{SmA})$—see Appendix B—and this is enough to consider them as the same topologically stable defect, according to the general topological theory (Michel, 1980; Kleman, 1989). Consider the two equalities

$$(2,a) = (0,a)(2,e),$$

$$(2,a) = (-1,e)(0,a)(1,e). \tag{33}$$

The first equality means that L'' is obtained by adding the dislocation $L_{2d} \mapsto (2,e)$ to L. In the Volterra sense, it is an addition; in the topological stability theory sense, it is the product of two homotopy classes $(0,a)$ and $(2,e)$. The second equality, which expresses that $(0,a)$ and $(2,a)$ are conjugate in $\Pi_1(V_{SmA})$, has a simple physical image: it expresses the effect of a complete circumnavigation of the disclination $L \mapsto (0,a)$ about a dislocation $L_d \mapsto (1,e)$. Such an operation cannot change the nature of the circumnavigating defect, although its homotopy class is modified. We refer the reader to Mermin (1979) for a pedagogical discussion and an illustration of this property.

In terms of Volterra invariants, L, L'', and all disclinations of the same conjugacy class carry rotations about twofold axes located in planes between layers; L' and all disclinations of the same conjugacy class carry rotations about twofold axes located in the middle planes of layers.

C. Nature of the defects attached to a quantized disclination

Taking stock of the specific examples discussed above, we now derive some general properties relating to attached defects. Various cases arise as follows.

1. Continuous attached defects (dislocations, disclinations, dispirations) and kinks

a. Topological stability

Continuous defect densities belong to the identity homotopy class, and therefore they do not modify the homotopy class of the master disclination L all along it. Or, stated otherwise, they are not visible when mapping a closed loop of the deformed medium into the order-parameter space V.

b. Volterra process

Because the existence of continuous defects has to comply, in an ordered medium, with the existence of broken symmetries, not all continuous defects are realizable, and thereby limits are put on the possible realizations of master disclinations, in particular their shapes (in dynamic terms, their flexibility). Equation (21), which derives from Eq. (1) and has been established for an isotropic uniform medium, is still valid it we take these limits into account.

2. Quantized attached defects of the first type: Full kinks

a. Topological stability

Inspired by the SmA example, we first refer to a case where $L \mapsto \{a\}$ is transformed into a disclination $L'' \mapsto \{a''\}$ belonging to the same conjugacy class $\{a''\} = \{u\}\{a\}\{u^{-1}\}$ of the first homotopy group $\Pi_1(V)$ as L, by the absorption or emission of a dislocation $\{v\}$. This dislocation hits the master disclination at some node, where we have the Kirchhoff relation, which is written in topological theory as $\{a''\} = \{a\}\{v\}$; this relation also reads

$$\{v\} = \{a^{-1}\}\{a''\} = \{a^{-1}\}\{u\}\{a\}\{u^{-1}\} \tag{34}$$

and therefore the attached defect is a commutator of $\Pi_1(V)$. The result is not restricted to attached dislocations; it is valid for a defect $\{v\}$ of any type. We now establish a reciprocity theorem, which extends the concept of the node, which is as yet not understood.

Recall that the commutators of a group G generate an invariant subgroup $D[G]$, also called the derived group. Not all elements of the derived group are commutators, but all are products of commutators. From the point of view of the physics of defects, it is important to observe that D contains entire conjugacy classes of $\Pi_1(V)$, and that the cosets of D in $\Pi_1(V)$ are also composed of entire conjugacy classes (Kleman, 1977; Trebin, 1984). As an example, in a SmA liquid crystal, dislocations having the same Burgers vector parity all belong to the same coset of $\Pi_1(V_{SmA})/D$; for the sake of clarity, consider only even dislocations: the two homotopy classes $(2r,e)$ and $(-2r,e)$, $r \neq 0$, form an entire class of conjugacy and they

belong to the same coset as the homotopy class $(0,e)$—the null defect, which constitutes by itself a full conjugacy class. This very fact means that the even dislocations are equivalent to the null dislocation $(0,e)$, in the following sense. It is possible to split the even dislocation $(2r,e)$ into two equal dislocations (r,e); let one of them circumnavigate about an (m,a) disclination, bringing it to the conjugate state $(-m,a)(r,e)(m,a)=(-r,e)$, while the other one stays in place. It is then possible for $(2r,e)$ to self-annihilate by letting the fixed and the returned dislocations mutually annihilate, i.e., generate a defect of homotopy class $(0,e)$. Similarly, any odd dislocation $(2r+1,e)$ is equivalent to $(1,e)$; but odd dislocations are not commutators.

One can therefore establish the following reciprocity theorem: if the attached defect $\{v\}$ is a commutator, then $\{a\}$ and $\{a''\}$ are either in the same conjugacy class, or belong to two conjugacy classes belonging to the same coset of $\Pi_1(V)/D$.

This is also true, by an easy extension, for any element of D, not only commutators. We can thereby state in all generality that any defect whose homotopy class belongs to the derived group $D[\Pi_1(V)]$ is eligible as an attached defect, and separates the master disclination into segments whose homotopy classes belong to the same coset of $\Pi_1(V)/D$.

We name such a defect an attached defect of the first type.

b. Volterra process

Insofar as defects of the first type are commutators, they can terminate on a singular point, since they are equivalent to the identity homotopy class, and this singular point can be the node where they meet the master disclination. This is the main result one can reach from the analysis of topological properties, but one cannot do more, because the topological theory does not properly separate dislocations and disclinations. In other words, the topological analysis does not say anything about the shape (the flexibility) of the master line, even though there is no doubt that the attachments are the tools for its changes of shape and the relaxation of the stresses.

Consider the geometry of a kink on a wedge disclination (Fig. 23); this geometry differs somewhat from that of Fig. 4 for a continuous disclination. According to the above discussion, the same dislocations that have been absorbed by the wedge segment L^-, say, are still outside the wedge segment L^+; we still have relaxation dislocations, terminating on the kink, an allowed process insofar as these dislocations are of the first type.

Friedel's relation [Eq. (1)] is established for an *a priori* Volterra description of line defects. Assume that, in Fig. 23, L^+ and L^- are $k=\pm\frac{1}{2}$ wedge disclination segments in a SmA phase, as in Fig. 20. According to Friedel's relation, as which can be written as, with $\mathbf{\Omega}=\pm\pi\mathbf{t}$,

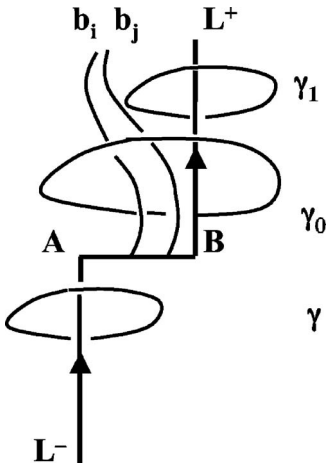

FIG. 23. L is a quantized disclination, AB a kink. The relaxation dislocations no longer cross the master line.

$$\sum_i \mathbf{b}_i = \pm 2\mathbf{t}\times\mathbf{AB}, \tag{35}$$

the relaxation dislocation Burgers vectors are perpendicular to the figure plane. If we assume that we are under the conditions of using this relation in a SmA liquid crystal, the lines are drawn in a medium that is not yet deformed by the Volterra process, and the layers are parallel to the L^+ and L^- lines. We do not lose generality by assuming further that the layers are perpendicular to the plane of the figure; **AB** is along the layer normal. Therefore the Burgers vectors $\mathbf{b}_i$ are parallel to the layers; the related dislocations are continuous. The layers in the transition region between L^+ and L^- suffer extra curvatures, which represent these dislocations. This is certainly not a small-energy geometry. But the geometry of Fig. 23 can be understood differently. If the relaxation dislocations are quantized, there should be layers parallel to the plane of the figure in the **AB** region (perpendicular to the Burgers vector), whereas **AB** is along the normal to the layers. This is possible only if we consider a medium already deformed by disclinations. Friedel's relation still works for **AB** joining a segment along L to a segment along L'; for example, in Fig. 20. It therefore works when applied locally to the tangent undistorted medium, on either sides of the disclination. We give an example in a SmA phase in Sec. V. We use the term full kinks for kinks that separate master disclination segments belonging to the same coset of $\Pi_1(V)/D$.

3. Quantized attached defects of the second type: Partial kinks

The discussion of the SmA case has shown that it is perfectly licit to consider a master line made of two wedge segments L and L' that do not belong to the same coset of $\Pi_1(V)/D$. The dislocation $\{\nu\}$ that hits the (now partial) kink is not a commutator, and the relation $\{a'\}=\{a\}\{\nu\}$ is no longer a trivial relation. In the above case it was possible, at least in a thought experiment, to abolish the node by smoothly turning the two segments to the same homotopy class—simultaneously abolishing

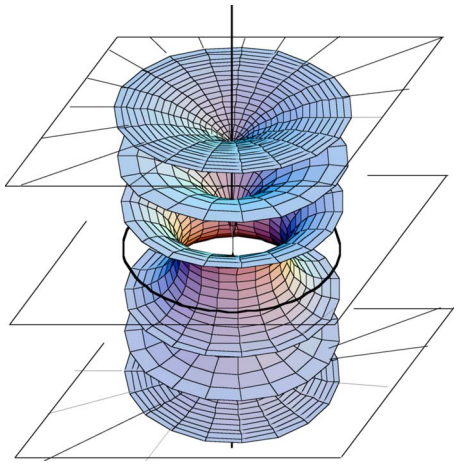

FIG. 24. (Color online) Toric FCD.

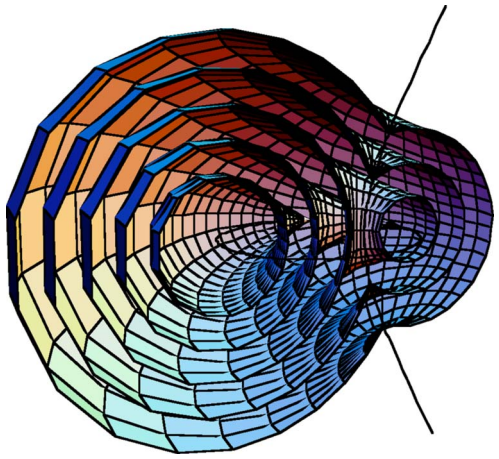

FIG. 25. (Color online) FCD with positive and negative Gaussian curvature surface elements From Kleman and Lavrentovich, 2003, Fig. 10.5.c, p. 348, with kind permission of Springer Science and Business Media.

the full kink. This is now forbidden. On the other hand, the attached defect exists only on one side of the master line, because $\{a'\}=\{a\}\{\nu\}$ is now the topological stability (TS) expression of a true Kirchhoff relation for three defects meeting at a node. In the Volterra process language, $\{a'\}=\{a\}\{\nu\}$ is nothing other than Eq. (35).

V. FOCAL CONICS IN SMECTIC *A* PHASES AS QUANTIZED DISCLINATIONS

The most remarkable defects in Sm*A* phases are focal conic domains (FCDs), whose geometrical properties were first investigated by Friedel and Grandjean (1910) and Friedel (1922). A FCD consists of a pair of confocal conics (an ellipse E and a hyperbola H), which are the focal lines of the set of normals to a family of parallel smectic layers folded into Dupin cyclides [Hilbert and Cohn-Vossen (1964)]. For a recent account of the physics behind this geometry, see Kleman and Lavrentovich (2003) and Kleman *et al.* (2004); an essential property of E and H is that they are disclination lines.

Consider the simple case where E degenerates into a circle C and thereby its conjugate conic C' is a straight line orthogonal to the plane of C, passing through its center. The Dupin cyclides are then nested tori (Fig. 24). They are restricted in this figure to the cyclides with a Gaussian curvature of negative sign, with planar continuations outside. This is the most frequent, if not the only, empirical occurrence of toric domains.

It is apparent that C and C' are both wedge disclination lines, C of strength $k=\frac{1}{2}$, C' of strength $k=1$. According to the analysis in Sec. II.G, there are no attached dislocations, only attached disclinations, whose density can be written as

$$\delta\mathbf{f}=\frac{2}{R}\mathbf{n}\,\delta s=2\mathbf{n}\,\delta\vartheta. \tag{36}$$

The Nye's edge dislocations that follow the latitude lines of the tori are of the type (call them the first type) that attends such disclinations; their (infinitesimal) Burgers vectors $\delta\mathbf{b}_{\mathrm{rot}}$ are along the meridian lines; they introduce extra matter that curves the C disclination. On the other hand, the Nye's edge dislocations (of the second type) that follow the meridian lines of the tori, whose (infinitesimal) Burgers vectors $\delta\mathbf{b}_{\mathrm{tr}}$ are along the latitude lines, relax the quantized dislocations that attend the C wedge disclination, after the manner already discussed for a straight $k=\frac{1}{2}$ line (Fig. 21). Note that the Burgers vector $\delta\mathbf{b}_{\mathrm{tr}}$ is variable along a dislocation of the second type, since the local frame of reference is continuously rotated by the dislocations of the first type.

All these results extend to more general FCDs. Figure 25 represents such a FCD with positive and negative Gaussian curvature surface elements.

In a local frame of reference where the one and two axes are along the lines of curvature of the Dupin cyclide, the three axis along the normal, the dislocation density tensor (defined in Appendix A) has components

$$\alpha_{11}=0,\quad \alpha_{12}=\frac{1}{R_2},\quad \alpha_{13}=0,$$

$$\alpha_{21}=-\frac{1}{R_1},\quad \alpha_{22}=0,\quad \alpha_{23}=0,$$

$$\alpha_{31}=\frac{1}{\rho_{g1}},\quad \alpha_{32}=\frac{1}{\rho_{g2}},\quad \alpha_{33}=0.$$

where $1/\rho_{g1}$ and $1/\rho_{g2}$ are the geodesic curvatures of the curvature lines. The geodesic curvatures vanish in the toric case, since then the lines of curvature are also geodesic lines. Recall that α_{ij} measures a dislocation content; the integral

$$\int\int_{\gamma}\alpha_{ij}dS_i$$

over an area bound by a loop γ is the j component of the Burgers vector of dislocations going through this area along the i direction. The dislocation tensor, being a ten-

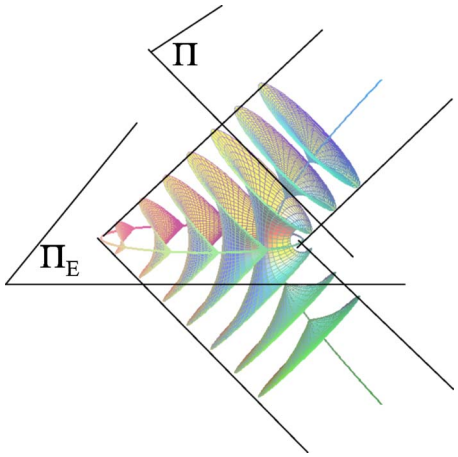

FIG. 26. (Color online) Generic FCD with negative Gaussian curvature layers; see text.

sor, is invariant under a change of coordinates; the choice of the curvature lines as coordinate lines has a simple physical interpretation in terms of $\delta\mathbf{b}_{\rm tr}$ and $\delta\mathbf{b}_{\rm rot}$, for the components α_{12} and α_{21}. The extra dislocation densities α_{31} and α_{32} also have Burgers vectors parallel to the smectic layers, as they must, for the symmetry reasons already mentioned. They correspond to edge lines along the normals to the layers, and contribute to the stability of the shape of the conics and their relaxation.

As observed (Kleman *et al.*, 2004), FCDs are restricted to the negative Gaussian curvature parts $\sigma_1\sigma_2<0$ of the cyclides (Fig. 26). The FCD is therefore confined inside a double cylinder lying on the ellipse, whose generatrices are parallel to the asymptotes of the hyperbola. Any layer inside this double cylinder is bordered by a curvature line of the cyclides, i.e., a circle (Fig. 26). The plane Π containing the circle is tangent to the cyclide, so that the outside extension of the layer can be along Π, without any cusp. Π is perpendicular to one or the other of the asymptotic directions of the hyperbola; thus the set of all planes Π forms two families of parallel planes that eventually cross on the plane of the ellipse. By limiting the corresponding material layers to the half space above or below the ellipse plane Π_E, Π_E appears as a tilt grain boundary of misorientation $\omega=2\sin^{-1}e$, where e is the ellipse eccentricity. E itself is a $k=\frac{1}{2}$ disclination line to which are attached the constitutive dislocations of the tilt grain boundary; see Appendix C for a detailed investigation of its characteristics.

VI. GEOMETRICAL FRUSTRATION: ROLE OF DISCLINATIONS

A. Geometrical frustration; A short overview

The concept of frustration covers a number of inhomogeneous structures which are all describable in terms of defects, in fact disclinations; see Kleman (1989) for a review. The word was introduced by Toulouse (1977b) in the frame of the theory of antiferromagnetic systems, where there exist closed paths of atoms with nearest-neighbor exchange interactions that cannot be satisfied simultaneously.

1. Unfrustrated domains separated by defects

By geometrical frustration (Kleman, 1985a, 1987), we mean an extension of the concept of frustration such that (i) it connotes systems where the short-range interactions are so dominant that they completely determine the local configuration, and (ii) it is possible to describe these interactions in geometrical terms—in a sense geometrical frustration is an extension of the notion of steric hindrance. The concept is therefore of interest when the local configuration is incompatible with long-range Euclidean ordering, i.e., is noncrystallographic in the usual sense of this term. The frustrated medium is thereby divided into small, unfrustrated, domains, of size ξ, say, separated by defect regions where the short-range order is broken.

In three dimensions, it is fruitful to introduce a crystal template where the unfrustrated domains spread without obstruction, if such a description is feasible. Such templates, where this local order extends homogeneously without distortion, are necessarily curved, non-Euclidean, with Riemannian habit spaces of constant curvature. The decurving of the template into an Euclidean medium employs disclinations of these curved crystals; they delimit the unfrustrated domains of the actual medium. Geometrical frustration connotes the existence of a particular type of incompatibility resulting from the different interactions in competition. Disorder at the scale ξ does not prevent the existence at larger scales of correlations between the unfrustrated domains; the resulting frustrated medium can be either a crystal with broken translations—if weak long-range interactions take over at some scale—or a medium truly disordered at all scales greater than ξ—if long-range interactions are very small. Very similar but simpler approaches in one or two dimensions were developed earlier to describe approximate epitaxy and surface reconstruction of crystals, helical magnetic order, and charge- or spin-density waves [cf. Friedel (1977b) for an introduction]. Chemists have also talked in the same spirit since the 1930s of nonalternating electronic structures of molecules and solids.

We first present a short overview of frustrated media with an emphasis on the presence of disclinations. In most of the examples below, the three-dimensional sphere S^3 is employed as a template habit space.

2. Covalent glasses, disclinations

For covalent glasses, frustration originates in the constancy of the coordination number z, which can be incompatible with certain ring configurations. For example, five- and seven-membered rings do not generate Euclidean order. A large literature exists on the subject, starting with the model of Zachariasen (1932) for continuous random networks; see Mosseri and Sadoc (1990) for covalent frustration models.

As pointed out by Rivier (1987), the underlying geometrical structure of a covalently bound material is a graph with a constant coordination at each node, except for dangling bonds and possible double bonds. There is no reason why covalent bonds should form polyhedra. A stacking of polyhedra is a particular graph. In that latter case, Rivier's theorem, which states that "odd-membered rings are not found in isolation, but are threaded through by uninterrupted lines which form closed loops or terminate on the boundaries of the specimen" (Rivier, 1979), is quite useful. But it applies also to nonpolyhedral structures, as soon as rings are recognizable. Rivier's lines are disclinations; see also Toulouse (1977b).

3. Double-twisted configurations of liquid crystal directors and polymers, disclinations

The most studied phenomenon of frustration in liquid crystals is the double-twist molecular arrangement of short molecules met in blue phases, and whose presence has been suggested in cholesterics of biological origin (DNA, etc.); see Livolant and Bouligand (1986); Livolant (1987); and Giraud-Guille (1988). The chromosome of dinoflagellates (Livolant and Bouligand, 1980) also displays a double-twisted geometry of DNA molecules of a type somewhat different from the type met in blue phases (Friedel, 1984; Kleman, 1985b). The idea has also been presented that the double twist is present in amorphous molten polymers (Kleman, 1985a).

Consider a liquid crystal of chiral molecules. If the director is an axis of cylindrical symmetry, all directions orthogonal to any director can act effectively as axes of helicity—in a classical N^* phase, this symmetry is broken and there is only one axis of helicity. The local unfrustrated arrangement can be described as in Fig. 27, where the integral lines of the director are helices of chirality opposite to the chirality of the rotation of the director about the radii. We have $n_r=0$, $n_\vartheta=\sin\psi(r)$, $n_z=\cos\psi(r)$, with $\psi(0)=0$. The molecules rotate with the inverse pitch

$$q(r)=\frac{2\pi}{p}=-\mathbf{n}\cdot\boldsymbol{\nabla}\times\mathbf{n}=\frac{d\psi}{dr}+\frac{\sin 2\psi}{2r},$$

which is of the same order of magnitude as the inverse pitch of the cholesteric phase. Double twist is entirely satisfied only for the director along the z axis ($r=0$); at a distance $r=p/4$ from the z axis, the director has rotated by $\pi/2$ along the r axis and is now perpendicular to the z axis; its vicinity is no longer double twisted; frustration sets in.

Blue phases are made of elements of double-twisted cylinders of matter assembled in space. Three cylinders can stack along three orthogonal directions; the region of highest frustration, in between, may show up a singularity of the director field, a $k=-\frac{1}{2}$ disclination. This local arrangement has been found in several cubic symmetries showing a 3D disclination segment network (Meiboom *et al.*, 1983; Barbet-Massin *et al.*, 1984). The blue fog is amorphous, and disclination lines are seemingly random; it has also been suggested that the blue fog is icosahedral, as in quasicrystals (Hornreich and Shtrikhman, 1986; Rokhsar and Sethna, 1986) achieving thereby another type of frustration.

FIG. 27. Double-twist configuration. From Kleman, Lavrentovich, and Nastishin, 2005, Dislocations and Disclinations in Mesomorphic Phases, Fig. 54, p. 246; copyright Elsevier.

Double twist can be thought of as resulting from a competition between a tendency to dense packing, ensuring parallel alignment of the integral lines, and a tendency to chirality. But a geometry with equidistant helices, which would result from such a competition (Kleman, 1985a), is not homogeneous in Euclidean space.

The template proposed by Sethna (1985) in an S^3 curved space ensures a homogeneous unfrustrated double twist; we denote it by {dtw/S^3}. The director is along a family of great circles of the habit three-sphere, all those great circles being equidistant and twisted, and parallel in the sense of spherical geometry. This is described in Appendix D (the Hopf fibration) and its defects are studied in Sec. VII.C; see also Dubois-Violette and Pansu (1988).

4. Tetrahedral and icosahedral local orders, disclinations

For amorphous metals and Frank and Kasper phases, the origin of frustration is the tendency toward dense packing of equal or quasiequal spheres, representing atoms.

a. Frank and Kasper phases

In complex metallic alloy structures, particularly those of transition metals, it occurs frequently that the struc-

ture is entirely determined by the requirements for sphere packing, i.e., atoms form tetrahedral clusters, and coordination polyhedra are triangulated.

Frank and Kasper (1958, 1959) made a thorough topological and geometrical study of crystalline structures submitted to such constraints, showing that—if one admits that the number of neighbors Z_S of an atom on the coordination polyhedra to which it belongs is either $Z_S=5$ or 6—there are only four types of coordination polyhedra, with $Z=12$, 14, 15, and 16. Frank and Kasper distinguish the sites $Z=12$ as *minor* sites, and the other ones as *major* sites. The edges which join neighboring major sites form a *skeleton*; sites of $Z=14$, 15, or 16 are meeting points of two, three, or four *bones*. This skeleton is much simpler to study than the structure as a whole. The description of the Frank and Kasper phases in terms of a skeleton of bones (i.e., a network of line defects) is contemporary to the development of disclination in liquid crystals [due to Frank (1958)], but it was only later that the topological nature of these defects as true disclinations was recognized (Nelson, 1983a).

The Frank and Kasper networks constitute a remarkable example where the main characteristics of geometrical frustration show up; frustrated atoms are along lines which structure a sea of unfrustrated atoms $Z=12$, and there is a typical distance between lines which scales with the lattice parameter. The existence of the skeleton of major sites is not dependent on the existence of a periodic lattice, and the only necessary hypothesis is that the medium be polytetrahedral.

b. Amorphous metals

Icosahedral order ($Z=12$) is met in Frank and Kasper phases, but also in amorphous metals, undercooled atomic systems (Frank, 1950a; Bernal, 1959, 1964), and quasicrystals (Schechtman *et al.*, 1984). It is also valid for small clusters less than a few hundreds of atoms; for metals and rare gases, see Friedel (1977a, 1984).

Bernal has used a polyhedral approach to analyze handmade systems of equal spheres, and has shown that a large majority of the polyhedra (approximately 86%) are tetrahedra; hence the predominance of local icosahedral order. Furthermore, these tetrahedra arrange frequently into *pseudonuclei* that are aggregates of face-sharing tetrahedra, two by two, and tend to build a connected lattice in the whole structure, wrapping themselves around the larger holes (i.e., rather low-density polyhedra with $V=8$, 9, or 10 vertices). Of course the tetrahedra cannot fill the whole three-dimensional space; however, since they can extend freely along one direction, one notices a large number of three-stranded spirals, right- or left-handed, formed by a one-dimensional array of regular tetrahedra. Their local density is large. They are reminiscent of the twisted great circles of S^3, and therefore fit locally into the curved-space crystal representative of the local order. The pseudonuclei are the regions of less frustrated order.

Numerous analyses of atomic packings have followed Bernal's pioneering work; we refer the interested reader to Zallen's (1979) review on dense random packings.

c. The {3, 3, 5} template

This is an example of a crystalline structure in a curved space. There are no icosahedral Euclidean crystals, but icosahedral order is compatible with a space of constant curvature, namely, the three-sphere S^3, which can be tiled with regular tetrahedra, 20 of them meeting at a vertex, i.e., generating an icosahedron. This structure is known, after Coxeter (1973), as the {3, 3, 5} polytope: elementary facets have three edges, and hence are equilateral triangles; three facets meet at a vertex, and hence elementary cells are regular tetrahedra; five cells share a common edge, and hence an edge is a fivefold axis.

This polytope has $N_0=120$ vertices, $N_1=720$ edges, $N_2=1200$ faces, and $N_3=600$ cells. The passage from this template to a disordered system, i.e., the decurving of {3, 3, 5} and its infinite extension to a Euclidean space, occurs through the introduction in the perfect {3, 3, 5} crystal (Kleman and Sadoc, 1979; Kleman, 1989) of disclinations of negative strength—i.e., which introduce extra matter—forming a 3D network in physical space, like the Frank and Kasper network. For a description of quasicrystals in terms of frustration, see Kleman and Ripamonti (1988) and Kleman (1989, 1990).

B. The decurving process

1. Rolling without glide and disclinations

We now focus our attention on the transformation of a curved template into an actual flat medium, under the constraint that the local order of the template is conserved. An isometric mapping continuous over the whole medium is not possible, because it would require that the Gaussian curvatures be equal at corresponding points (Darboux, 1894; Hilbert and Cohn-Vossen, 1964; Singer and Thorpe, 1996).

However, isometric mapping can be achieved locally, by parallel transport along a line L, according to Cartan (1963). Letting M (S^3, say) roll without glide upon E^3, along any path $L\subset S^3$, lengths and angles along the path are conserved at corresponding points in E^3. If L is a geodesic of S^3, it maps along a straight line L in E^3: this is the so-called Levi-Cività connection. In general, such a mapping transforms a closed line $L\subset M$ into an open line in E^3. The closure failure can be described as a disclination.

Consider a material cone: the curvature is concentrated at the apex, a useful feature here, for it maps isometrically on the plane as a whole, except at the apex, which becomes the vertex of an empty wedge bordered by two generatrices. This is clearly the picture of the Volterra process for a disclination, whose angle, called here the *deficit angle*, is a measure of the concentrated curvature. In order to complete the mapping, it suffices to fill the void with perfect matter. The final object does not carry stresses, if the material cone is amorphous; but

it cannot be so if the medium is ordered, since then disclinations are quantized.

We show next that the decurving process yields generically two sets of disclinations: (i) those resulting from the mapping of M onto the Euclidean space E^3; these disclinations are of negative (respectively positive) strength if M has positive (respectively negative) Gaussian curvature; (ii) those resulting from an elastic relaxation (disclinations of a sign opposite to the former ones).

The relationship between disclination lines and curvature has been emphasized long ago by Kondo (1955–1967) and Bilby (1960). Their approach is opposite to the present one; Kondo and Bilby start from E^3, which they consider as the habit space of the physical crystal, and map it on a space that is curved due to the presence of disclinations in E^3. In contrast, the physics of the disordered system, which lives in E^3, is contained in its curved representation.

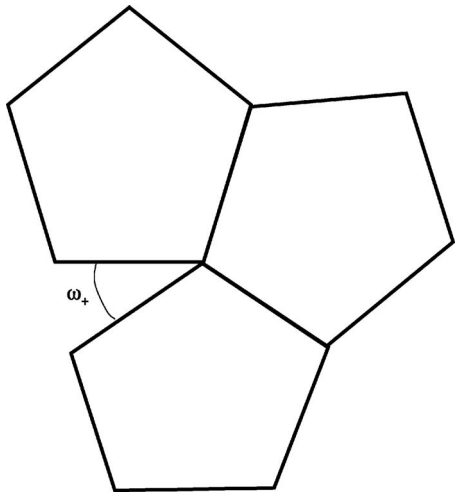

FIG. 28. Deficit angle at a merging vertex of three regular pentagons, $\omega_+ = \pi/5$.

2. The Volterra process in a curved crystal

It is useful to approximate a Riemannian manifold by a piecewise flat manifold. Such a process of triangulation has been proposed by Regge (1961) to calculate properties of curved manifolds in general relativity without using coordinates. For instance, in {3, 3, 5}, the edges of the lattice are replaced by straight lines in the embedding Euclidean space, and the faces and cells by Euclidean faces and cells. The edges, on which all the curvature is now concentrated, form the skeleton of the triangulated manifold (the one-bones), which is articulated at the vertices (the zero-bones). Consider a $D=2$ example, {5, 3} (three pentagons at each vertex); its Regge image is a dodecahedron with flat pentagonal faces. By mapping the pentagons around a vertex (where the curvature is concentrated) onto the plane, one allows the appearance of a deficit angle

$$\omega_+ = 2\pi - 3 \times \frac{3\pi}{5} = \frac{\pi}{5} \tag{37}$$

(Fig. 28), which is not equal to the angle of a quantized disclination in {5, 3}, namely, $\Omega = 3\pi/5$. The stress field produced by the Volterra process at such a vertex is that of a negative disclination of strength $\omega_- = \Omega - \omega_+ = -2\pi/5$. This angle also measures the deficit angle of the local negative Gaussian curvature generated by the introduction of extra matter; this negative Gaussian curvature would manifest itself as a locally hyperbolic surface element, if the disclinated {5, 3} is allowed to relax elastically in three dimensions.

It is energetically unfavorable that the only disclinations present in the actual medium be of negative strength. Therefore all vertices are not the seats of mapping disclinations, and those which are not are flattened by force, which yields stresses characteristic of positive disclinations of strength ω_+.

In three dimensions, the curvature is concentrated along the one-bones; if one moves a vector by parallel transport on a closed circuit L about an edge i, it rotates by an angle ω_i (the deficit along i),

$$\omega_i = 2\pi - \sum \alpha_k, \tag{38}$$

which does not depend on the precise location of L as long as it is traced in Euclidean space and does not cross another edge; α_k is the dihedral angle of the local flat polyhedron k with edge i. One can perform a Volterra process, now truly reminiscent of the usual Volterra process in flat space, either by gluing the two lips across the angle ω_i or by inserting (removing) a lattice unit cell Ω in the space separating the lips. According to which case one considers, one introduces a topological disclination of strength $\pm|\omega_i|$ or $\mp|\omega_i - \Omega|$. These disclinations are wedge disclinations, since they lie along a rotation vector $\mathbf{\Omega}$. The Volterra process for twist disclinations does not add or remove matter; therefore it does not change the curvature.

The deficit vectors $\boldsymbol{\omega}_i$ that are merging at a vertex and are parallel to the corresponding edges obey the Kirchhoff relation

$$\sum \boldsymbol{\omega}_i = \mathbf{0}, \tag{39}$$

here written for small ω_i's. This expression is in fact the Bianchi identity for curvatures when the deficit angles are small (Regge, 1961).

To summarize, the actual medium contains two sets of disclinations; we call them D_s lines when they carry spherical curvature and are positive strength disclinations, D_h lines otherwise. Notice the duality between D_s and D_h lines; it means that one can start equally from a spherical crystal or from a hyperbolic crystal to construct a disordered system (Kleman, 1982a, 1983). The precise location and density ϱ_s and ϱ_h of the D_s and D_h lines are, of course, subject to great arbitrariness, and it is the best elastic balance which decides the final choice. From that point of view, an amorphous solid with local icosahedral order is certainly closer to a spherical crystal than a hyperbolic crystal, and one expects $\varrho_s > \varrho_h$.

C. The concept of a non-Euclidean amorphous medium

The foregoing model of an amorphous medium, based on the existence of a frustrated order, does not forbid the conceptual possibility of a homogeneous, isotropic, structureless, medium in S^3, whose defects we can investigate after the manner of the amorphous medium discussed in Sec. II.

The model we consider has no relation whatsoever with any kind of local order. We denote it $\{am/S^3\}$. Because of the curvature imposed by the habit space S^3, the singularities that break the continuous rotation and (noncommutative) translation symmetries are somehow at variance with disclinations and dislocations in flat Euclidean space. This is also true for the {3, 3, 5} case, but the continuous case is expected to be easier to understand. Furthermore, the concept itself of a curved amorphous medium is new and worth investigating in its own right. As we just observed, a pending question in the {3, 3, 5} case is how to decurve such a template in order to get an atomic liquid or amorphous medium with icosahedral local order. The difficulty lies in the fact that the {3, 3, 5} disclinations are quantized, and the answer is not unique; stresses remain. The same question for $\{am/S^3\}$ yields a unique answer with no stresses remaining, since defects are continuous in strength and distribution.

Finally there is the question of disclination networks, analogous in spirit to Frank dislocation networks. Disclination networks are apparent in polynanocrystals (Sec. III.C) and in Frank and Kasper phases (Sec. VI.A.4). They might also be important in undercooled liquids, but the true local geometry is that one of a spherical crystal with icosahedral symmetry (Sec. VI.A.4). This situation requires reconsidering the Kirchhoff relations in a curved habit space, either amorphous (as a generalization of Sec. II.F.2, see Sec. VII.E) or icosahedral (i.e., with quantized disclinations, see Sec. VII.F).

VII. DEFECTS IN THREE-SPHERE TEMPLATES

A. Geometry and topology of a three-sphere: A reminder

A point **M** on the three-sphere S^3 of unit radius will be defined by its Cartesian coordinates in E^4, $\{x_0,x_1,x_2,x_3\}$, or more concisely by the unit quaternion x,

$$x = x_0 + x_1 i + x_2 j + x_3 k,$$

$$|x|^2 = x\tilde{x} = x_0^2 + x_1^2 + x_2^2 + x_3^2 = 1, \tag{40}$$

where $\tilde{x}$ stands for the (complex) conjugate of x.

1. The rotation group SO(3) in quaternion notation

The set of unit quaternions forms a group that is related to the group of rotations SO(3) in E^3, as follows. The unit quaternion x,

$$x = \cos\vartheta + q\sin\vartheta, \quad q = \frac{x_1 i + x_2 j + x_3 k}{\sqrt{x_1^2 + x_2^2 + x_3^2}}, \tag{41}$$

is representative of a rotation ϑ along the direction $\{x_1,x_2,x_3\}$; two antipodal points x, $-x$ on S^3 embedded in E^4 are representative of the same rotation ϑ and $\vartheta+\pi$ along the same direction x_1,x_2,x_3; q is called a pure unit quaternion; its real part vanishes, $q^2=-1$, $q\tilde{q}=1$. All SO(3) rotations are therefore represented by a sphere S^3 with antipodal points identified, namely, $P^3=S^3/Z_2$, the projective plane in three dimensions. Reciprocally, $Q=S^3$, the multiplicative group of unit quaternions, is the double covering of P^3 and, as a topological group, is isomorphic to SU(2) and homomorphic 2:1 to the group SO(3) of all rotations that leave the origin fixed,

$$\mathrm{SO}(3) = \mathrm{SU}(2)/Z_2, \tag{42}$$

the kernel of the homomorphism being generated by the rotation 2π.

Because of the validity of Moivre's formula for unit quaternions, x can also be denoted

$$x = \exp\left(\frac{\vartheta}{2}q\right). \tag{43}$$

2. The rotation group SO(4) in quaternion notation

The quaternion notation provides an easy analysis of the basic isometric transformations of E^4 (Coxeter, 1991) that conserve a fixed point (the center of S^3). These are as follows.

(i) The *single rotation*, with one pointwise fixed 2D plane, the so-called axial plane containing the origin **O**; this plane is the E^4 generalization of the rotation axis in E^3. For that reason, one shall often call the single rotation in E^4 as the *rotation*.

(ii) The *double rotation* (with one fixed point only, the center of S^3), which is the commutative product of two rotations about two completely orthogonal axial planes.

a. The single rotation

The basic formula for a rotation of angle α about the axial plane $\Pi_{1,w}=(0,1,w)$, defined by three points in E^4, namely, (i) the origin {0, 0, 0, 0}—denoted {0}, (ii) {1, 0, 0, 0}—denoted {1}, (iii) $\{0,w_1,w_2,w_3\}$—denoted $\{w\}$, is

$$x' = e^{-(\alpha/2)w} x e^{(\alpha/2)w}. \tag{44}$$

The transformation (44) leaves invariant any point x of $\Pi_{1,w}$, i.e., $x=\lambda+\mu w$ (λ, μ real), and no other points,

$$\lambda + \mu w = e^{-(\alpha/2)w}(\lambda + \mu w)e^{(\alpha/2)w}.$$

If x is a pure quaternion (not necessarily a unit one), Eq. (44) gives the rotation of its representative point **x** by an angle α about the axis **w**, on a two-sphere S^2 of radius $|x|$. Therefore a pair of two conjugate unit quaternions $(e^{-(\alpha/2)w}, e^{-(\alpha/2)w})$ represents one element of SO(3); the pair $(-e^{-(\alpha/2)w}, -e^{-(\alpha/2)w})$ represents the same element; the representation is 2:1, as already noted.

$\Pi_{1,w}$ intersects the habit sphere S^3 or {3, 3, 5} or $\{am/S^3\}$, radius R, along a great circle $C_{1,w}$, radius R, which is thereby pointwise invariant in the rotation given by Eq. (44); $\{R\}$ and $\{Rw\}$ belong to this great circle.

The vector αt tangent to $C_{1,w}$ at **M** is the local rotation vector in S^3 induced by the single rotation in E^4.

With Eq. (44), we have considered a special axial plane. A rotation of angle α about a generic axial plane passing through the origin in E^4 is

$$x' = e^{-(\alpha/2)p} x e^{(\alpha/2)q}, \tag{45}$$

$p \neq \pm q$, with axial plane

$$\Pi_{p,q} = (0, 1 - pq, p + q). \tag{46}$$

It is easy to show that $1-pq$ and $p+q$ are invariant in the transformation given by Eq. (45). Notice that p and q are pure unit quaternions.

This is now the place to introduce the plane

$$\Pi^{\perp}_{p,q} = (0, 1 + pq, p - q), \tag{47}$$

which is the plane completely orthogonal to $\Pi_{p,q}$; the directions denoted by $1+pq$ and $p-q$ are both orthogonal to $1-pq$ and to $p+q$. A rotation of angle β about $\Pi^{\perp}_{p,q}$ taken as an axial plane reads

$$x' = e^{(\beta/2)p} x e^{(\beta/2)q} \tag{48}$$

Since the four directions $1-pq$, $p+q$, $1+pq$, and $p-q$ are mutually orthogonal, they can be used as the directions of a Cartesian frame of reference in E^4.

b. The double rotation: Right and left helix turns

The rotations about two completely orthogonal planes are commutative. Consider the product of two rotations of the same angle α about $\Pi_{p,q}$ and $\Pi^{\perp}_{p,q}$. According to Eqs. (45) and (48), we have

$$x' = e^{-(\alpha/2)p}(e^{(\alpha/2)p} x e^{(\alpha/2)q}) e^{(\alpha/2)q},$$

i.e.,

$$x' = x e^{\alpha q}. \tag{49}$$

This double rotation conserves S^3 (and any three-sphere centered at the origin) globally, and leaves only one point invariant, the intersection of the two planes $\Pi_{p,q}$ and $\Pi^{\perp}_{p,q}$, i.e., the center {0} of S^3. It leaves no point invariant in S^3; thereby it is akin to a translation in Euclidean space; *E*. Cartan introduced the term *transvection* to connote such an operation in a Riemannian space (Cartan, 1963).

The term p does not appear any longer in Eq. (49); hence this transformation can be given a geometric interpretation in any pair of a large set of completely orthogonal plane pairs. For instance, it is a transformation that, in the two-plane $\Pi_{1,q}$ containing the origin {0} and the directions {1, 0, 0, 0} and $q=\{0, q_1, q_2, q_3\}$, is a rotation of angle α, and in the completely orthogonal two-plane $\Pi^{\perp}_{1,q}$ is a rotation of the same angle α (Montesinos 1987).

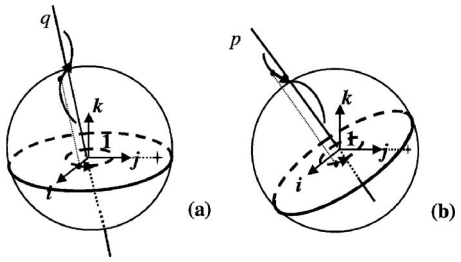

FIG. 29. Helix turns. (a) Right helix turn $x' = x e^{\alpha q}$ and (b) left helix turn $x' = e^{-\alpha p} x$ in stereographic projection.

It can also be called a *right helix turn*, for the following reason. Consider the transvection $x' = x e^{\alpha i}$. In order to visualize it, we employ the stereographic projection of S^3 from its pole $\{-1, 0, 0, 0\}$ onto the hyperplane spanned by the directions i, j, and k (the imaginary part of the quaternion set); $x' = x e^{\alpha i}$ turns the *equator* plane spanned by the directions j and k (i.e., the plane $\Pi^{\perp}_{1,i}$ completely orthogonal to $\Pi_{1,i}$) to the right by an angle α about the axis i, and pushes it forward by the same angle [Fig. 29(a)]. The same is true, also in stereographic projection, for the transformation $x' = x e^{\alpha q}$, where q is any pure unit quaternion chosen as the axis of the rotation, since any axis q results from the axis i by a rotation in the 3D $\langle i, j, k \rangle$ hyperplane; all pure unit quaternions are visualizable in stereographic projection, as well as their corresponding equator planes.

The *left helix turn*

$$x' = e^{-\alpha p} x \tag{50}$$

results from the product of two rotations of the same angle and of opposite signs, $x' = e^{-(\alpha/2)p}(e^{-(\alpha/2)p} x e^{(\alpha/2)q}) e^{-(\alpha/2)q}$, performed on two completely orthogonal planes; it turns the equator of p also to the right by an angle α, but pushes its equator plane backward by the same angle [Fig. 29(b)]. A left helix turn and a right helix turn are commutative, but two left (or right) helix turns are not. Therefore these transformations are akin to noncommutative translations.

3. Group of direct isometries in the habit three-sphere S^3

Any product of a right translation by a left translation is a direct isometry in S^3:

$$x' = e^{-\beta p} x e^{\alpha q}; \tag{51}$$

it is also the product of two commutative rotations of angles $\alpha+\beta$ and $\alpha-\beta$ about two completely orthogonal axial planes $\Pi_{p,q}$ and $\Pi^{\perp}_{p,q}$; a right (or left) helix turn is given by Eq. (51), with β (or α) $=0, 2\pi$. $\{-e^{\alpha p}, -e^{-\beta q}\}$ generates the same isometry as $\{e^{\alpha p}, e^{-\beta q}\}$.

Since any isometry in S^3 is generated by a combination of two commutative helix turns $\{e^{\alpha p}, e^{-\beta q}\}$, one right, one left—each belonging to the group SU(2)—the maximal group that leaves S^3 invariant is

$$\mathrm{SO}(4) = G(S^3) \sim \mathrm{SU}(2) \times \mathrm{SU}(2)/Z_2 = S^3 \times \mathrm{SO}(3). \tag{52}$$

It is a direct product. Its universal cover is $\bar{G}(S^3)=S^3\times S^3$, i.e., the group of unit quaternions, squared.

A discussion on some geometric characteristics of S^3 can be found in Appendix D.

B. Disclinations and disvections in S^3

The notion of line defect easily generalizes to any ordered medium in S^3. In terms of the Volterra process, we have two types of defects.

1. Disclinations in S^3

Disclinations break a single rotation in E^4, defined by the SO(4) group element $\{e^{-(\Omega/2)p},e^{(\Omega/2)q}\}$ about some axial plane $\Pi_{p,q}$; they conserve the habit sphere S^3 globally. The plane $\Pi_{p,q}$ intersects S^3 along a great circle C. For an observer confined to the habit sphere, this rotation appears as a set of rotation vectors $\mathbf{\Omega t}$ tangent to C all along, as already indicated. The points x of the cut surface are displaced by the single rotation

$$x' = e^{-(\Omega/2)p}xe^{(\Omega/2)q}.$$

Remember that any great circle is a geodesic of S^3, so that this operation is clearly a generalization of a disclination in E^3, where the rotation vectors are along straight lines, i.e., Euclidean geodesics.

2. Disvections in S^3

Disvections break transvection symmetries and are thereby generalizations of dislocations, which break translation symmetries. A right (say) transvection

$$x_i' = x_i e^{\alpha q}, \quad |x_i| = R,$$

brings $\mathbf{M}_i(x_i)$ to $\mathbf{M}_i'(x_i')$, at a distance $|b|=|x_i'-x_i| = 2R\sin\frac{\alpha}{2}$, along the great circle C_i through $\mathbf{M}_i$ and $\mathbf{M}_i'$. $\mathbf{M}_i'$ in turn is moved by the same distance $|b|$ along the same great circle. Any point $\mathbf{M}_j$ outside C_i likewise follows another great circle C_j which is equidistant from C_i, with the same $|b|$, i.e., which turns about C_i in a double-twisted manner. The points x of the cut surface are displaced by the double rotation

$$x' = xe^{\alpha q}.$$

This operation is clearly a generalization of a dislocation in E^3, with $\mathbf{b}$ the analog of the Burgers vector.

The term disvection was introduced to connote line defects that break noncommutative translation symmetries in quasicrystals (Kleman, 1992).

C. Defects of the double-twist S^3 template

The topological classification of line defects in the double-twist template $\{\mathrm{dtw}/S^3\}$ is the same as that of the uniaxial nematic (Sethna, 1985), namely,

$$\Pi_1(V_{\mathrm{dtw}}) = Z_2, \tag{53}$$

since $V_{\mathrm{dtw}}=\mathrm{SO}(4)/\mathrm{SU}(2)\times D_{2h}=P_2$, the projective plane. In this expression, $\mathrm{SO}(4)=\mathrm{SO}(3)\times\mathrm{SU}(2)$ is the group of isometries of S^3 [Eq. (52)], SU(2), in the denominator, is isomorphic to the group of left or right transvections—the template has a definite chirality, and D_{2h} is the rotation point group, as in a N phase. These results can be obtained using the geometric picture of the Hopf fiber bundle (see Fig. 36 in Appendix D), which is the geometrical representation of $\{\mathrm{dtw}/S^3\}$.

Whereas the topological stability analysis provides only one class of topological defects, namely, $|k|=\frac{1}{2}$, the Volterra process provides many more, exactly as the N phase. Therefore one has to differentiate $k=-\frac{1}{2}$ disclinations, which add matter, and $k=\frac{1}{2}$ disclinations, which remove matter. In principle, only the first category of disclinations is liable to decurve $\{\mathrm{dtw}/S^3\}$ a Euclidean medium; this is precisely the result that is claimed in the current BP structural models (Meiboom *et al.*, 1983). However, a caveat is in order: Because viscous relaxation operates at constant density, a negative sign for the decurving disclinations should not be a prerequisite; Sethna (1985) has proposed a model where there are no disclinations at all, with, however, the same cubic structure.

D. Continuous defects in a 3D spherical isotropic uniform medium

1. The wedge disclination

First, a few remarks about the great circles of S^3, which are geodesics of S^3, i.e., the equivalent of straight lines in flat space.

a. Wedge disclinations are along great circles

Let $\Pi_{p,q}=\{0,1-pq,p+q\}$ be the plane that intersects the habit sphere along the great circle C. We have $|1-pq|^2=|p+q|^2=2-pq-qp$, where

$$-pq-qp = 2\mathbf{p}\cdot\mathbf{q} = 2\cos\phi_{p,q},$$

$\phi_{p,q}$ being the angle between $\mathbf{p}$ and $\mathbf{q}$; $1-pq$ and $p+q$ are orthogonal. We then have, for any point u on C,

$$u = a(1-pq)+b(p+q), \quad |u| = R.$$

We choose the origin of the angles in the $\Pi_{p,q}$ plane along the direction $1-pq$; one then gets

$$\begin{aligned} u(\vartheta) &= RN_{p,q}e^{(\vartheta/2)p}(1-pq)e^{(\vartheta/2)q} \\ &= RN_{p,q}[(1-pq)\cos\vartheta+(p+q)\sin\vartheta], \end{aligned} \tag{54}$$

where

$$N_{p,q} = (2-pq-qp)^{-1/2} = \left(2\cos\frac{\phi_{p,q}}{2}\right)^{-1}.$$

The first equality expresses the fact that the points of C are obtained by a rotation $\{e^{(\vartheta/2)p},e^{(\vartheta/2)q}\}$ about $\Pi_{p,q}^{\perp}=\{0,1+pq,p-q\}$ in E^4. Observe that the rotation

$\{e^{(\vartheta/2)p}, e^{(\vartheta/2)q}\}$ keeps pointwise invariant the intersection of $\Pi_{p,q}^{\perp}$ with S^3, which is a great circle $C^{\perp}$ orthogonal to C. The angular distance between any pair of points $\mathbf{M} \in C$, $\mathbf{M}^{\perp} \in C^{\perp}$ is equal to $\pi/2$ (the two vectors **OM** and $\mathbf{OM}^{\perp}$ are orthogonal). The circles C and $C^{\perp}$, which have the same center and the same diameter, have no point in common.

b. Volterra elements of a wedge disclination

Consider now the rotation $\{e^{-(\Omega/2)p}, e^{(\Omega/2)q}\}$ about $\Pi_{p,q}$; it conserves S^3 globally. The plane $\Pi_{p,q}$ intersects S^3 along C. In S^3, this rotation is a set of rotation vectors $\Omega\mathbf{t}$ tangent to C throughout. It is therefore a rotation that builds C Volterra-wise as a line of wedge character, of strength Ω. Its constitutive dislocations are as follows. Let $x = x^{\parallel} + x^{\perp}$ be the quaternion representation of a point $\mathbf{P} = \mathbf{x}^{\parallel} + \mathbf{x}^{\perp}$ on the cut surface $\Sigma_{\mathbf{C}}$ of C (it is not useful to select a special cut surface), split into its two components, one, $x^{\parallel}$, belonging to $\Pi_{p,q}$ (invariant in the rigid Volterra rotation $\{e^{-(\Omega/2)p}, e^{(\Omega/2)q}\}$ that moves apart the two lips of the cut surface), the other one, $x^{\perp}$, belonging to $\Pi_{p,q}^{\perp}$ (not invariant in the rotation under consideration). Hence

$$x'^{\parallel} = x^{\parallel} = e^{-(\Omega/2)p} x^{\parallel} e^{(\Omega/2)q}, \quad x'^{\perp} = e^{-(\Omega/2)p} x^{\perp} e^{(\Omega/2)q}.$$

Thus $|x^{\perp}|$ is the distance of **P** from the axial plane $\Pi_{p,q}$ of the Volterra process we are considering.

The sum total of the Burgers vectors of the constitutive dislocations between the wedge line and **P** is, in quaternion notation,

$$b = x' - x = e^{-(\Omega/2)p} x e^{(\Omega/2)q} - x, \tag{55}$$

which can also be written

$$b = \sin\frac{\Omega}{2} e^{-(\Omega/2)p}(xq - px) = \sin\frac{\Omega}{2}(xq - px)e^{(\Omega/2)q}. \tag{56}$$

But, because $x^{\parallel}$ belongs to $\Pi_{p,q}$ and $x^{\perp}$ to $\Pi_{p,q}^{\perp}$, we have

$$x^{\perp} = e^{(\vartheta/2)p} x^{\perp} e^{(\vartheta/2)q}, \quad x^{\parallel} = e^{-(\vartheta/2)p} x^{\parallel} e^{(\vartheta/2)q},$$

for any ϑ. Hence

$$x^{\perp} q + p x^{\perp} = 0, \quad x^{\parallel} q - p x^{\parallel} = 0, \tag{57}$$

and eventually

$$b = -2\sin\frac{\Omega}{2} p x^{\perp} e^{(\Omega/2)q} \equiv 2\sin\frac{\Omega}{2} e^{-(\Omega/2)p} x^{\perp} q. \tag{58}$$

To connect with the discussion concerning Eq. (1), we make use of two remarks: (i) the modulus of b, calculated from Eq. (58), is

$$|b| = 2|x^{\perp}|\sin\frac{\Omega}{2}; \tag{59}$$

(ii) the Burgers vector **b** is perpendicular to $\Pi_{p,q}$. Notice that it is also orthogonal to $\mathbf{x}^{\perp}$ and to $\mathbf{x}'^{\perp}$, which both belong to $\Pi_{p,q}^{\perp}$; hence $\mathbf{b}\cdot\mathbf{OP} = \mathbf{b}\cdot\mathbf{OP}' = 0$.

These two properties also belong to the constitutive dislocations of a wedge line in $\{\mathrm{am}/E^3\}$. Note that Eq. (59) reproduces the integral of Eq. (1) performed on the interval between the line and a point **P** on the cut surface for a wedge disclination, since $|x^{\perp}|$ is in both cases the distance to the invariant manifold [in Eq. (1) it is the distance to the rotation axis of the disclination]. The fact that **b** is orthogonal to the axial plane $\Pi_{p,q}$ compares to the fact that in Eq. (1) the Burgers vector is orthogonal to the axis of rotation.

The Burgers vector db of the constitutive dislocations situated between x and $x+dx$ on the cut surface is

$$db = e^{-(\Omega/2)p} dx e^{(\Omega/2)q} - dx,$$

which can also be written

$$db = -2\sin\frac{\Omega}{2} p dx^{\perp} e^{(\Omega/2)q} \equiv 2\sin\frac{\Omega}{2} e^{-(\Omega/2)p} dx^{\perp} q. \tag{60}$$

To summarize, Eq. (60), valid in $\{\mathrm{am}/S^3\}$, is the equivalent of Eq. (1), valid in $\{\mathrm{am}/E^3\}$. It describes the constitutive dislocations of a wedge disclination Ω located at the intersection of the habit three-sphere and the two-plane $\Pi_{p,q} = \{0, 1-pq, p+q\}$.

It then remains to find the manifolds along which $d\mathbf{b}$ is constant not only in magnitude, but also in direction, i.e., the geometry of the constitutive dislocation lines. The relation $x^{\perp} = \text{const}$ defines a two-plane parallel to $\Pi_{p,q}$, which intersects the habit sphere along a circle $C_{x^{\perp}}$, of radius $|x^{\parallel}|$, which is not a great circle, except if $x^{\perp} = 0$, in which case $C_{x^{\perp}}$ is the disclination C itself. The circles C and $C_{x^{\perp}}$ are parallel and perpendicular to some direction $d_{x_{\perp}}$ belonging to $\Pi_{p,q}^{\perp}$; b, which depends only on $x^{\perp}$, is constant on $C_{x^{\perp}}$, which is indeed a constitutive dislocation of the wedge disclination. The set of constitutive dislocations $C_{x^{\perp}}$ for $0 \leqslant |x^{\parallel}| \leqslant R$, so chosen that these circles are in parallel planes, all perpendicular to the same direction $d_{x^{\perp}}$ in $\Pi_{p,q}^{\perp}$, describes half a great sphere, which is a geodesic manifold of S^3, and consequently the equivalent of a half plane in flat space. There is a one-parameter family of such half great spheres, depending on the direction $d_{x^{\perp}}$ in $\Pi_{p,q}^{\perp}$, each of them playing the role of a possible cut surface $\Sigma_{\mathbf{C}}$ for the wedge disclination C.

Equation (58) can be given an interpretation in terms of disvections. We introduce the quaternion $z_{\perp} = -px^{\perp} = x^{\perp} q$; it results geometrically from a rotation by an angle of $\frac{\pi}{2}$ of the vector $\mathbf{x}^{\perp}$ in the $\Pi_{p,q}^{\perp}$ plane, so that $z^{\perp} = e^{-(\pi/4)p} x^{\perp} e^{(\pi/4)q}$; $z^{\perp}$ is constant all along $C_{x^{\perp}}$. Hence

$$db = 2\sin\frac{\Omega}{2}(dz^{\perp} e^{(\Omega/2)q}) \equiv 2\sin\frac{\Omega}{2}(e^{-(\Omega/2)p} dz^{\perp}) \tag{61}$$

appears as either a left screw or a right screw.

2. Defects attached to a disclination in $\{am/S^3\}$

a. Useful identities and relations

We introduce two great circles at each point **M** of a generic disclination line L; one of them, C_m, is tangent to L at **M** along the direction **m**, the other one, C_μ, is tangent to the local rotation vector $\mathbf{\Omega}=\Omega\boldsymbol{\mu}$; $m\tilde{m}=\mu\tilde{\mu}=1$. Their analogs in $\{am/E^3\}$ are the straight lines along **m**—the tangent to the disclination line—and $\boldsymbol{\mu}$—along the rotation vector. The two-planes to which these circles belong are denoted $\Pi_{p,q}=\{0,1-pq,p+q\}$ for C_m, and $\Pi_{\varrho,\sigma}=\{0,1-\varrho\sigma,\varrho+\sigma\}$ for C_μ; p, q, ϱ, σ, are defined as in Eqs. (62) and (63):

$$p=-\frac{1}{R}u\tilde{m}=\frac{1}{R}m\tilde{u},\quad q=\frac{1}{R}\tilde{u}m=-\frac{1}{R}\tilde{m}u, \tag{62}$$

$$\varrho=-\frac{1}{R}u\tilde{\mu}=\frac{1}{R}\mu\tilde{u},\quad \sigma=\frac{1}{R}\tilde{u}\mu=-\frac{1}{R}\tilde{\mu}u, \tag{63}$$

Full details are given in Appendix D. Notice that the relations $m\tilde{u}+u\tilde{m}=0$ and $\tilde{u}m+\tilde{m}u=0$, easily deduced from Eq. (62), express the orthogonality of **m** and **u**, $\mathbf{m}\cdot\mathbf{u}=0$. Likewise, $\mu\tilde{u}+u\tilde{\mu}=0$, and so on.

Observe that m is invariant in any rotation about $\Pi_{p,q}$, and that μ is likewise invariant in any rotation about $\Pi_{\varrho,\sigma}$; this yields

$$e^{-(\vartheta/2)p}me^{(\vartheta/2)q}=m,\quad e^{-(\vartheta/2)\varrho}\mu e^{(\vartheta/2)\sigma}=\mu,$$

for any ϑ; hence

$$pm-mq=0,\quad \varrho\mu-\mu\sigma=0. \tag{64}$$

These relations also stem from Eqs. (62) and (63), but it is worth retrieving them in this way, in order to emphasize the role of invariance by rotation. Since **M** belongs to both axial planes $\Pi_{p,q}$ and $\Pi_{\varrho,\sigma}$, we have

$$e^{-(\vartheta/2)p}ue^{(\vartheta/2)q}=u,\quad e^{-(\vartheta/2)\varrho}ue^{(\vartheta/2)\sigma}=u,$$

for any ϑ; hence

$$pu-uq=0,\quad \varrho u-u\sigma=0. \tag{65}$$

also stemming from Eqs. (62) and (63).

More generally, the quaternion components $a^\parallel$ and $a^\perp$, respectively, in $\Pi_{p,q}$ and $\Pi^\perp_{p,q}$, of any vector $a=a^\parallel+a^\perp$ obey

$$pa^\parallel-a^\parallel q=0,\quad pa^\perp+a^\perp q=0, \tag{66}$$

and similar relations for its components $a_\parallel$ and $a_\perp$ in $\Pi_{\varrho,\sigma}$ and $\Pi^\perp_{\rho,\sigma}$,

$$\varrho a_\parallel-a_\parallel\sigma=0,\quad \varrho a_\perp+a_\perp\sigma=0. \tag{67}$$

By differentiating, one also gets

$$e^{(\vartheta/2)p}udqe^{(\vartheta/2)q}=udq,\quad e^{(\vartheta/2)p}dpue^{(\vartheta/2)q}=dpu,$$

$$e^{(\vartheta/2)\varrho}ud\sigma e^{(\vartheta/2)\sigma}=ud\sigma,\quad e^{(\vartheta/2)\varrho}d\varrho ue^{(\vartheta/2)\sigma}=d\varrho u,$$

$$e^{(\vartheta/2)p}mdqe^{(\vartheta/2)q}=mdq,\quad e^{(\vartheta/2)p}dpme^{(\vartheta/2)q}=dpm,$$

$$e^{(\vartheta/2)\varrho}\mu d\sigma e^{(\vartheta/2)\sigma}=\mu d\sigma,\quad e^{(\vartheta/2)\varrho}d\varrho\mu e^{(\vartheta/2)\sigma}=d\varrho\mu. \tag{68}$$

All these relations are easy to establish directly, by employing identities of the type

$$e^{(\vartheta/2)\varrho}d\varrho=d\varrho e^{-(\vartheta/2)\varrho},\quad d\sigma e^{(\vartheta/2)\sigma}=e^{-(\vartheta/2)\sigma}d\sigma, \tag{69}$$

which express rotational invariance about $\Pi^\perp_{p,q}$ and $\Pi^\perp_{\varrho,\sigma}$. The quaternions udq, dpu, mdq, dpm belong to the plane $\Pi^\perp_{p,q}$; they are invariant in any rotation about the axial plane $\Pi^\perp_{p,q}$. The quaternions $ud\sigma$, $d\varrho\sigma$, $\mu d\sigma$, $d\varrho\mu$ belong to the plane $\Pi^\perp_{\varrho,\sigma}$; they are invariant in any rotation about the axial plane $\Pi^\perp_{\varrho,\sigma}$.

More generally, the quaternions $b^\parallel$ and $b^\perp$ in $\Pi_{p,q}$ and $\Pi^\perp_{p,q}$, and the quaternions $b_\parallel$ and $b_\perp$ in $\Pi_{\varrho,\sigma}$ and $\Pi^\perp_{\varrho,\sigma}$, $b=b^\parallel+b^\perp=b_\parallel+b_\perp$, are such that

$$b^\parallel dq,\quad dpb^\parallel,\quad b^\perp q,\quad pb^\perp$$

belong to the plane $\Pi^\perp_{p,q}$,

$$b^\perp dq,\quad dpb^\perp,\quad b^\parallel q,\quad pb^\parallel \tag{70}$$

belong to the plane $\Pi_{p,q}$,

$$b_\parallel d\sigma,\quad d\varrho b_\parallel,\quad b_\perp\sigma,\quad \varrho b_\perp$$

belong to the plane $\Pi^\perp_{\varrho,\sigma}$,

$$b_\perp d\sigma,\quad d\varrho b_\perp,\quad b_\parallel\sigma,\quad \varrho b_\parallel \tag{71}$$

belong to the plane $\Pi_{\varrho,\sigma}$. Other useful relations are obtained by considering small rotations $d\vartheta$ about an axial plane. For instance, we have

$$u+du=e^{(d\vartheta/2)p}ue^{(d\vartheta/2)q},$$

which yields

$$du=\frac{1}{2}(pu+uq)d\vartheta. \tag{72}$$

Since $pu-uq=0$ [Eq. (65)], Eq. (72) yields

$$du=pu\,d\vartheta=uq\,d\vartheta=Rm\,d\vartheta, \tag{73}$$

the last equality also originating in the expressions for p and q [Eq. (62)].

b. A general expression for the attached defect density

We reproduce the extended Volterra process approach used for Euclidean crystals. Because $\{am/S^3\}$ is amorphous, any disclination L, whatever its strength, can be constructed as a sum of infinitesimal constitutive defects attached to L if L has twist character. The wedge disclination case has already been discussed; the constitutive defects are disvections [one set of disvections, whose chirality is ambiguous, left or right, Eq. (61)]. Disvections are the analogs in $\{S^3\}$ of dislocations in $\{E^3\}$, so that one can consider this result as the $\{S^3\}$ analog of the result in $\{E^3\}$. Contrarily, as we show, in the twist or mixed line case, the attached defects are generically disclinations, which, however, can be defined as the sum of two sets of disvections of opposite chiralities.

Now assume that L is any loop in the habit three-sphere, and consider two neighboring points $\mathbf{M}$ and $\mathbf{M}+d\mathbf{M}$ on this line, u and $u+du$ in quaternion notations, with $u\tilde{u}=(u+du)(\tilde{u}+d\tilde{u})=R^2$, i.e., $d\tilde{u}u+\tilde{u}du=0$. In order to compare the Volterra processes at two neighboring points $\mathbf{M}$ and $\mathbf{M}+d\mathbf{M}$, we proceed as follows.

Let $\mathbf{\Omega}=\Omega\boldsymbol{\mu}$ be the rotation vector of the disclination at $\mathbf{M}$. Being a rotation vector, $\boldsymbol{\mu}$ belongs to the axial plane $\Pi_{\varrho,\sigma}=\{0,1-\varrho\sigma,\varrho+\sigma\}$ that intersects the habit sphere along the great circle C_μ running through $\mathbf{M}$, and to which $\boldsymbol{\mu}$ is tangent. This is akin to the situation investigated in the case of the wedge disclination, where C_μ is the wedge line itself and where $\boldsymbol{\mu}$ is tangent to the wedge line (observe that $\boldsymbol{\mu}$ does not belong to the habit three-sphere but to the 3D flat tangent space to the sphere at $\mathbf{M}$). We therefore have $\boldsymbol{\mu}\cdot\mathbf{OM}=0$.

Consider now two close points $\mathbf{M}$ and $\mathbf{M}+d\mathbf{M}$ on the disclination L, with rotation vectors along μ and $\mu+d\mu$, and a point $\mathbf{P}$ (x in quaternion notation) on the cut surface $\Sigma_{\mathbf{L}}$. The variation in displacement observed from $\mathbf{M}$ to $\mathbf{M}+d\mathbf{M}$ at the same point $\mathbf{P}$ is

$$db_{\mathbf{M}}=e^{-(\Omega/2)(\varrho+d\varrho)}xe^{(\Omega/2)(\sigma+d\sigma)}-e^{-(\Omega/2)\varrho}xe^{(\Omega/2)\sigma}$$

$$=\sin\frac{\Omega}{2}(e^{-(\Omega/2)\varrho}xd\sigma-d\varrho xe^{(\Omega/2)\sigma}). \tag{74}$$

If the line L is a great circle and the local rotation vector is along the tangent of this circle, which means that one can choose ϱ, σ constant (independent of the point on C), then $d\varrho=d\sigma=0$; the line is of wedge character, as expected, and $db_{\mathbf{M}}=0$. There are no *attached* defects. We retrieve the results of Sec. VII.D.1.

Equation (74) is the fundamental equation related to attached defect densities in $\{\mathrm{am}/S^3\}$.

We show now that it cannot be interpreted the same way as Eq. (4) in $\{\mathrm{am}/E^3\}$, although the extended Volterra process from which it results is similar.

c. Attached disclination densities

As a matter of fact, Eq. (74) appears as the difference between two disclinations of axial planes $\Pi_{\varrho,\sigma}$ and $\Pi_{\varrho+d\varrho,\sigma+d\sigma}$; this difference can be expressed as a unique disclination carrying an infinitesimally small angle of rotation.

The quaternions $\varrho+d\varrho$ and $\sigma+d\sigma$ are pure unit quaternions, if second-order terms in $d\sigma^2$, $d\varrho^2$, etc. are neglected; $d\varrho$ and $d\sigma$ are pure quaternions, of equal moduli $|d\varrho|=|d\sigma|=d\lambda$ real and positive. We introduce the two pure unit quaternions t_ϱ, t_σ such that $d\lambda t_\varrho=d\varrho, d\lambda t_\sigma=d\sigma$.

We define

$$d_{\mathbf{M}}=e^{-(d\Omega_F/2)t_\varrho}xe^{(d\Omega_F/2)t_\sigma}-x. \tag{75}$$

Equation (75) is the displacement $d_{\mathbf{M}}(x)$ at $\mathbf{P}(x)$ due to an infinitesimal disclination of angle $d\Omega_F$ about the axial plane Π_{t_ϱ,t_σ}. Notice that $d_{\mathbf{M}}(u)=0$, which confirms that the infinitesimal disclination just defined is attached at $\mathbf{M}$ to L. We now show that Eq. (74) can be given the same form as Eq. (75), with the following choice of $d\Omega_F$:

$$d\Omega_F=2\sin\frac{\Omega}{2}\cos\frac{\Omega}{2}d\lambda, \tag{76}$$

justified below. Equation (76) can also be written as $d\Omega_F=2d(\sin\frac{\Omega}{2})$, $d\Omega_F$ thus appearing as the differential of the modulus of the Frank vector introduced in Sec. II.F.2, if one assumes that the variation $d\Omega$ of the argument equals $2d\lambda\sin\frac{\Omega}{2}$; we see later on why it should be so.

We now give hints how to identify Eqs. (74) and (75), and find *passim* an interesting simplification of the expressions of $db_{\mathbf{M}}$, $d_{\mathbf{M}}$.

Split $x=x_\parallel+x_\perp$ into its components $x_\parallel\in\Pi_{\varrho,\sigma}$ and $x_\perp\in\Pi^\perp_{\varrho,\sigma}$. According to Eq. (71), $x_\parallel d\sigma$ and $d\varrho x_\parallel$ belong to $\Pi^\perp_{\varrho,\sigma}$. Hence, $e^{-(\Omega/2)\varrho}x_\parallel d\sigma=x_\parallel d\sigma e^{(\Omega/2)\sigma}$, and

$$db_{\mathbf{M}}=\sin\frac{\Omega}{2}(\{x_\parallel d\sigma-d\varrho x_\parallel\}e^{(\Omega/2)\sigma}$$

$$+\{e^{-(\Omega/2)\varrho}x_\perp d\sigma-d\varrho x_\perp e^{(\Omega/2)\sigma}\}). \tag{77}$$

Because $x_\parallel\in\Pi_{\varrho,\sigma}$, we have

$$x_\parallel\sigma-\varrho x_\parallel=0.$$

Likewise, because $x_\perp\in\Pi^\perp_{\varrho,\sigma}$, we have

$$x_\perp\sigma+\varrho x_\perp=0.$$

We differentiate these relations, keeping x constant, and get

$$x_\parallel d\sigma-d\varrho\, x_\parallel=0,\quad x_\perp d\sigma+d\varrho\, x_\perp=0.$$

Hence

$$db_{\mathbf{M}}=\sin\frac{\Omega}{2}\{e^{-(\Omega/2)\varrho}x_\perp d\sigma-d\varrho x_\perp e^{(\Omega/2)\sigma}\}. \tag{78}$$

The terms depending on $x_\parallel$ have disappeared. The remaining terms can be transformed in many ways, using the equalities just derived and the rotation invariances of Eqs. (70) and (71). We get for $db_{\mathbf{M}}$

$$db_{\mathbf{M}}=-2\sin\frac{\Omega}{2}\cos\frac{\Omega}{2}d\lambda t_\varrho x_\perp$$

$$=2\sin\frac{\Omega}{2}\cos\frac{\Omega}{2}d\lambda x_\perp t_\sigma, \tag{79}$$

and using similar transformations for $d_{\mathbf{M}}$,

$$d_{\mathbf{M}}=-d\Omega_{\mathbf{F}}t_\varrho x_\perp=d\Omega_{\mathbf{F}}x_\perp t_\sigma. \tag{80}$$

Hence, to summarize, $db_{\mathbf{M}}$ and $d_{\mathbf{M}}$ describe the same infinitesimal disclination attached to L at $\mathbf{M}$, of angle $d\Omega_{\mathbf{F}}$, of axial plane Π_{t_ϱ,t_σ}.

Notice that the definition of $\delta\Omega=2d\lambda\sin\frac{\Omega}{2}$ is not mere chance; it originates in expressions of the type $e^{(\Omega/2)(\sigma+d\sigma)}$, which can also be written as

$$e^{(\Omega/2)(\sigma+d\sigma)}=e^{(\Omega/2)\sigma}+\sin\frac{\Omega}{2}d\lambda t_\sigma=e^{(\Omega/2)\sigma}+\frac{d\Omega}{2}t_\sigma.$$

For the sake of completeness, we write some other expressions for $db_{\mathbf{M}}$:

$$db_{\mathbf{M}} = \sin\frac{\Omega}{2}\{-e^{-(\Omega/2)\varrho}d\varrho x_\perp + x_\perp d\sigma e^{(\Omega/2)\sigma}\},$$

$$= \sin\frac{\Omega}{2}\{-d\varrho e^{(\Omega/2)\varrho}x_\perp + x_\perp e^{-(\Omega/2)\sigma}d\sigma\}. \quad (81)$$

We make use of Eq. (81).

Also, because $x_\perp \in \Pi^\perp_{\varrho,\sigma}$,

$$v_\perp \equiv e^{(\Omega/2)\varrho}x_\perp = x_\perp e^{-(\Omega/2)\sigma},$$

we can write

$$db_{\mathbf{M}} = \sin\frac{\Omega}{2}(-d\varrho v_\perp + v_\perp d\sigma),$$

where $v_\perp \in \Pi^\perp_{\varrho,\sigma}$, because

$$e^{-(\Omega/2)\varrho}(e^{(\Omega/2)\varrho}x_\perp)e^{-(\Omega/2)\sigma} \equiv x_\perp e^{-(\Omega/2)\sigma} = e^{(\Omega/2)\varrho}x_\perp$$

(the first member of this equation is a rotation of $v_\perp$ with axial plane $\Pi^\perp_{\varrho,\sigma}$).

d. Infinitesimal Burgers vectors and disclination lines

Starting from Eq. (74) or (81), we calculate $|db_{\mathbf{M}}|$ using $|db_{\mathbf{M}}|^2 = db_{\mathbf{M}}d\tilde{b}_{\mathbf{M}}$. The calculation, not reproduced here, uses some of the equalities established above. One finds

$$|db_{\mathbf{M}}| = 2\sin^2\frac{\Omega}{2}|x_\perp|d\lambda. \quad (82)$$

This equation compares to Eq. (61) (wedge disclination) by the common presence of the $|x_\perp|$ term—again, the relevant distance is the distance to the axial plane that carries the rotation vector of the disclination. The presence of the $\sin^2\frac{\Omega}{2}$ term is interpreted as follows. We can split $db_{\mathbf{M}}$ into two Burgers vectors, appearing in Eq. (81), related to two disvections, one right, one left,

$$db_{\mathbf{M},\sigma} = \sin\frac{\Omega}{2}x_\perp d\sigma e^{(\Omega/2)\sigma},$$

$$db_{\mathbf{M},\varrho} = -\sin\frac{\Omega}{2}e^{-(\Omega/2)\varrho}d\varrho x_\perp. \quad (83)$$

$db_{\mathbf{M},\varrho}$ and $db_{\mathbf{M},\sigma}$ have the same Burgers vector modulus, namely, $|db_{\mathbf{M},\varrho}| = |db_{\mathbf{M},\sigma}| = \sin\frac{\Omega}{2}|x_\perp|d\lambda$. The extra $\sin\frac{\Omega}{2}$ factor in $|db_{\mathbf{M}}|$ means that the two vectors $d\mathbf{b}_{\mathbf{M},\varrho}$ and $d\mathbf{b}_{\mathbf{M},\sigma}$ make a constant angle, equal to Ω. One can check directly that $d\mathbf{b}_{\mathbf{M},\rho}\cdot d\mathbf{b}_{\mathbf{M},\sigma} = \frac{1}{2}(db_{\mathbf{M},\varrho}d\tilde{b}_{\mathbf{M},\sigma} + d\tilde{b}_{\mathbf{M},\varrho}db_{\mathbf{M},\sigma}) = \cos\Omega$.

The description of the infinitesimal defects related to the disclination L in terms of disvections is equivalent to the description in terms of attached disclinations. Notice that the disvection lines, which are those lines along which $db_{\mathbf{M},\varrho}$ and $db_{\mathbf{M},\sigma}$ are constant, are not attached to L—which would require that $x_\perp = 0$, since the points of L are characterized by the quaternion coordinate u which obeys $u_\perp = 0$. The line L itself is a particular disvection line, of vanishing Burgers vector. Hence the infinitesimal disvection lines form two sets of lines surrounding L, each comparable to the set of disvections surrounding a wedge disclination line.

3. Twist disclination along a great circle

By constant rotation vector we mean that the local rotation axis of the disclination L, namely, $\Omega\mu$ in quaternion notation, with $\mu\tilde{\mu} = 1$, is parallel transported along a line with the natural connection of the sphere S^3. If such a line is a great circle, i.e., a geodesic, the rotation axis makes a constant angle with this circle, $\boldsymbol{\mu}\cdot\mathbf{m} = \cos\varphi$. This configuration is equivalent to a straight disclination line in $\{\mathrm{am}/E^3\}$, with constant rotation vector. A point $\mathbf{M}$ on L depends on the variable u or the arc angle ϑ. Let C^ϑ_μ be the great circle tangent to $\mu(\vartheta)$ at $\mathbf{M}(\vartheta) \in L$; it belongs to the plane $\Pi_{\varrho,\sigma} = \{0, 1-\varrho\sigma, \varrho+\sigma\}$; $\varrho = \varrho(\vartheta)$ and $\sigma = \sigma(\vartheta)$ are given by Eq. (63). $\Pi_{p,q} = \{0, 1-pq, p+q\}$ is the two-plane that contains the great circle L; p and q are constant.

The parallel transport of μ along L, a geodesic, is also a rotation about the axial plane $\Pi^\perp_{p,q} = \{0, 1+pq, p-q\}$, completely orthogonal to $\Pi_{p,q}$. Such a rotation can be written as

$$\mu + d\mu = e^{(d\vartheta/2)p}\mu e^{(d\vartheta/2)q},$$

which yields

$$d\mu = \frac{1}{2}(p\mu + \mu q)d\vartheta. \quad (84)$$

Using Eqs. (84) and (63), the following expressions for $d\varrho$ and $d\sigma$ are obtained:

$$d\varrho = \frac{1}{2}(p\varrho - \varrho p)d\vartheta, \quad d\sigma = -\frac{1}{2}(q\sigma - \sigma q)d\vartheta. \quad (85)$$

We also have

$$d\lambda = \frac{1}{2}d\vartheta|p\varrho - \varrho p| = \frac{1}{2}d\vartheta|q\sigma - \sigma q|.$$

We then have $\boldsymbol{\mu}\cdot\mathbf{m} = \cos\varphi = \frac{1}{2}(m\tilde{\mu} + \mu\tilde{m})$, a constant. We can show, again using Eqs. (62) and (63), that

$$(p\varrho - \varrho p)^2 = (q\sigma - \sigma q)^2 = 4\sin^2\varphi,$$

which yields

$$d\lambda = |\sin\varphi|d\vartheta. \quad (86)$$

As indicated by the presence of the coefficient $|\sin\varphi|$ in the expression of $d\lambda$, the only component of $\boldsymbol{\mu}$ that is relevant in the twist properties of the line is its component orthogonal to $\mathbf{m}$. Hence we split the rotation vector as follows:

$$\mu(\vartheta) = \mu^\perp + \mu^\parallel, \quad (87)$$

where $\mu^\perp$ belongs to the plane $\Pi^\perp_{p,q}$ and is therefore invariant in any rotation about this plane; $\mu^\parallel = m\cos\varphi$ belongs to the plane $\Pi_{p,q}$. It is a question of simple algebra to show that the $\mu_\parallel$ component does not contribute to

$\sigma q - q\sigma$ or to $p\varrho - \varrho p$. The only component of the rotation vector that contributes to the dislocation densities attached to C is $\mu_\perp$ (which is a constant all along the disclination), through the $|\sin\varphi|$ factor. But notice that the rotation vector is still $\Omega\boldsymbol{\mu}$.

The same discussion as in Secs. VII.D.1 and VII.D.2 is valid, with the simplifications of Eqs. (85) and (86).

E. Kirchhoff relations

Any isometry of S^3 has the form $x' = e^{-\beta q} x e^{\alpha p}$, Eq. (51), and can be split into the product of two commutative helix turns, one right, one left. Therefore a product of isometries can be written

$$x' = l_Q^{(1)} \cdots l_Q^{(i)} l_Q^{(i+1)} \cdots x \cdots r_Q^{(i+1)} r_Q^{(i)} \cdots r_Q^{(1)}, \tag{88}$$

where $l_Q^{(i)}, r_Q^{(i)} \in Q = \mathrm{SU}(2)$. n disclinations meeting at a node can be split into two sets of disvections meeting at this node, n left disvections and n right disvections. Thus we first investigate the Kirchhoff relations for (left or right) disvections.

1. Three disvections meeting at a node

Let $h_Q^{(1)} = e^{\alpha p}$, $h_Q^{(2)} = e^{\beta q}$, $h_Q^{(3)} = e^{\gamma r}$ be the elements of symmetry of three right (say) disvections meeting at a node. We then have

$$h_Q^{(1)} h_Q^{(2)} h_Q^{(3)} = \{\pm 1\}. \tag{89}$$

Remember that the group of all unit quaternions is 2:1 homomorphic to the group of all rotations of a two-sphere that leave the origin fixed. In that sense, h_Q and $-h_Q$ represent the same rotation in SO(3), but they do not represent the same transvection in SU(2). $\{-1\}$ transforms x into $-x$ by a helix turn of angle π about any axis $\mathbf{w}$: $\{-1\} = e^{\pi w}$. However, it will appear as a fundamental necessity to introduce the quaternion $\{-1\}$ in Eq. (89), as we shall see.

Denote by a, b, and c the angles between the directions defined by the three pure unit quaternions p, q, and r, namely, $a = \angle(\mathbf{q},\mathbf{r})$, $b = \angle(\mathbf{r},\mathbf{p})$, and $c = \angle(\mathbf{p},\mathbf{q})$. Equation (89), which also reads, e.g., $h_Q^{(1)} h_Q^{(2)} = \pm \tilde{h}_Q^{(3)}$, yields three relations coming from the real part of this relation, of the type

$$\cos\alpha\cos\beta - \cos c \sin\alpha \sin\beta = \pm\cos\gamma, \tag{90}$$

where $\cos c = \mathbf{p}\cdot\mathbf{q} = p_1q_1 + p_2q_2 + p_3q_3$, and nine relations coming from the pure quaternion part, of the type

$$q_1 \sin\beta\cos\alpha + p_1 \sin\alpha\cos\beta + s_{c,1} \sin c \sin\alpha \sin\beta = \mp r_1 \sin\gamma, \tag{91}$$

where the unit vector $\mathbf{s}_c$ (i.e., the pure unit quaternion s_c), defined by the cross product $\mathbf{s}_c \sin c = (\mathbf{p}\times\mathbf{q})$, has been introduced; similarly, $\mathbf{s}_a \sin a = (\mathbf{q}\times\mathbf{r})$ and $\mathbf{s}_b \sin b = (\mathbf{r}\times\mathbf{p})$.

Multiplying Eq. (91) by $s_{c,1}$ and summing over the three Eqs. (91) containing $s_{c,1}, s_{c,2}, s_{c,3}$, one gets

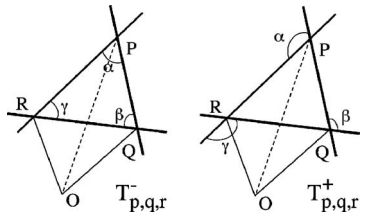

FIG. 30. Spherical 2D representation of Kirchhoff relations for disvections. **P**, **Q**, and **R** are on the sphere centered at **O**; see text.

$$\frac{\sin^2 a}{\sin^2\alpha} = \frac{\sin^2 b}{\sin^2\beta} = \frac{\sin^2 c}{\sin^2\gamma} = \mp \frac{V_{p,q,r}}{\sin\alpha\sin\beta\sin\gamma}, \tag{92}$$

where $V_{p,q,r} = \mathbf{r}\cdot(\mathbf{p}\times\mathbf{q})$ is the scalar triple product; $V_{p,q,r} = \mathbf{p}\cdot\mathbf{s}_a \sin a = \mathbf{q}\cdot\mathbf{s}_b \sin b = \mathbf{r}\cdot\mathbf{s}_c \sin c$.

One recognizes in Eqs. (90) and (92) expressions much akin to those met in 2D spherical trigonometry. The geometric interpretations of Eq. (89) in terms of spherical triangles are different, whether one has a $\{-1\}$ or a $\{1\}$ in the right-hand member.

a. $h_Q^{(1)} h_Q^{(2)} h_Q^{(3)} = \{-1\}$

One finds that there are two conjugate spherical triangles, here after denoted $T^-_{p,q,r}$ and $T^-_{s_a,s_b,s_c}$, whose angles and angular arcs yield $\{-1\}$ in the right-hand member:

(i) The vertices of $T^-_{p,q,r}$ are extremities $\mathbf{P},\mathbf{Q},\mathbf{R}$, of the three-vectors $\mathbf{p},\mathbf{q},\mathbf{r}$; the angles of the triangles are α,β,γ, and the angular arcs are a,b,c (see Fig. 30). Standard results in spherical trigonometry yield (Weisstein, 1999)

$$-\cos\gamma = \cos\alpha\cos\beta - \cos c \sin\alpha\sin\beta, \tag{93}$$

$$\frac{\sin\alpha}{\sin a} = \frac{\sin\beta}{\sin b} = \frac{\sin\gamma}{\sin c} = \frac{V_{p,q,r}}{\sin a \sin b \sin c}. \tag{94}$$

Equation (93) is obtained by applying the "cosine rules for the angles," specialized to the angle γ. The construction of a triangle of angles α,β,γ, of angular arcs a,b,c, requires that the following inequalities are obeyed:

$$\alpha+\beta+\gamma \geqslant \pi, \quad a+b+c \leqslant 2\pi. \tag{95}$$

(ii) The vertices of $T^-_{s_a,s_b,s_c}$ are extremities $\mathbf{A},\mathbf{B},\mathbf{C}$, of the three-vectors $\mathbf{s_a},\mathbf{s_b},\mathbf{s_c}$; the angles of the triangles are $\pi-a,\pi-b,\pi-c$, the angular arcs are $\pi-\alpha,\pi-\beta,\pi-\gamma$. One checks that $\mathbf{s}_a\cdot\mathbf{s}_b = (\mathbf{q}\times\mathbf{r})\cdot(\mathbf{r}\times\mathbf{p}) = (\cos a\cos b - \cos c)/\sin a \sin b$ etc., i.e., $\mathbf{s}_a\cdot\mathbf{s}_b = -\cos\gamma$, etc., by applying the cosine rules for the angles, specialized to the angle $\pi-c$. Equation (93) is also satisfied (it is obtained by applying the cosine rules for the edges, specialized to the edge of arc $\pi-\gamma$), and Eq. (94) is replaced by

$$\frac{\sin a}{\sin\alpha} = \frac{\sin b}{\sin\beta} = \frac{\sin c}{\sin\gamma} = \frac{V_{s_a,s_b,s_c}}{\sin\alpha\sin\beta\sin\gamma}. \tag{96}$$

Equations (94) and (96) are identical, and both are identical to Eq. (92), as can be shown by employing the standard identities

$$V_{p,q,r} \equiv \sin a \sin b \sin \gamma \equiv \sin b \sin c \sin \alpha \equiv \cdots,$$

$$V_{s_a,s_b,s_c} \equiv \sin \alpha \sin \beta \sin c \equiv \cdots,$$

which yield

$$V_{p,q,r} V_{s_a,s_b,s_c} = \sin \alpha \sin \beta \sin \gamma \sin a \sin b \sin c,$$

$$V_{p,q,r}^2 = \sin a \sin b \sin c V_{s_a,s_b,s_c},$$

$$V_{s_a,s_b,s_c}^2 = \sin \alpha \sin \beta \sin \gamma V_{p,q,r}.$$

The construction of a triangle of angular arcs $\pi-\alpha, \pi-\beta, \pi-\gamma$, of angles $\pi-a, \pi-b, \pi-c$, requires that the same inequalities are obeyed as for $T^{-}_{p,q,r}$.

Remark. The two tetrahedra **OABC** and **OPQR** are in conjugate positions on the two-sphere; the edge $\mathbf{s_a}$ of **OABC** is perpendicular to the facet (**OQR**) of **OPQR**, and the edge **p** of **OPQR** is perpendicular to the facet (**OBC**) of **OABC**, etc. Hence the appearance of the arc angles $\pi-\alpha$, conjugate to the angles α, etc., of the angles $\pi-a$, conjugate to the arc angles a, etc.

Both geometrical representations **OABC** and **OPQR** of the Kirchhoff relation for three disvections are equivalent; we retain the first one. They express that the set of disvections terminate on a disvection of angle π, whose direction w is not given a fixed value. In that sense, the terminal node can be interpreted as a singular point.

Notice also that the same {−1} disvection can be assigned to the spherical triangle (**PQR**)* outside the smaller triangle (**PQR**). This shows that, in the present representation of transvections, the full two-sphere S^2 has to be assigned the identity disvection {+1}, with angle 2π.

b. $h_Q^{(1)} h_Q^{(2)} h_Q^{(3)} = \{1\}$

Notice that $e^{-\pi p} = e^{-\pi q} = e^{-\pi r} = \{-1\}$. Hence the {+1} Kirchhoff relation of Eq. (89), for the angles α, β, γ and the angular arcs a, b, c, can be transformed to the following:

$$e^{(\pi-\gamma)r} e^{(\pi-\beta)q} e^{(\pi-\alpha)p} = \{-1\}, \tag{97}$$

which can be discussed like the previous one for the angles $\pi-\alpha, \pi-\beta, \pi-\gamma$ and the angular arcs $\pi-a, \pi-b, \pi-c$. The inequalities of Eq. (95) are now replaced by

$$a+b+c \geqslant \pi, \quad \alpha+\beta+\gamma \leqslant 2\pi, \tag{98}$$

i.e., the complementary ones to those for the case {−1}.

For the spherical representation of Eq. (97), see Fig. 30. Now the relevant angles are the external angles. There is no {−1} disvection at the point where the three disvections merge.

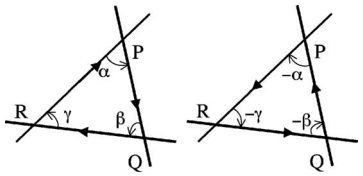

FIG. 31. Sketches representing conjugate disvections; see text.

2. Orientation vs handedness of a disvection

The *handedness* of a disvection is a topological concept; its *orientation* is related to the Volterra process; it does not make sense topologically.

We have not yet taken care of the orientations (of the disvection lines, or of the edges of the triangles $T^{\pm}_{p,q,r}$) and of the signs of the angles α, β, and γ. In the usual dislocation theory, the orientation of a dislocation line is fixed arbitrarily, from which orientation the sign of the related Burgers vector is deduced, but still depending on a convention, generally the so-called FS/RH (final start/right hand) convention (Nabarro, 1967). For a given orientation, the change of Burgers vector has a topological meaning, because **b** and **−b** are different translation symmetries. We have here a somewhat more subtle situation.

a. Topological considerations only

(i) The change of sign of a transvection, viz., $x \to x e^{\alpha p}$ changing to $x \to -x e^{\alpha p}$, does not connote the same disvection, for in such a case the triple node $e^{\alpha p} e^{\beta q} e^{\gamma r} = \{\pm 1\}$ changes sign: $e^{\alpha p} e^{\beta q} e^{\gamma r} = \{\mp 1\}$ is a different disvection. Hence a change of sign does not correspond to an arbitrariness in the orientation.

(ii) The change of sign of the angle of a transvection, viz., $x \to x e^{\alpha p}$ changed to $x \to x e^{-\alpha p}$, does not connote the same disvection. The triple nodes $e^{\alpha p} e^{\beta q} e^{\gamma r} = \{\pm 1\}$ and $e^{-\alpha p} e^{-\beta q} e^{-\gamma r} \neq \{\pm 1\}$ are different disvections, because of the noncommutativity of the transvections. A change of sign of the angle does not correspond to an arbitrariness in the orientation.

(iii) Two conjugate disvections, viz., $x \to x e^{\alpha p}$ and $x \to e^{-\alpha p} x$, are equivalent disvections. They are not equal, because they differ by the disclination $e^{-\alpha p} x e^{-\alpha p}$, which breaks a proper rotation, but a proper rotation does not modify chirality in the usual sense. This emphasizes the concept of conjugacy (change of handedness). The two equations $e^{\alpha p} e^{\beta q} e^{\gamma r} = \{\pm 1\}$ and $e^{-\gamma r} e^{-\beta q} e^{-\alpha p} = \{\pm 1\}$ are conjugate. The two oriented triangles of Fig. 31 (illustrating the case {−1}) are conjugate triangles.

b. Volterra process

The topological considerations above indicate that the lips of the cut surface of a disvection are displaced at x by the quantity $b(x) = x e^{\alpha p} - x$ (expressed as a quaternion), but there is no hint whether this process adds or removes matter. Once the choice is made, it can be related to an arbitrary orientation and a convention on the

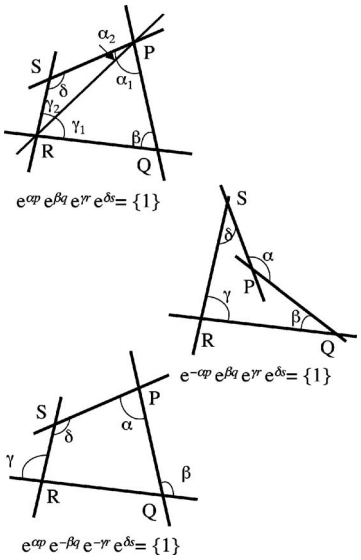

FIG. 32. Four disvections meeting at a node; representation on the unit two-sphere.

sign $\pm|\mathbf{b}|$, in the manner of dislocations. The situation is then much the same, and is independent of the handedness.

The situation is different with disclinations, because the opposite rotations $e^{-\alpha p}xe^{\alpha p}$ and $e^{\alpha p}xe^{-\alpha p}$ are both allowed topologically.

3. More than three disvections meeting at a node

Let

$$e^{\alpha p}e^{\beta q}e^{\gamma r}e^{\delta s}=\{1\} \tag{99}$$

be four disvections meeting at a node, $\mathbf{P},\mathbf{Q},\mathbf{R},\mathbf{S}$ the terminations of the directions $\mathbf{p},\mathbf{q},\mathbf{r},\mathbf{s}$ on the unit two-sphere, $\alpha=\angle(\mathbf{SPQ})$, $\beta=\angle(\mathbf{PQR})$, $\gamma=\angle(\mathbf{QRS})$, $\delta=\angle(\mathbf{RSP})$. They are represented in Fig. 32 (top) as a spherical quadrangle that can be split into two triangles $T^{-}_{p,q,r}$ and $T^{-}_{r,s,p}$. Equation (99) also holds if the triangles are of types $T^{+}_{p,q,r}$ and $T^{+}_{r,s,p}$, i.e., if the angles are all complementary to the inside angles of the quadrangle (not represented in Fig. 32). The two other sketches of Fig. 32 correspond to other possibilities mixing inside and outside angles.

More generally, a n-gon is the graphical representation of the meeting at a node of n disvections; the n-gon can be split into n triangles (in many ways), each of them of type $T^{+}_{p_i,p_j,p_k}$ or $T^{-}_{p_i,p_j,p_k}$.

4. Kirchhoff relations for disclinations

It suffices to consider one set of right disvections and one set of left disvections, separately. The results of the previous section apply to each set.

a. Three disclinations meeting at a node

Assume first that the right and left transvections in Eq. (88) are complex conjugate, $l^{(i)}_Q=\tilde{r}^{(i)}_Q$, and that the angles α_i and the directions p_i are such that they form a $\{-1\}$ triangle. The same triangle represents as well the left and right transvections (Fig. 31). Hence, because $\{-1\}^2=\{1\}$, the left and the right transvections all together amount to an identity isometry. The representative triangle, which is at the same time left and right, has then to be thought of as a $\{1\}$ triangle, i.e., a disclination of angle 2π. Taking into account the complementary triangle on the two-sphere, the full S^2 has to be assigned the identity isometry $\{+1\}^2$, with angle 4π.

Also, the rotation $l^{(i)}_Q x r^{(i)}_Q$ (with $l^{(i)}_Q=\tilde{r}^{(i)}_Q$) is of angle $2\alpha_i$, each disvection taking part by an angle α_i. We consider the Euclidean limit in the **OABC** representation. Keeping in mind that the rotation $l^{(i)}_Q x r^{(i)}_Q$ ($l^{(i)}_Q=\tilde{r}^{(i)}_Q$) is of angle $2\alpha_i$ ($\alpha_i=\frac{\omega_{\alpha_i}}{2}$, half the angle of the related disclination), and noticing that, in this limit, the quantities $\sin\alpha_i$, etc., are proportional to the edge lengths of a flat triangle, it appears that in this limit the vectors $\mathbf{f}_{\alpha_i}=2\sin\frac{\omega_{\alpha_i}}{2}\mathbf{p_i}$, etc., obey a Kirchhoff relation, as already observed for disclinations in $\{am/E^3\}$.

b. Extension to the generic case, when $l^{(i)}_Q$ and $r^{(i)}_Q$ are not complex conjugate

It is possible, as noted in Sec. VII.A.3, to split a rotation $l^{(i)}_Q x r^{(i)}_Q$ into two rotations with complex conjugate transvections. Such a splitting having been performed, we are back to the previous case.

5. Mixed case

Figure 33 indicates with two simple examples how disclinations and disvections can merge at nodes, in the particular case when the involved disvections all have the same strength, up to chirality (complex conjugacy). Notice that three disclinations of the same strength cannot meet at the same node, a seemingly obvious result, easily demonstrated by using the splitting of each disclination into two disvections of opposite hands.

These results are entirely topological, and do not take into account the orientations and signs of the disvections that have been previously discussed (Sec. VII.E.2). For

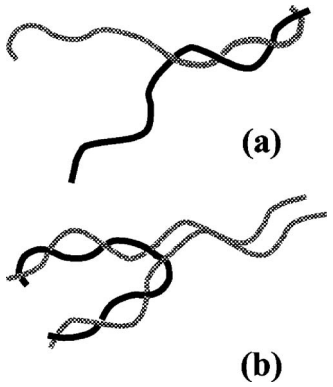

FIG. 33. Node relations for disvections and disclinations, mixed. A disvection is either left (black lines) or right (shaded lines). (a) Disclination split into two disvections of opposite hands; (b) disvection split into two disclinations.

example, in Fig. 33(b), one can assume that the two bundled right disvections are of opposite signs and the same Burgers vectors. Therefore the bundle annihilates and the two remaining disclinations are oriented the same way, making them together a unique disclination. Hence Fig. 33(b) is not at variance with the result of Sec. VII.D.2, established in the extended Volterra process fashion, which states that a twist disclination carries continuous disclinations, not disvections.

F. The {3,3,5} defects

A short discussion of the {3,5} and {3,3,5} groups is given in Appendix F.

We distinguish between disclinations, disvections, and defects that combine both types. In this section, we restrict to defects in the *nondecurved* {3,3,5} polytope.

1. Disclinations

There are 60 Volterra disclinations, when identifying "antipodal" elements in $\bar{Y}$. This number goes up to 120 in the TS classification, for which $\Pi_1(V_{\{3,3,5\}}) \sim \bar{Y} \times \bar{Y}$. Each element of rotation symmetry leaves invariant a great circle C_ω. For instance, for $|\omega| = 2\pi/5$, C_ω follows a sequence of ten spherical edges of the {3, 3, 5} polytope; in the locally Euclidean version of {3,3,5}, in which each spherical facet is approximated by a planar facet and each spherical edge by a straight segment in E^4, C_ω is a polygon with ten edges. Observe that a wedge disclination is a disclination loop along such a C_ω. The local rotation vector $\boldsymbol{\omega t}$ is along the tangent to C_ω; no attached dislocations (disvections) are necessary to curve the disclination line. See Nicolis *et al.* (1986) for a quantitative description of a disclinated {3,3,5} crystal in its habit three-sphere.

2. The disvection Burgers vectors

There are 60 left disvections $h_{\bar{\mathbf{Y}}} x\{1\} \equiv h_{\bar{\mathbf{Y}}} x$, and 60 right disvections $\{1\} x h_{\bar{\mathbf{Y}}} \equiv x h_{\bar{\mathbf{Y}}}$, when identifying antipodal elements in $\bar{Y}$. These numbers go up to 120 right disvections and 120 left disvections in the TS classification. Disvections leave no fixed point in {3,3,5}.

Consider the right screw $xe^{\alpha q}$, $x = x_0 + x_1 i + x_2 j + x_3 k$ being some {3,3,5} vertex **M** on the habit sphere S^3 of radius R. The displacement of **M** is $\Delta x = xe^{\alpha q} - x$, whose absolute value $|\Delta x|$ is $|x||e^{\alpha q} - 1| = 2R \sin \frac{\alpha}{2}$. The left screw $e^{-\alpha q} x$ has the same Burgers modulus $|\Delta x|$ as the right screw; it is a constant independent of x. However, the direction of $\Delta\mathbf{x}$ varies with **M** in {3,3,5}: it is tangent to the Clifford parallels belonging to the Hopf fibration related to q (Fig. 36), Appendix D.

There are two such Burgers vectors at each point, one right and one left. Thereby, $\Delta\mathbf{x}$ is not a Burgers vector in the ordinary sense, but it would tend to a constant vector if the radius R of {3,3,5} is allowed to increase without limit; however, this process has no physical meaning, and we see later on another method to transform $\Delta\mathbf{x}$ into a genuine Burgers vector.

Taking $\alpha_5 = \frac{\pi}{5}$, we find $|\Delta\mathbf{x}|_5 = R\tau^{-1}$, which is precisely the length of an edge of the polytope {3,3,5}. This Burgers vector is the smallest possible. It displaces **x** to one of its 12 nearest neighbors, which are at the vertices of an icosahedron. The orbit of **x** under the repeated action of the right screw is a geodesic circle $C_{5,\text{right}}$ that is approximated by a ten-edge polygon. The coordinate x_0 measures the distance to the geodesic circle C_p along the 0 axis. The angle β_5 made by the orbit of **x** with C_p is $\text{arc}(x_0)/2R$ (Sommerville, 1967). The same considerations apply to a left screw, yielding the same absolute value for the Burgers vector, but directed now along another great circle $C_{5,\text{left}}$ at **x**, with angle $-\text{arc}(x_0)/2R$. Hence, the spherical angle between the two circles $C_{5,\text{right}}$ and $C_{5,\text{left}}$ at **x** is $\text{arc}(x_0)/R$, which has to be equal to $2\pi/5$ (five ten-edge great circles emanating from any vertex and belonging to a geodesic two-sphere). Observe that the notion of right or left is relative to C_p. A C_5 has an intrinsic meaning; there are 72 different C_5s, since there are 120 vertices and since 6 C_5s are incident at each vertex ($6 \times 120/10 = 72$). There are 48 right (48 left) screws whose angle is a multiple of $\pi/5$ (72° of arc, 288° of arc, 144° of arc, 216° of arc) along six possible directions from each vertex. The Burgers vectors have respective lengths $R\tau^{-1}$, $R(3-\tau)^{1/2}$, $R\tau$, and $R(2+\tau)^{1/2}$. They all join **x** to the vertices of icosahedra of edge lengths $R\tau^{-1}$ for the first and R for the three others. The Burgers vectors of length $R(3-\tau)^{1/2}$ join **x** to its 12 third nearest neighbors, which also form an icosahedron (Coxeter, 1973).

We also have $|\triangle x|_3 = R$ for $\alpha_3 = \frac{\pi}{3}$—this is the distance from the center x of a dodecahedron (edge length $R\tau^{-1}$) to its 20 vertices, which are the next-nearest neighbors of **x**; these are not the vertices of the {3,3,5} polytope, but the centers of the {3,3,5} triangular facets; $|\Delta x|_2 = \sqrt{2}R$ for $\alpha_2 = \frac{\pi}{2}$—this is the distance from the center **x** of an icosidodecahedron (edge length $\sqrt{2}R$) to its 30 vertices, which are the fourth nearest neighbors of **x**. Observe that the edge length can be larger than the radius of the habit sphere (Coxeter, 1973). These vertices are the midpoints of the {3,3,5} edges.

3. Screw disvections

In analogy with the Euclidean case, we define a *screw disvection* as a disvection line parallel to the Burgers vector, which in our case points out a great circle C_n, $n = 2$, 3, or 5. We have emphasized above the $n = 5$ case. The cut surface can be any surface bound by C_5, for example, half a great two-sphere. Now, in analogy with the classical Euclidean case, we are interested in an ideal cut surface Σ_s that slips along itself in the Volterra process. An ideal cut surface of a screw disvection (i.e., a loop) has to be parallel to the Burgers vectors, which are supported by a set of Clifford parallels. Several possibilities exist.

(i) C_p being the axis about which C_5 is twisted, drop a segment of geodesic $C_\perp$ (an arc of great circle) perpendicular to C_p between any point of C_5 and C_p; this operation determines a unique point on C_p if C_5 and C_p are not conjugate, any point on C_p if $C_5=\tilde{C}_p$.

(ii) The surface generated by the great Clifford circles parallel to C_5 and lying on $C_\perp$. In effect, consider two conjugate great circles C_5 and $\tilde{C}_5$, generated by a fivefold axis; these conjugate geodesics are indeed ten-edge great circles, as shown by Coxeter (1991). Assume that the screw disvection line is along C_5. The Burgers vector varies in direction along C_5 and the cut surface, but has a constant modulus, as shown above. It is along the tangent to C_5. The cut surface is made of Clifford parallels to C_5 and $\tilde{C}_5$ which stretch on the skew surface Σ_s between C_5 and $\tilde{C}_5$. The Burgers vector attached to each point of Σ_s is, by construction, along the local Clifford parallel, and the Volterra process consists in a movement of Σ_s in its surface.

4. Edge disvections

An ideal cut surface Σ_e of an edge disvection loop has to be orthogonal to the Burgers vectors, which are supported by a set of Clifford parallels. Therefore according to the previous discussion, Σ_e is a cap of a great sphere, bound by a loop of any shape.

VIII. DISCUSSION

The foregoing discussions present a general view of disclinations and dislocations. The emphasis is on (i) their interplay with continuous defects (themselves characterized as continuous dislocations, disclinations, or dispirations) in the constitution of defect textures in all media with continuous and frustrated symmetries; (ii) their various relaxation processes as they can be approached by the consideration of defects, in particular continuous ones.

These questions are not entirely new, as can be seen from the literature, but they have been largely ignored in the ill-ordered media community. The purpose of the present article is to stress the changes of perspective which occur in the theory of defects in mesomorphic phases (liquid crystals) and other ill-ordered media, when the notions of disclination and continuous defects and the correlated use of the Volterra process are fully used, in concurrence with the topological stability theory of defects. Central to that analysis is the concept of the extended Volterra process, essential to the understanding of disclinations: this considers, in the last stage of the process, a viscous or plastic relaxation of the elastic stresses developed.

The other approaches to the defects in ill-ordered media are of two sorts. Only the second one is directly comparable to the Volterra process approach.

(i) In liquid crystals with quantized translation symmetries, like smectics or columnar phases, many observations can be described in purely geometrical terms as isometric singular textures, largely inspired by the work of Georges Friedel in the first decades of the twentieth century (Friedel and Grandjean, 1910; Friedel, 1922); focal conic domains and developable domains, which obey rather restrictive geometric properties, are of this sort. But the geometrical approach to defects is limited to situations where the role of continuous defects can be set aside. For a review, see Kleman *et al.* (2004). It is a rather remarkable fact that some mesomorphic liquid phases adopt, on rather huge sizes compared to molecular sizes, configurations that obey very precise geometrical rules, and that these configurations are directly related to the structural symmetries of the medium. These configurations are worth investigation and they continue to be of interest today. But these investigations did not inspire considerations leading to the present theory of defects.

(ii) In contrast to the emphasis on the geometrical point of view, and since the late 1970s, when the theory appeared, the basic concepts of defect classification in mesomorphic phases and in frustrated media are those of topological theory. The topological theory relates the stability of defects to the topological properties of the order parameter; it is concerned only with discrete, quantized, defects. That topological stability leads to energetic metastability is in many cases a reasonable assumption, which, however, cannot distinguish between different topologically equivalent configurations.

A. The extended Volterra process

1. Pure Volterra process in the absence of plastic relaxation: Constitutive defect densities

The pure Volterra process has been widely employed in the study of material deformation (Frank, 1950b; Friedel, 1964); it applies to the construction of a Volterra disclination in a solid, but only to a limited extent. One distinguishes two cases.

a. Perfect disclinations

The only case is that one of a straight, wedge, disclination line in a Volterra continuous elastic body or in a crystalline solid, with rotation vector $\mathbf{\Omega}$ parallel to the line, $\mathbf{\Omega}$ being a symmetry operation of the crystal.

b. Imperfect disclinations

This includes (i) straight wedge Frank grain boundaries, which are analyzable: in an amorphous medium, in terms of parallel infinitesimal dislocations, uniformly distributed, and in a solid crystal, in terms of finite dislocations, at least for small rotations; (ii) straight twist lines or lines of a more general shape, which absorb or emit constitutive dislocations attached to the line or in its vicinity. In a solid medium with no relaxation, these disclinations require very large energies to be created and also to move: their creation involves large stress concentrations extending over large regions; their motion would, whatever their nature, leave behind a stream of dislocations that could be dispersed only by slip

and/or climb. These properties are related to the fact that, in such a solid without relaxation, the long-range elastic energy is large as long as Ω is finite and the solid is of macroscopic size; the core energy is also large when the position of the lines deviates from the axis of rotation. Except for borderline cases involving disclinations of very small rotations, connected with weakly polygonized grain boundaries in crystals, disclinations in solids have not been observed as isolated objects, but only regrouped in close parallel strands with compensating strengths: parallel wedge pairs of opposite rotations in single crystals [described, e.g., by Friedel (1964)] or triplets with rotations following a Kirchhoff relation, at the edges of the grains in relaxed polycrystals, as in Sec. III. In this last case, the twist components of the involved disclinations exchange their constitutive dislocations. In the absence of possible relaxation by slip or climb, these are all sessile defects.

Remark. The pure Volterra process applies only if $\Omega > -2\pi$, since below this limit there is no matter left. But any value in the range defined is allowed, even if the configuration is topologically unstable. Notice also that there is no limitation on the choice of the cut surface Σ with respect to crystalline symmetries, but this yields different dislocation configurations with different energies, e.g., a tilt grain boundary if the rotation vector $\mathbf{\Omega}$ [Eq. (1)] is in the plane of Σ, with a set of parallel edge dislocations; a twist grain boundary if the rotation vector is perpendicular to the plane of Σ, with two crossing sets of parallel screw dislocations.

2. Extended Volterra process: Relaxation defect densities

Some plasticity of the medium can allow dislocations to relax. Disclinations are relaxed either by Nye dislocations or/and by absorbed or emitted attached defects.

a. Nye dislocations

Nye dislocations compensate as far as possible for dislocations of the grain boundaries associated with the disclination. They widen the singular core of topologically unstable disclinations (as for a $k=n$ line in a nematic). They can be included in the extended Volterra process, in the last step which takes into account the plastic relaxations allowed by the boundary conditions and symmetries.

Notice that the extended Volterra process includes $\Omega \leqslant -2\pi$.

b. Emitted or absorbed dislocations

Emitted or absorbed dislocations play a prevailing role when the disclination moves or changes its shape, in interplay with Nye dislocations. And, like Nye dislocations, they can be included in the extended Volterra process, also taking into account the allowed plastic relaxations. They can be induced: in a solid, either by high-temperature diffusion or by plastic deformation at low temperature (or twinning, or crack formation), in a liquid crystal by the anisotropic flow of matter.

3. Mostly liquid crystals

It has been known for a long time, since well before the emergence of the topological theory, that the geometrical variability, the energetic (as opposed to topological) stability, and the elastic relaxation of defects in cholesterics (Friedel and Kleman, 1969) are largely controlled by relaxation defect densities. This occurs through mechanisms, not yet thoroughly investigated, that involve continuous symmetries of the medium. A continuous defect, just like a quantized defect in the Volterra classification, is related to a symmetry element of the liquid crystal, precisely a continuous symmetry. In topological theory, it always belongs to the identity element $\{1\}$ of the first homotopy group $\Pi_1(V)$; in that sense, a continuous defect is never topologically stable. Continuous defects are often attached to quantized disclinations, whose flexibility and relaxation they control. Similar results apply to all mesomorphic phases, as they display continuous symmetries. The extended Volterra process was presented by Friedel and Kleman (1969), but has not been developed since. It is interesting to note that even Georges Friedel's "rigid" defect geometries show different aspects when discussed in terms of continuous dislocations.

Remark. Some noncontinuous Volterra disclinations also belong to $\{1\}$. For instance, in uniaxial nematics N, the Volterra process provides two types of quantized disclinations, those whose rotation angle is an odd multiple of π, and those whose rotation angle is a multiple of 2π. Only the defects of the first type are recognized as being topologically stable (i.e., differing from $\{1\}$); the defects of the second type belong to $\{1\}$. This is so because the liquid-crystal symmetries contain a continuous rotation subgroup (not present in solid crystals) whose presence drives the first homotopy group finite, whereas the group of Volterra defects is infinite. In practice, quantized defects that are not allowed by the topological theory are also of interest, as it may happen, for instance with suitable boundary conditions, that the energetic stability of the defect prevails over its topological stability. In this sense these quantized disclinations which carry an angle of rotation multiple of 2π are true disclinations.

Since a deformed mesomorphic phase is a liquid, there are no strains at rest; but there are large curvature deformations that can be analyzed in terms of Nye densities (Kleman, 1982b), continuous dislocations, or continuous dispirations. Since continuous defects are topologically related to the continuous symmetries of the mesomorphic phase, this puts limitations on the possible curvature deformations of the medium in the vicinity of quantized disclinations, and on the shape modifications and mobility of those defects.

Indeed, a continuous transition between Hooke strain elasticity for solids and Frank-Oseen curvature elasticity for mesomorphic phases is ensured by a continuously growing density of dislocations whose Burgers vectors decrease and vanish in such a way that the total Burgers vector remains constant.

4. Extended Volterra process vs topological stability

a. The topological stability theory

The topological stability theory considers only defects that cannot be suppressed by plastic relaxation. It provides an *a posteriori* description that results from a mapping of the distorted medium onto the order-parameter space $V=E^3/H$. Quantized dislocation and disclination invariants $\{a_i\}$ belong to the first homotopy group of the order-parameter space $\Pi_1(V)$, which is usually non-Abelian.

The topological approach has the advantage of being extendible to defects of any dimensionality (point, line, and wall defects, and configurations). It is a more condensed process but a poorer one than the Volterra process, as it neglects the boundary conditions and makes equivalent all configurations that can be deduced one from the other by continuous deformations. For such deformations to occur, a high degree of plasticity is required, which does not occur in solids at low temperatures, whether crystals or glasses, and other amorphous systems, but is present in liquid crystals and ferromagnetics. The approach does not always allow prediction of the stabler configuration in ordered media, still less prediction of the finer details of any configuration. By neglecting the topologically unstable situations, TS makes the bet that the corresponding singularities do reduce their energy by dissipating in some way. This bet is most often justified; however, it might fail in the presence of special boundary conditions, as the $k=1$ nematic line in a capillary tube (Cladis and Kleman, 1972; Meyer, 1973) and more generally in thin samples, where their broad core was well known to Friedel (1922). Also, in the presence of strong material constant anisotropies, a $k=1$ disclination core may be singular—this latter situation is met in nematic main-chain polymers (Mazelet and Kleman, 1986).

b. The extended Volterra process

The extended Volterra process is an *a priori* description of defects, as it gives a process of creation of line defects (only) whose characteristic invariants are classified by the elements of the symmetry group H of the medium in a medium free of stresses.

It yields the same conclusions as the topological stability theory, but at a finer level, by properly handling all plastic relaxations, including those related to line-attached defects. This approach can be useful when investigating dynamical aspects, when the viscosity is large as in solids, in most smectics, and in polymeric liquid crystals (Friedel, 1979; Kleman, 1984). It is also useful when dealing with nanostructures. This is at the price of an often much more complex analysis.

5. Reconsideration of *a posteriori* Volterra description of a defect in an amorphous medium

A Volterra constructed disclination is qualified by the line direction with respect to the rotation vector: it is a wedge, twist, or mixed disclination line. Similarly, a dislocation is a screw, edge, or mixed dislocation line. Such specificity does not characterize a line defined by its topological invariant. The question therefore arises as to whether it is possible to qualify any given line of the deformed medium in the same terms. This requires an *a posteriori* description of the defect, i.e., some kind of mapping that brings back the deformed medium to a stress-free reference medium, from which the line has been supposedly constructed in the Volterra mode.

This program seems feasible when the reference medium is endowed with a 3D crystal lattice L whose equivalent directions and equivalent points can be recognized in the deformed medium. Directions can be followed along circuits surrounding disclinations, and a rotation or Frank vector obtained that is unique in the reference lattice. This is how the Kirchhoff relations are established.[7]

This consideration, namely, the possibility of fully characterizing an isolated dislocation or disclination, extend to the continuous theory of defects of Bilby, Kröner, and so on, which always assumes explicitly the presence of a lattice, whose repeat distances are most certainly taken infinitesimally small, but this does not invalidate our reasoning. The continuous theory, in a way, contemplates continuous sets of isolated defects, whose Burgers vector is nonetheless infinitesimally small. For this purpose it employs the methods of differential geometry on manifolds. It is precisely the existence of a lattice that justifies the use of the Cartan-Levi-Cività distant parallelism method in the continuous theory of defects. For if equivalent points and directions did not exist in the deformed medium, the comparison of vectors at two distant points would make no sense. It then follows that there are quantized disclinations in an amorphous medium, but their characteristics depend on the gedanken lattice drawn on it; therefore they do not present physical interest. We have considered only continuous disclinations in amorphous media in this article.

B. Volterra processes in various media compared

The Volterra process applies to amorphous and frustrated media as well as to liquids, solid crystals, and templates of frustrated media. There are, however, some differences worth stressing.

a. Amorphous medium

In an amorphous medium, the translation vector and the rotation vector that define the relative displacement of the cut surface are elements of the full Euclidean group E^3. The related defects are not topologically stable. Dislocations and finite disclinations are noninde-

[7]Notice that the Burgers vector of a dislocation surrounding a disclination $\mathbf{\Omega}$ is not uniquely determined this way; it is defined but to a rotation $\mathbf{\Omega}$, as first noticed by Sleeswyk (1966), see also de Wit (1971) and Harris and Scriven (1970, 1971). This is a small complication stressed in Sec. II.E.1, whose effect on the Kirchhoff relations has not been investigated.

pendent defects. A finite disclination carries a field comprising constitutive and relaxation dislocations. It also possibly carries infinitesimal disclinations. The constitutive and relaxation dislocations relate to the strength of the line and to a part of its curvature (through the kink mechanism); the infinitesimal disclinations relate to another curvature component. These infinitesimal disclinations correspond to infinitesimal rotations belonging to the rotational part of the Euclidean group, whereas the strength of a finite disclination is characterized by invariants associated to the constitutive and relaxation dislocations, i.e., belonging to the translational part of the Euclidean group only; these translations generate the Frank vector associated with the finite disclination.

b. Solid crystal

In the solid crystal, the characteristic Volterra invariants of the defects are the translation and rotation elements of its Euclidean symmetry group H, whose elements classify dislocations and disclinations (necessarily finite) as now independent defects. However, the concepts of constitutive and relaxation dislocations still make sense. Because there are no infinitesimally small rotations in H, a line can be curved only by the kink mechanism, which makes use of finite relaxation dislocations. On the other hand, a straight disclination line is necessarily of wedge character, as there are no infinitesimal dislocations to give it a twist character.

Notice that this description applies better to coarse-grained crystals with a quasi-perfectly-polygonized, annealed structure. Most grain boundaries in a polycrystal are strongly misorientated, like polynanocrystalline materials below.

c. Polynanocrystal

In a polynanocrystal, the nanograins are separated by generally large misorientation grain boundaries which thereby are not analyzable in terms of quantized dislocations (those of the crystal) but rather in terms of continuous dislocations. In an ideal picture, three grains meet along a segment of (continuous) disclination, and these segments meet at quadruple nodes, forming then a 3D disclination network. The plastic deformation of polynanocrystals is at variance with that one of usual polygonized crystals; it is governed by the disclinations, which yields considerable stresses. Disclination-governed plastic deformation has long been a subject of the Saint Petersburg Russian school [see Romanov and Vladimirov (1992) for a review], without attracting much attention elsewhere.

d. Liquid crystal

In a liquid crystal, the characteristic invariants of the defects are as above the translation and rotation elements of a Euclidean group H, whose elements classify dislocations and disclinations as independent defects. But, according to the case, the corresponding translation and rotation symmetries are finite or/and continuous, including infinitesimally small elements. In a nematic (N) liquid crystal, translation symmetries are continuous, including infinitesimally small elements, and rotation symmetries are of both types. In a SmA liquid crystal, there are quantized and continuous translation and rotation symmetries. Line defect curvatures are therefore related to both the kink mechanism, through (quantized or continuous) dislocations, and the presence of infinitesimally small strength disclinations.

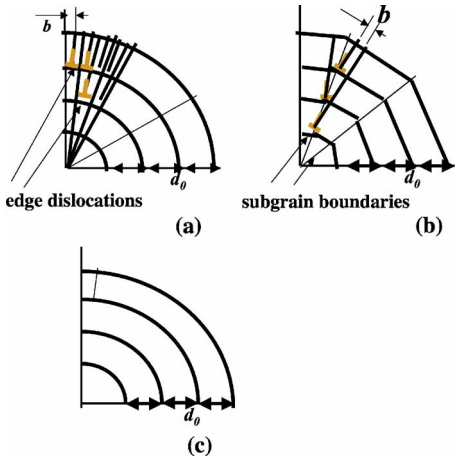

FIG. 34. (Color online) Genealogy of Nye's dislocations. These represent the gradual passage from a situation where (a) a random density of finite dislocations imposes curvature and strain to a situation where (c) the Burgers vectors becoming infinitesimal, the strain vanishes but the curvature subsists. In between (b), the dislocations of (a) have organized into subgrain boundaries.

e. Curved habit spaces of frustrated media

In the curved habit spaces of frustrated media, like $\{\mathrm{am}/S^3\}$, $\{3,3,5/S^3\}$, and $\{dtw/S^3\}$, dislocations (which we call disvections) are not commutative, and disclinations can still be defined, with the same differences as above between amorphous media and crystalline media. Generically, disvections do not attach to disclinations, but disclinations do. Three-dimensional disclination networks are therefore important features of the habit curved spaces, if one draws one attention to the plastic deformation of such spaces at constant Gaussian curvature.

Disclinations also form 3D networks in actual, Euclidean, amorphous systems, liquid crystals such as cholesteric blue phases, Frank and Kasper phases, and probably in undercooled liquids or quasicrystals. In such 3D networks, the disclinations have to be somewhat flexible, which is possible, whether these disclinations are quantized or not, only if other defects, dislocations (defined in the Euclidean decurved medium) or disclinations, continuous or not, attach to them.

ACKNOWLEDGMENTS

We thank Yves Bréchet, Jean-Luc Martin, and Helena Van Swygenhoven for discussions on nanocrystals, and Randall Kamien for a useful remark on the TGBA

phase and for encouragement. We are also grateful to Claire Meyer, Yuriy Nastishin, and Oleg Lavrentovich for permission to reproduce some of their artworks. M.K. would like to thank Claire Meyer and Yuriy Nastishin for discussions on continuous defects in mesomorphic phases.

APPENDIX A: CONTINUOUS DISLOCATIONS IN SOLIDS AND NYE'S DISLOCATION DENSITIES

This is a simplified presentation of a topic that has been very inspiring for the theory of continuous dislocations.

We consider a deformed body described in terms of deformations β_{ij} or of strains $e_{ij}=\frac{1}{2}(\beta_{ij}+\beta_{ji})$, and assume that these quantities are so small that it is permissible to ignore second-order terms. As is well known, it suffices to know the strains e_{ij} in order to derive the stresses and the elastic energy, so that the deformations β_{ij} are generally ignored. In the absence of elastic singularities (dislocations, disclinations), the β_{ij}'s are derived from a displacement $\beta_{ij}=u_{j,i}$ (we use the notation $u_{i,j}=\partial u_i/\partial x_j$). The Beltrami conditions (that the strains have to obey in order to ensure the existence of a displacement function) are

$$(inc\mathbf{e})_{ij} \equiv \varepsilon_{ijk}\varepsilon_{lmn}e_{jm,kn} = 0. \tag{A1}$$

Here we have introduced the incompatibility tensor $(inc\mathbf{e})_{ij}\equiv\varepsilon_{ijk}\varepsilon_{lmn}e_{jm,kn}$; it does not vanish in the presence of elastic singularities.

The condition for the existence of a displacement function takes a much simpler form in terms of the β_{ij}'s,

$$\alpha_{ij} \equiv -\varepsilon_{ikl}\beta_{lj,k} = 0. \tag{A2}$$

The theory of continuous dislocation densities emphasizes the role of the tensor α_{ij}; when there is no displacement function, it does not vanish, and it can be interpreted in terms of dislocation densities; we refer the reader for details to Kröner (1981); see also Kröner (1958) and Nabarro (1967), Chaps. 1 and 8.

The integral $\Delta u_i=-\int_{\partial\sigma}\beta_{ij}dx_i=-\int\int_{\sigma}\alpha_{kj}dS_k$ on a loop $\partial\sigma$ that bounds the surface element σ vanishes if the strain derives from a displacement function ($\beta_{ij}=u_{j,i}$); if this is not the case, the one-form $\beta_{ij}dx_i$ is not integrable, and the integral measures a displacement vector Δu_i. $\Delta\mathbf{u}$ is interpreted as the Burgers vector of the dislocation densities that pierce the surface bounded by $\partial\sigma$; α_{ij} is the density of dislocations along the x_i axis; it measures the total Burgers vector component along the x_j axis of the set of dislocations through the unit area perpendicular to the x_i axis. For a dislocation L of finite Burgers vector $\mathbf{b}$ along a direction $\mathbf{t}$, one gets $\alpha_{ij}=-t_ib_j\delta(L)$.

Now, again after Kröner, we write α_{ij} as

$$\alpha_{ij} = -\varepsilon_{ikl}e_{lj,k} + \omega_{i,j} - \omega_{k,k}\delta_{ij}, \tag{A3}$$

by splitting $\beta_{ij}=e_{ij}+\omega_{ij}$ into a symmetric part e_{ij} and an antisymmetric part ω_{ij}. We have introduced $\omega_i=\frac{1}{2}\varepsilon_{ikl}\omega_{kl}$ (reciprocally, $\omega_{ij}=\varepsilon_{ijk}\omega_k$), which yields $\omega_i=\frac{1}{2}\varepsilon_{ikl}\beta_{kl}$; hence the relation (A3). If e_{ij} is "compatible," i.e., $\alpha_{ij}=0$, we have $\omega_i=\frac{1}{2}\varepsilon_{ikl}u_{l,k}$. In the generic incompatible case, the β_{ij}'s and ω_i's have to be given new interpretations, which we detail below.

For the time being, notice that ω_i measures the rotation of an element of volume with respect to the lattice directions (ω_3 is a rotation about the x_3 axis with respect to the x_1 axis and the x_2 axis); according to Eq. (A3) it contains two contributions to the rotations, one coming from the strains and the other from the dislocation densities α_{ij}. This splitting into two contributions makes sense, because it is possible to conceive an ordered medium with no strains but a density of dislocations, the Nye's dislocation densities (Nye, 1953), at the origin of the rotation distortions. An example is given in Fig. 34, directly inspired by Nye's analysis. In a strainless medium, these densities read

$$\alpha_{ij} = \omega_{i,j} - \omega_{k,k}\delta_{i,j}, \tag{A4}$$

which can also be written

$$\omega_{i,j} = \alpha_{ij} - \frac{1}{2}\alpha_{kk}\delta_{i,j}. \tag{A5}$$

In the general case, the gradient tensor of the rotations is

$$\omega_{i,j} = \varepsilon_{ikl}e_{lj,k} + \alpha_{ij} - \frac{1}{2}\alpha_{kk}\delta_{i,j}, \tag{A6}$$

where the two contributions (from the strains, and dislocation densities) are separately nonintegrable.

Of course, this model is valid as long as the rotations ω_i are small. In the smectic case discussed, the ω_i's measure the rotation of the orthonormal Darboux-Ribaucour trihedron from its equilibrium position along the principal axes of the shell (Darboux, 1894).

There is no equivalence between a description in terms of Nye's dislocation densities and a description in terms of strain dislocation densities; in other words, the solutions in β_{ij} of the equation $\alpha_{ij}\equiv-\varepsilon_{ikl}\beta_{lj,k}=\omega_{i,j}-\omega_{k,k}\delta_{i,j}$ are such that $\beta_{ij}+\beta_{ji}=0$. Reciprocally, the solutions in β_{ij} of the equation $\alpha_{ij}\equiv-\varepsilon_{ikl}\beta_{lj,k}=-\varepsilon_{ikl}e_{lj,k}$ are such that $\beta_{ij}-\beta_{ji}=0$. Descriptions in terms of Nye's dislocations and of strain dislocations are exclusive one from the other.

The gradual passage depicted in Fig. 34 can also be thought of as a gradual transformation of a solid (with quantized dislocations carrying strains) into a SmA phase (with continuous Nye dislocations only). In this transformation, the distorted solid crystal elasticity gradually becomes the elasticity of the distorted smectic phase. More generally, the prevalence in mesomorphic phases of Nye's dislocations over quantized dislocations is the sign of their liquid character, and the origin of the Frank-Oseen elasticity (Frank, 1958), replacing the Hookean elasticity.

Returing to the physical meaning of the β_{ij}'s and ω_i's in the generic incompatible case, β_{21} describes a *plastic* distortion that displaces an element of volume with a finite section $\Delta x_1\Delta x_2$ along the x_1 axis, by a quantity $\beta_{21}\Delta x_2$. This distortion can be managed by the *glide*

along the same axis of a set of edge dislocations parallel to the x_3 axis, with Burgers vectors along the x_1 axis. There is no change of volume density.

β_{22} describes a plastic distortion that elongates (or shortens, according to the sign) an element of volume with a finite section $\Delta x_1 \Delta x_2$ along the x_2 axis, by a quantity $\beta_{22}\Delta x_2$. This distortion can be managed by the *climb*, along the same axis, of a set of edge dislocations parallel to the x_3 axis, with Burgers vectors along the x_2 axis. There is a relative change of volume density equal to β_{22}.

ω_3, discussed above, can also be thought of as the result of two glide operations, β_{21} and $-\beta_{12}$.

In the present theory, no account is taken of disclination densities, since the rotation $d\omega_i = \omega_{i,j} dx_j$ is, of course, integrable: the density of disclinations vanishes.

In fact this theory computes the minimum density of dislocations necessary to produce a given distortion of the medium. It assumes that this results from dislocation creation and annihilation, as well as from motion by glide and climb. Such hypotheses are well satisfied in magnets or liquids or (partly) in liquid crystals. They are not generally satisfied in solids, except partly at very high temperatures. As in TS theory, it assumes perfect plastic relaxations, but for given boundary conditions.

APPENDIX B: TOPOLOGICAL STABILITY AND VOLTERRA PROCESS COMPARED, CONJUGACY CLASSES AND HOMOLOGY

To begin, notice that $L \mapsto (0,a)$ and $L'' \mapsto (2,a)$ are in the same conjugacy class of the first homotopy group; in fact, all elements $(2p,a)$, $p \in Z$, belong to the same conjugacy class and represent the same core type of disclination; the other type of core corresponds to the conjugacy class $(2q+1,a)$, $q \in Z$. Each core-type of disclination, i.e., each conjugacy class can be identified in the Volterra classification with two types of disclinations, $k = \pm\frac{1}{2}$, differing by the sign: the topological classification does not distinguish $k=\frac{1}{2}$ and $k=-\frac{1}{2}$. There is an infinite number of other conjugacy classes, corresponding to the dislocations, each defined by a positive integer r and containing two elements $\{(r,e),(-r,e)\}$, i.e., two Burgers vectors equal in modulus, opposite in signs. All together one has $\infty+2$ conjugacy classes:

$$\left.\begin{array}{c} C_r:\{(r,e),(-r,e)\} \quad r \in Z^+ \cup \{0\} \\ C_1:\{(2p+1,a)\} \quad p \in Z \\ C_2:\{(2q,a)\} \quad q \in Z \end{array}\right| . \tag{B1}$$

Each conjugacy class therefore corresponds to an element of the Volterra classification, although it does not specify whether the line is twist, wedge, etc. This assertion can be made more accurate as follows. The classes C_{2r}—they represent dislocations whose Burgers vector is even—are commutators of $\Pi_1(V_{\mathrm{Sm}A})$; it is indeed not difficult to prove that any element of the form $uvu^{-1}v^{-1}$, where $u,v=(n,a)$, belong to a C_{2r}. The commutators generate a normal subgroup of $\Pi_1(V_{\mathrm{Sm}A})$—the so-called derived group D—such that $\Pi_1(V_{\mathrm{Sm}A})$ can be partitioned into cosets c_i,

$$\Pi_1(V_{\mathrm{Sm}A}) = \sum_i c_i = \sum_i u_i D = D + u_1 D + u_2 D + u_3 D, \tag{B2}$$

with $c_0 = D$, $c_1 = (2p+1,a)D$, $c_2 = (2q,a)D$, $c_3 = (2r+1,e)D$. It is easy to check that the content of each coset is independent of the values of the integers p, q, and r. Furthermore, all elements of C_1 belong to c_1, those of C_2 belong to c_2, and those of all C_{2r+1} belong to c_3. Finally, $\Pi_1(V_{\mathrm{Sm}A})/D = \{c_0,c_1,c_2,c_3\}$ is an Abelian group whose identity element is c_0. It is the dihedral group D_2; its multiplication rules $c_1c_3 = c_2$, $c_2c_3 = c_1$ reproduce the effects described above of the emission or absorption of a dislocation with an odd Burgers vector at the core of a disclination. Two disclinations of different core types give an odd dislocation, when merging: $c_1c_2 = c_3$. All the odd dislocations appear as one and the same element c_3; the even dislocations appear in the identity element c_0. More generally, $\Pi_1(V)/D$ is an Abelian group, called the first homology group, noted $H_1(V,Z)$.

Let Ω_1 be some rotation symmetry axis in a SmA liquid crystal; an axis Ω_2 obtained by any rotation of Ω_1 about the normal to the layers is also a rotation symmetry axis. However, the two wedge disclinations L_1 and L_2 are not distinguished by the topological classification, which assigns indifferently the element $(0,a)$ to both. The latter result is another weakness of the topological classification, which originates in the presence of a continuous rotation symmetry about the layer normal in a SmA phase. The same difficulty does not arise with a SmC phase, whose first homology group is also D_2, whereas the conjugacy classes are twice as numerous as in a SmA phase; $\Pi_1(V_{\mathrm{Sm}C}) = Z \square Z_4$; see Bouligand (1974), Bouligand and Kleman (1979). Observe that the symmetry point group of a SmC phase is $H_{\mathrm{Sm}C} = Z \square Z_2$ (reflections excluded), and that D_2 is precisely the quotient of the point group by its derived group. $Z \square Z_2$ is the Volterra group of defects (it is easy to check that it contains the two kinds of rotation axes, those in the layer planes, and those in the midlayer planes, all perpendicular to the mirror plane), and D_2 can be understood as the Volterra group restricted to its Abelian properties. The SmC point group is a quantized group, and the relation just indicated between the Volterra group and the homology group can be extended to any medium with a quantized point group (reflections excluded). The same relation does not hold when the point group is continuous, as it is for SmA ($H_{\mathrm{Sm}A} = Z \square D_\infty$); see Kleman (1982b), Chap. 10.

But in both cases the even dislocations are lumped in the identity element of $H_1(V,Z)$. In both cases, and eventually in all cases of ordered media, the Volterra

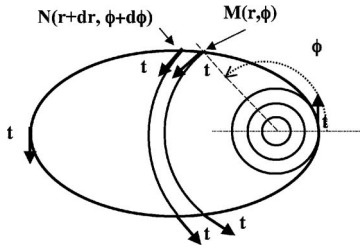

FIG. 35. Distribution of the rotation vectors $\mathbf{\Omega}=\pi\mathbf{t}$ on an ellipse in a focal domain. The layers intersect the plane of the ellipse along circles centered in one of the foci.

classification has a stronger kinship with the set of conjugacy classes of $\Pi_1(V)$ than with $H_1(V,Z)$. The lumping of even dislocations in the identity element of the first homology group is, of course, a weakness of the homology classification; a tentative explanation has been given by Kleman (1982b), Chap. 10, where a more general discussion of the conjugacy classes and of the homology classification in any ordered medium can be found [see also Kleman (1977)].

APPENDIX C: THE ELLIPSE IN A FCD AS A DISCLINATION

In a generic FCD (Fig. 26), the hyperbola H is completely embedded in the domain and is a wedge disclination of strength $k=1$; indeed any direction along it is a 2π symmetry axis. On the other hand, the ellipse E, which is usually on the boundary of the domain, is a disclination of strength $k=\frac{1}{2}$ for the full layer geometry, which contains the FCD and two sets of outside layers that meet on the plane of E. But E is not in general of wedge character, because the tangent to the ellipse is not a folding axis for the local smectic layers. An obvious solution is given in Fig. 35, where the local rotation vector $\mathbf{\Omega t}$, with $\Omega=\pi$, is tangent to the layers, which are folded symmetrically with respect to the plane of the ellipse (Kleman *et al.*, 2006). Other solutions are possible, with $\mathbf{\Omega}$ off this plane (but then necessarily nonsymmetric with respect to the ellipse plane), which would correspond to a different set of attached dislocations, most probably of higher energy.

We apply Eq. (1), rewritten

$$d\mathbf{b}_{tr}=2\mathbf{t}\times\mathbf{MN}, \tag{C1}$$

to the ellipse, Fig. 35; $d\mathbf{b}_{tr}$ is perpendicular to the plane of the ellipse, and one easily gets $d\mathbf{b}_{tr}=2dr$; therefore the total Burgers vector attached to one side of the ellipse $(0<\phi<\pi)$ is (Kleman and Lavrentovich, 2000)

$$\mathbf{b}_{tr}=\int_{\phi=0}^{\phi=\pi} d\mathbf{b}_{tr}=4c. \tag{C2}$$

Taking $dr=d_0$—an approximation which makes sense (up to second order), since d_0 is so small compared to the size a of the ellipse—it is visible that the points M, of polar coordinates $\{r,\phi\}$, and N, of polar coordinates $\{r+dr,\phi+d\phi\}$, are on two parallel smectic layers at a distance d_0, and the total Burgers vector attached to a layer is equal to $2d_0$. There are no dislocations attached to the singular circle of a toric FCD, as the eccentricity e vanishes, and $\delta r=0$. The Burgers vector attached to a layer that is transverse to the perimeter of the ellipse is a constant, $2d_0$. Consider one such dislocation of Burgers vector $2d_0$; it spreads outside the ellipse in the shape of a quantized dislocation, on both sides of the ellipse, and goes across it in the shape of curved layers, in a manner akin to the $k=\frac{1}{2}$ case (Fig. 21). The full balance of Burgers vectors has to take into account the Nye dislocations, including those related to the infinitesimal disclinations,

$$-d\mathbf{f}=d\mathbf{t}=-\{\cos\phi,\sin\phi\}d\phi. \tag{C3}$$

$d\mathbf{t}$ is a vector along the normal of the layer, as required by symmetry (the normal to the layer is an axis of continuous rotational symmetry). But there is no *a priori* reason that the total Burgers vector carried by the Nye dislocations balances topologically the quantized attached dislocations; it is the attachment that provides a balance equation.

If the dislocation segments outside the ellipse belong to a plane, they build a grain boundary limited by the ellipse. It is a simple matter to check that the misorientation angle is $\omega=2\sin^{-1}e$. This grain boundary is a pure tilt boundary if it occupies the plane of the ellipse. Notice that $\boldsymbol{\omega}$ (the tilt vector, along the direction of the ellipse minor axis) and $\mathbf{\Omega t}$ (along the ellipse) define both the same tilt grain boundary; as described in Sec. II.E.1, Eq. (9).

We know from topological stability theory that the defect geometry of the ellipse as a disclination does not break the constancy of its conjugacy class in $\Pi_1(V_{\mathrm{Sm}A})$ along E. The variation of the representative homotopy class (inside the same class of conjugacy) for a circuit embracing the line depends on the quantized dislocations (not the infinitesimal dislocations which belong to the identity class of the homotopy group) attached to it, which it also embraces.

APPENDIX D: A FEW GEOMETRICAL CHARACTERISTICS OF THE THREE-SPHERE

Details on the topics that follow can be found in Sommerville (1967), Montesinos (1987), and Coxeter (1998).

1. Clifford parallels and Hopf fibration

The trajectory of a point $M\in S^3$ under the action of a right screw, say, $x'=xe^{\alpha q}$, $0<\alpha\leqslant 2\pi$, is a great circle C_{right} of S^3. Two right (respectively, left) great circles that rotate helically about the same q are equidistant all along their length and mutually twisted with a pitch $\varpi=2\pi$ (respectively, -2π): they form a congruence of so-called right (respectively, left) Clifford parallels that fill S^3 uniformly. All great circles of this congruence are

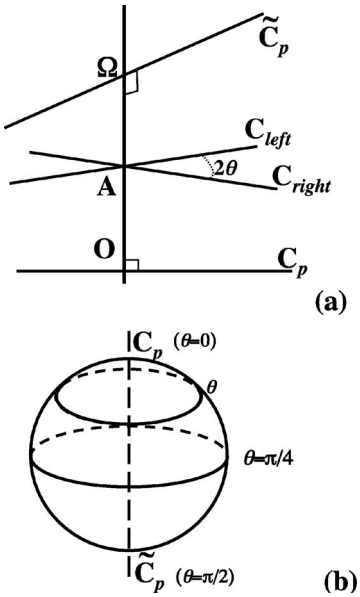

FIG. 36. (a) C_p and $\tilde{C}_p$ are conjugate great circles (represented as straight lines in reason of their geodesic character); C_{right} and C_{left} are equidistant to C_p and $\tilde{C}_p$ ($OA=\vartheta$, $A\Omega=\pi/2-\vartheta$). All right and left Clifford parallels at the same distance ϑ generate a ruled Clifford surface with two axes of revolution C_p and $\tilde{C}_p$. (b) Representation on the basis S^2 of a Hopf fibration of S^3, with C_p and $\tilde{C}_p$ as particular fibers. Each fiber is represented by a point on the basis; Clifford surfaces (the small circles on S^2) $\vartheta=$const; spherical torus $\vartheta=\pi/4$.

equivalent. Because any of those great circles can be considered as the axial line of cylindrical double-twist geometry for the other parallel great circles, the geometry of Clifford parallels has inspired a nonfrustrated model of the blue phase (Sethna, 1984). The great sphere S^2 defined by the intersection of the hyperplane $q_1x_1+q_2x_2+q_3x_3=0$ and S^3 intersects the great circles of the congruence orthogonally; this geometry defines S^3 as a fiber bundle of great circles S^1 over a great sphere S^2, the Hopf fibration (see Fig. 36). Notice that great circles are the geodesic lines of S^3 and great spheres the geodesic surfaces of S^3.

2. Spherical torus

The axis p and the circle of unit radius in its equator plane (Fig. 29) play identical roles in the double rotation: p is the stereographic projection of a great circle of S^3, here denoted C_p, which is the intersection of the sphere of unit quaternions $x_0^2+x_1^2+x_2^2+x_3^2=1$ with the two-plane $\frac{x_1}{p_1}=\frac{x_2}{p_2}=\frac{x_3}{p_3}$; the equator circle, here denoted $\tilde{C}_p$, is a great circle intersection of the unit quaternion sphere with the two-plane $x_0=0$, $p_1x_1+p_2x_2+p_3x_3=0$. These two great circles are conjugate; they have this remarkable property that the arc of any great circle C_g joining any point on C_p to any point on $\tilde{C}_p$ is perpendicular to both and has arc length $\pi/2$. Select any C_g and transform it under the action of the right screw $x'=xe^{\alpha p}$, $0<\alpha\leqslant 2\pi$, say; this yields a set (C_g) of great circles, all stretching between C_p and $\tilde{C}_p$. The surface obtained is called the spherical torus; it is generated by two families of great circles: (C_g) and (C_p) made of the Clifford parallels that are parallel to C_p (and to $\tilde{C}_p$). These two families form a rectangular network on the spherical torus.

3. Clifford surfaces

Consider now the action of a left screw $y'=e^{\beta p}x'$ about the same axis p, i.e., $y'=e^{\beta p}xe^{\alpha}p$ on C_{right} when $\mathbf{M}(\alpha)$ traverses the geodesic line C_{right}, and β varies in the range $0<\beta\leqslant 2\pi$: each point on C_{right} develops into a full geodesic trajectory C_{left} (a great circle) whose entire set forms a Clifford surface, which is a closed surface with two conjugate axes of revolution; these axes are precisely the conjugate geodesic circles of the double rotation p. The geometric properties of the Clifford surface depend on the angular distance ϑ of C_{right} to C_p. This is illustrated Fig. 36.

The particular Clifford surface $\vartheta=\pi/4$ is a spherical torus, whose axes of revolution are C_p and $\tilde{C}_p$.

APPENDIX E: GEOMETRICAL ELEMENTS RELATED TO A GREAT CIRCLE IN S^3

1. Great circle defined by two points

Consider two points $\mathbf{M}$ and $\mathbf{M}'$ on the three-sphere S^3, in quaternion notation u and u', in vector notation $\mathbf{u}$ and $\mathbf{u}'$. We have

$$\mathbf{u}\cdot\mathbf{u}' = R^2\cos\vartheta, \quad u\tilde{u}' + u'\tilde{u} = 2R^2\cos\vartheta. \tag{E1}$$

ϑ is the angle between the directions $\mathbf{u}$ and $\mathbf{u}'$.

We define the geometric elements related to the great circle C (centered at the origin $\{0\}$) going through u and u'.

We introduce two quaternions $u+u'$ and $u-u'$, corresponding to orthogonal vectors. We now show that there are two pure unit quaternions ϱ and σ such that

$$u+u' \propto 1-\varrho\sigma,$$

$$u'-u \propto \varrho+\sigma, \tag{E2}$$

with the same coefficient of proportionality, a real number. In effect, multiplying the second equation by ϱ (on the left) in order to get an expression for ϱ, and by σ (on the right) in order to get an expression for σ, and substituting then in the first equation, it becomes

$$\varrho \propto (u'-u)(\tilde{u}'+\tilde{u}) = u'\tilde{u} - u\tilde{u}',$$

$$\sigma \propto (\tilde{u}'+\tilde{u})(u'-u) = \tilde{u}u' - \tilde{u}'u, \tag{E3}$$

where $u\tilde{u}=u'\tilde{u}(=R^2)$. It is easy to check that ϱ and σ are pure quaternions. It remains to renormalize, in order to get pure unit quaternions. Using

$$|u\tilde{u}'-u'\tilde{u}|^2=(u\tilde{u}'-u'\tilde{u})(u'\tilde{u}-u\tilde{u}')=4R^4\sin^2\vartheta$$

and the same expression for $|\tilde{u}u-\tilde{u}u'|^2$, ϱ and σ eventually read

$$\varrho=\frac{u'\tilde{u}-u\tilde{u}'}{2R^2|\sin\vartheta|},\quad \sigma=\frac{\tilde{u}u'-\tilde{u}'u}{2R^2|\sin\vartheta|}. \tag{E4}$$

The two-plane in which lies the great circle C, defined by u, u', and the origin of the coordinates (which is the center of C), contains the directions $1-\varrho\sigma$ and $\varrho+\sigma$. It is denoted $\Pi_{\varrho,\sigma}=\{0,1-\varrho\sigma,\varrho+\sigma\}$. Any rotation of angle ϑ that leaves invariant this plane leaves invariant the great circle C that contains u and u'; it transforms any point $y\in E^4$ into $y'\in E^4$ according to

$$y'=e^{-(\vartheta/2)\varrho}ye^{(\vartheta/2)\sigma}.$$

$\Pi_{\varrho,\sigma}$ is the axial plane of the rotation. The plane $\Pi^{\perp}_{\varrho,\sigma}\{0,1+\varrho\sigma,\varrho-\sigma\}$ is completely orthogonal to $\Pi_{\varrho,\sigma}$.

2. Great circle defined by the tangent at a point

We look for the great circle going through two very close points u and $u+du$, when du vanishes continuously; one gets

$$\varrho=\frac{du\,\tilde{u}-u\,d\tilde{u}}{2R^2d\vartheta}=\frac{1}{2R}\left(\frac{du}{ds}\tilde{u}-u\frac{d\tilde{u}}{ds}\right),$$

$$\sigma=\frac{\tilde{u}\,du-d\tilde{u}\,u}{2R^2d\vartheta}=\frac{1}{2R}\left(\tilde{u}\frac{du}{ds}-\frac{d\tilde{u}}{ds}u\right),$$

where $ds=R\,d\vartheta$ is the arc element on C.

Let μ be the unit tangent at u to C, $|\mu|=1$; we have

$$\varrho=\frac{1}{2R}(\mu\tilde{u}-u\tilde{\mu}),\quad \sigma=\frac{1}{2R}(\tilde{u}\mu-\tilde{\mu}u). \tag{E5}$$

Because of the relation of orthogonality $\boldsymbol{\mu}\cdot\boldsymbol{\mu}=0$, we can also write

$$\varrho=\frac{1}{R}\mu\tilde{u}=-\frac{1}{R}u\tilde{\mu},\quad \sigma=\frac{1}{R}\tilde{u}\mu=-\frac{1}{R}\tilde{\mu}u. \tag{E6}$$

One easily checks that ϱ and σ are two pure unit quaternions; $\varrho^2=\sigma^2=-1$.

APPENDIX F: THE {3,5} AND {3,3,5} SYMMETRY GROUPS

The symmetry group of the {3,3,5} curved crystal is related to the symmetry group Y of the icosahedron, since any vertex is the center of an icosahedron.

1. The group of the icosahedron {3,5}

The group Y is finite with 60 elements, represented by rotations about the 6 fivefold axes, the 10 threefold axes, and the 15 twofold axes of the icosahedron. The order-parameter space of the icosahedron {3,5} is $V_{\{3,5\}}=\mathrm{SO}(3)/Y$, whose first homotopy group $\Pi_1(V_{\{3,5\}})\sim\bar{Y}$ is the lift of Y in the covering group of SO(3), i.e., in SU(2). $\bar{Y}$ is also known as the binary group (5,3,2) (Coxeter, 1973); it has twice as many elements as Y.

The topological theory defect classes of the icosahedron have been investigated by Nelson (1983b). $\bar{Y}$ is perfect (i.e., the commutator subgroup $D[\bar{Y}]=\bar{Y}$), so that in principle all defects can mutually annihilate (Trebin, 1984).

The icosahedron vertices can be expressed in terms of quaternions, so that we have the analytical tools to represent the symmetry actions on {3,5}. A caveat: Since all symmetry elements $h_{\mathbf{Y}}\in Y$ are rotations about axes having the center of the icosahedron as a fixed point, going through the two-sphere S^2 on which {3, 5} lives, any action on a point x of the icosahedron has the form $h_{\bar{\mathbf{Y}}}xh_{\mathbf{Y}}$ and connotes a disclination, in the Volterra process terms. Therefore there are no disvections generated by the point group Y in {3,5}.

2. The group of the {3,3,5} polytope

The 120 elements of $\bar{Y}$, in quaternion representation, occupy on S^3 precisely the locations of the 120 vertices of a {3,3,5}. Thus the binary icosahedral group constitutes a group isomorphic to the group built by these vertices (Coxeter, 1973). The {3,3,5} symmetry point group (indirect isometries excluded) is

$$H=Y\times\bar{Y}, \tag{F1}$$

whose lift in $\bar{G}(S^3)=S^3\times S^3$ is

$$\bar{H}=\bar{Y}\times\bar{Y}. \tag{F2}$$

H has 7200 elements. The displacement of a point x of {3,3,5} under the action of the symmetry group is

$$x'=h_{\mathbf{Y}}xh_{\bar{\mathbf{Y}}},\quad h_{\bar{\mathbf{Y}}}\in\bar{Y},\quad h_{\mathbf{Y}}\in Y \tag{F3}$$

(or, taking the conjugate, a point $y'=\tilde{h}_{\bar{\mathbf{Y}}}y\tilde{h}_{\mathbf{Y}}$), where $h_{\bar{\mathbf{Y}}}$ and $\tilde{h}_{\mathbf{Y}}$ are not necessarily conjugate, i.e., Eq. (F3) composes any right action and any left action.

REFERENCES

Achard, M.-F., M. Kleman, Y. A. Nastishin, and H. T. Nguyen, 2005, Eur. Phys. J. E **16**, 37.
Anderson, P. W., and G. Toulouse, 1977, Phys. Rev. Lett. **38**, 508.
Barbet-Massin, R., P. E. Cladis, and P. Pieranski, 1984, Phys. Rev. A **30**, 1161.
Bernal, J. D., 1959, Nature (London) **183**, 141.
Bernal, J. D., 1964, Proc. R. Soc. London, Ser. A **280**, 299.
Bilby, B. A., 1960, Prog. Solid Mech. **1**, 329.

Bilby, B. A., R. Bullough, and E. Smith, 1955, Proc. R. Soc. London, Ser. A **231**, 263.
Bohsung, J., and H.-R. Trebin, 1987, Phys. Rev. Lett. **58**, 2277.
Bollmann, W., 1970, *Crystal Defects and Crystalline Interfaces* (Springer, Berlin).
Bouligand, Y., 1972, J. Phys. (Paris) **33**, 715.
Bouligand, Y., 1973, J. Phys. (Paris) **34**, 603.
Bouligand, Y., 1974, J. Phys. (Paris) **35**, 959.
Bouligand, Y., 1981, in *Physics of Defects*, Les Houches Session XXXV, edited by R. Balian, M. Kleman, and J.-P. Poirier (North-Holland, Amsterdam), Chap. 4.
Bouligand, Y., B. Derrida, V. Poénaru, Y. Pomeau, and G. Toulouse, 1978, J. Phys. (Paris) **39**, 863.
Bouligand, Y., and M. Kleman, 1970, J. Phys. (Paris) **31**, 1041.
Bouligand, Y., and M. Kleman, 1979, J. Phys. (Paris) **40**, 79.
Branagan, D. J., Y. L. Tang, A. V. Sergueeva, and A. K. Mukherjee, 2003, Nanotechnology **14**, 1216.
Burgers, J. M., 1939a, Proc. K. Ned. Akad. Wet. **47**, 293.
Burgers, J. M., 1939b, Proc. K. Ned. Akad. Wet. **47**, 378.
Calini, A., and T. Ivey, 1998, J. Knot Theory Ramif. **7**, 719.
Cartan, E., 1963, *Leçons sur la Géométrie des Espaces de Riemann*, 2nd ed. (Gauthier-Villars, Paris).
Champion, Y., C. Langlois, S. Guérin-Mailly, P. Langlois, J. L. Bonnentien, and M. Hÿtch, 2003, Science **300**, 310.
Chen, M., E. Ma, K. J. Hemker, H. Sheng, Y. Wang, and X. Cheng, 2003, Science **300**, 1275.
Cladis, P. E., and M. Kleman, 1972, J. Phys. (Paris) **33**, 591.
Coble, R. L., 1963, J. Appl. Phys. **34**, 1679.
Coxeter, H. S. M., 1973, *Regular Polytopes*, 3rd ed. (Dover, New York).
Coxeter, H. S. M., 1991, *Regular Complex Polytopes*, 2nd ed. (Cambridge University Press, Cambridge, England).
Coxeter, H. S. M., 1998, *Non-Euclidean Geometry*, 6th ed. (The Mathematical Association of America, Washington, D.C.).
Crussard, C., 1944a, Rev. Metall. **41**, 118.
Crussard, C., 1944b, Rev. Metall. **41**, 139.
Darboux, G., 1894, *Leçons sur la Théorie Générale des Surfaces* (Gauthier-Villars, Paris).
de Gennes, P. G., and J. Friedel, 2007, Philos. Mag. **87**, 39.
de Wit, R., 1971, J. Appl. Phys. **42**, 3304.
Dubois-Violette, E., and B. Pansu, 1988, Mol. Cryst. Liq. Cryst. **165**, 151.
Dzyaloshinskii, I. E., 1981, in *Physics of Defects*, Les Houches Session XXXV, edited by R. Balian, M. Kleman, and J.-P. Poirier (North-Holland, Amsterdam), Chap. 4.
Dzyaloshinskii, I. E., and G. E. Volovik, 1980, Ann. Phys. (N.Y.) **125**, 67.
Fivel, M., 2006, private communication.
Frank, F. C., 1950a, Proc. Phys. Soc., London, Sect. A **62**, 131.
Frank, F. C., 1950b, *Report on the Symposium on the Plastic Deformation of Crystalline Solids*, Carnegie Institute of Technology, Pittsburgh Conference, p. 150.
Frank, F. C., 1958, Discuss. Faraday Soc. **25**, 19.
Frank, F. C., 1969, Montpellier Symposium on Liquid Crystals, oral communication.
Frank, F. C., and J. Kasper, 1958, Acta Crystallogr. **11**, 184.
Frank, F. C., and J. Kasper, 1959, Acta Crystallogr. **12**, 483.
Friedel, G., 1922, Ann. Phys. (Paris) **18**, 273.
Friedel, G., 1926, *Leçons de Cristallographie* (Berger-Levrault, Nancy, France).
Friedel, G., and F. Grandjean, 1910, Bull. Soc. Fr. Mineral. **33**, 409.
Friedel, J., 1959a, *Fracture* (Wiley, New York), p. 498.
Friedel, J., 1959b, *Symposium on Internal Stresses and Fatigue in Metals* (Elsevier, Amsterdam), p. 220.
Friedel, J., 1964, *Dislocations* (Pergamon, Oxford).
Friedel, J., 1977a, J. Phys. (Paris), Colloq. **38**, C2-1.
Friedel, J., 1977b, in *Electron-Phonon Interactions and Phase transitions*, NATO Advanced Study Institute, Series B: Physics, edited by T. Riste (Plenum, New York).
Friedel, J., 1979, J. Phys. (Paris), Colloq. **40**, C3-45.
Friedel, J., 1984, *Trends in Physics*, edited by J. Sauter and R. Pantofliček (Union of Czechoslovak Mathematicians and Physicists, Prague).
Friedel, J., 1985, Conference held in honor of Jean Mandel, Ecole Polytechnique, Palaiseau.
Friedel, J., C. Boulanger, and C. Crussard, 1955, Acta Metall. **3**, 380.
Friedel, J., B. D. Cullity, and C. Crussard, 1953, Acta Metall. **1**, 79.
Friedel, J., and M. Kleman, 1969, J. Phys. (Paris), Colloq. **30**, C4-43.
Giraud-Guille, M. M., 1988, Calcif. Tissue Int. **42**, 167.
Harris, W. F., 1970, Philos. Mag. **22**, 949.
Harris, W. F., 1977, Sci. Am. **237**(12), 130.
Harris, W. F., and L. E. Scriven, 1970, Nature (London) **228**, 827.
Harris, W. F., and L. E. Scriven, 1971, J. Appl. Phys. **42**, 3309.
Hehl, F. W., P. von der Heyde, G. D. Kerlick, and J. M. Nester, 1976, Rev. Mod. Phys. **48**, 393.
Hilbert, D., and S. Cohn-Vossen, 1964, *Geometry and the Imagination* (Chelsea, New York).
Hilgenfeldt, S., A. M. Kraynik, S. A. Koehler, and H. A. Stone, 2001, Phys. Rev. Lett. **86**, 2685.
Hornreich, R. M., and S. Shtrikhman, 1986, Phys. Rev. Lett. **56**, 1723.
Huang, X., N. Hansen, and N. Tsuji, 2006, Science **312**, 249.
Julia, B., and G. Toulouse, 1979, J. Phys. (France) Lett. **40**, L395.
Kamien, R. D., and T. C. Lubensky, 1999, Phys. Rev. Lett. **82**, 2892.
Kleman, M., 1967, Ph.D. thesis (Université de Paris, Faculté des Sciences).
Kleman, M., 1973, Philos. Mag. **27**, 1057.
Kleman, M., 1974, J. Appl. Phys. **45**, 1377.
Kleman, M., 1977, J. Phys. (France) Lett. **38**, L199.
Kleman, M., 1982a, J. Phys. (Paris) **43**, 1389.
Kleman, M., 1982b, *Points, Lines and Walls* (Wiley, Chichester).
Kleman, M., 1983, J. Phys. (France) Lett. **44**, L295.
Kleman, M., 1984, in *Dislocations 1984*, edited by P. Vayssière, L. Kubin, and J. Castaing (Editions du CNRS, Paris), p. 1.
Kleman, M., 1985a, J. Phys. (France) Lett. **46**, L723.
Kleman, M., 1985b, J. Phys. (Paris) **46**, 1193.
Kleman, M., 1987, Phys. Scr. **T19**, 565.
Kleman, M., 1989, Adv. Phys. **38**, 605.
Kleman, M., 1990, in *Proceedings of the IIIrd International Conference on Quasicrystals, and Incommensurate Structures in Condensed Matter Physics*, edited by M. Yacaman *et al.* (World Scientific, Singapore), p. 109.
Kleman, M., 1992, J. Phys. II **2**, 69.
Kleman, M., and O. D. Lavrentovich, 2000, Eur. Phys. J. E **2**, 47.
Kleman, M., and O. D. Lavrentovich, 2003, *Soft Matter Physics, an Introduction* (Springer, New York).
Kleman, M., O. D. Lavrentovich, and Y. A. Nastishin, 2004,

Dislocations and Disclinations in Mesomorphic Phases, Dislocations in Solids Vol. 12, edited by F. R. N. Nabarro and J. P. Hirth (Elsevier, Amsterdam), p. 147.
Kleman, M., C. Meyer, and Y. A. Nastishin, 2006, Philos. Mag. **86**, 4439.
Kleman, M., and C. Ripamonti, 1988, C. R. Acad. Sci. **307**, 335.
Kleman, M., and J.-F. Sadoc, 1979, J. Phys. (France) Lett. **40**, L569.
Koch, C. C., 2003, Scr. Mater. **49**, 657.
Kondo, K., 1955–1967, *RAAG Memoirs of the Unifying Study of Basic Problems in Engineering and Physical Sciences by Means of Geometry* (Gakujutsu Bunken Fukyu-Kai, Tokyo), Chaps. 1–4.
Kröner, E., 1958, *Kontinuum Theorie des Versetzungen und Eigenspannungen* (Springer, Berlin).
Kröner, E., 1981, in *Physics of Defects*, Les Houches Session XXXV, edited by R. Balian, M. Kleman, and J.-P. Poirier (North-Holland, Amsterdam), Chap. 3.
Kröner, E., 1982, *Gauge Field Theories of Defects*, Discussion Meeting, Max-Planck Institut für Festkörperforschung und Metallforschung, Stuttgart.
Kuczinski, W., J. Pavel, and H. T. Nguyen, 1999, Phase Transitions **68**, 643.
Kumar, K. S., H. Van Swygenhoven, and S. Suresh, 2003, Acta Mater. **51**, 5743.
Lacombe, P., and L. Beaujard, 1948, Report of the Bristol Conference on Strength of Solids (Phys. Soc., London).
Lejček, L., 2002, Czech. J. Phys. **52**, 865.
Letelier, P. S., 1995, Class. Quantum Grav. **12**, 471.
Livolant, F., 1987, J. Phys. (Paris) **48**, 1051.
Livolant, F., and Y. Bouligand, 1980, Chromosoma **80**, 97.
Livolant, F., and Y. Bouligand, 1986, J. Phys. (Paris) **47**, 1813.
Lu, L., M. L. Sui, and K. Lu, 2000, Science **287**, 1463.
Ma, E., 2004, Science **305**, 623.
Ma, E., T. D. Shen, and X. L. Wu, 2006, Nat. Mater. **5**, 515.
MacFadden, S. X., R. S. Mishra, R. Z. Valiev, A. P. Zhilaev, and A. K. Mukherjee, 1999, Nature (London) **398**, 684.
Massey, W. S., 1967, *Algebraic Topology: An Introduction* (Harcourt, Brace and World, New York).
Mazelet, G., and M. Kleman, 1986, Polymer **27**, 714.
Meiboom, S., M. Sammon, and D. W. Berreman, 1983, Phys. Rev. A **28**, 3553.
Mermin, N. D., 1979, Rev. Mod. Phys. **51**, 591.
Meyer, R. B., 1973, Philos. Mag. **27**, 405.
Michel, L., 1980, Rev. Mod. Phys. **52**, 617.
Montesinos, J. M., 1987, *Classical Tessellations and Three-Manifolds* (Springer, Berlin).
Mosseri, R., and J. F. Sadoc, 1990, in *Geometry in Condensed Matter Physics*, edited by J. F. Sadoc (World Scientific, Singapore), p. 233.
Nabarro, F. R. N., 1967, *Theory of Crystal Dislocations* (Clarendon, Oxford).
Nelson, D. R., 1983a, Phys. Rev. Lett. **50**, 982.
Nelson, D. R., 1983b, Phys. Rev. B **28**, 5515.
Nicolis, S., R. Mosseri, and J.-F. Sadoc, 1986, Europhys. Lett. **1**, 571.
Nye, J. F., 1953, Acta Metall. **1**, 153.
Ovid'ko, I. A., 2002, Science **295**, 2386.
Ovid'ko, I. A., 2005, Rev. Adv. Mater. Sci. **10**, 89.
Puntigam, R. A., and H. H. Soleng, 1997, Class. Quantum Grav. **14**, 1129.
Read, W. T., and W. Shockley, 1950, Phys. Rev. **78**, 275.
Regge, T., 1961, Nuovo Cimento **19**, 558.
Renn, S. R., and T. C. Lubensky, 1988, Phys. Rev. A **38**, 2132.
Rivier, N., 1979, Philos. Mag. A **40**, 859.
Rivier, N., 1987, Adv. Phys. **36**, 97.
Rogula, D., 1976, *Large Deformations of Crystals, Homotopy and Defects*, Trends in Applications of Pure Mathematics to Mechanics, edited by G. Fichera (Pitman, New York), p. 311.
Rokhsar, D., and J. P. Sethna, 1986, Phys. Rev. Lett. **56**, 1727.
Romanov, A. E., and V. I. Vladimirov, 1992, *Disclinations in Crystalline Solids*, Dislocations in Solids No. 9, edited by F. R. N. Nabarro (North-Holland, Amsterdam), p. 191.
Schechtman, D., I. Blech, D. Gratias, and J. W. Cahn, 1984, Phys. Rev. Lett. **53**, 1951.
Schiøtz, J., F. D. Di Tolla, and K. W. Jacobsen, 1998, Nature (London) **391**, 561.
Schuh, C., T. G. Nieh, and T. Yamasaki, 2002, Scr. Mater. **46**, 735.
Sethna, J. P., 1984, Phys. Rev. Lett. **51**, 2198.
Sethna, J. P., 1985, Phys. Rev. B **31**, 6278.
Shan, Z. W., E. A. Stach, J. M. K. Wiezorek, J. A. Knapp, D. M. Follstaedt, and S. X. Mao, 2004, Science **305**, 654.
Singer, I. M., and J. A. Thorpe, 1996, *Lecture Notes on Elementary Topology and Geometry* (Springer-Verlag, New York).
Sleeswyk, A. W., 1966, J. Phys. (Paris), Colloq. **27**, C3-78.
Sommerville, D. M. Y., 1967, *The Elements of Non-Euclidean Geometry* (Dover, New York).
Steenrod, N., 1957, *The Topology of Fiber Bundles* (Princeton University Press, Princeton, NJ).
Tanakashi, Y., H. Takezoe, A. Fukuda, and J. Watanabe, 1992, Phys. Rev. B **45**, 7684.
Toulouse, G., 1977a, J. Phys. (France) Lett. **38**, 67.
Toulouse, G., 1977b, Commun. Phys. (London) **2**, 115.
Toulouse, G., and M. Kleman, 1976, J. Phys. (France) Lett. **37**, L149.
Trebin, H.-R., 1982, Adv. Phys. **31**, 194.
Trebin, H.-R., 1984, Phys. Rev. B **30**, 4338.
Van Petegem, S., S. Brandstetter, H. Van Swygenhoven, and J.-L. Martin, 2006, Appl. Phys. Lett. **89**, 073102.
Van Swygenhoven, H., 2002, Science **296**, 66.
Van Swygenhoven, H., P. M. Derlet, and A. G. Froseth, 2006, Acta Mater. **54**, 1975.
Van Swygenhoven, H., D. Farkas, and A. Caro, 2000, Phys. Rev. B **62**, 831.
Van Swygenhoven, H., and J. R. Weertman, 2006, Mater. Today **9**, 24.
Vilenkin, A., and E. P. S. Shellard, 1994, *Cosmic Strings and Other Topological Defects* (Cambridge University Press, Cambridge, England).
Volovik, G. E., and V. P. Mineev, 1976, Pis'ma Zh. Eksp. Teor. Fiz. **24**, 605 [JETP Lett. **24**, 561 (1976)].
Volovik, G. E., and V. P. Mineev, 1977, Zh. Eksp. Teor. Fiz. **72**, 2256 [Sov. Phys. JETP **45**, 1186 (1977)].
Volterra, V., 1907, Ann. Sci. Ec. Normale Super. **24**, 401.
von Neumann, J., 1952, *Metals Interfaces* (ASM, Cleveland, Ohio), p. 108.
Wang, Y. M., M. W. Chen, F. H. Zhou, and F. Ma, 2002, Nature (London) **419**, 912.
Washburn, J., and E. R. Parker, 1952, J. Met. **4**, 1076.
Weaire, D., and S. Hutzler, 2000, *The Physics of Foams* (Oxford University Press, Oxford).
Weertman, J. R., D. Farkas, K. Hemker, H. Kung, M. Mayo, R. Mitra, and H. Van Swygenhoven, 1999, MRS Bull. **24**, 44.
Weisstein, E. W., 1999, *Spherical Geometry*, MathWorld, URL

http://mathworld.wolfram.com/SphericalTrigonometry.html
Wolf, D., V. Yamakov, S. R. Philpot, A. K. Mukherjee, and H. Gleiter, 2005, Acta Mater. **53**, 1.
Yip, S., 1998, Nature (London) **391**, 532.
Zachariasen, N., 1932, J. Am. Chem. Soc. **54**, 3841.
Zallen, R., 1979, in *Fluctuation Phenomena*, edited by E. W. Montroll, and J. L. Leibovitz (North-Holland, Amsterdam), p. 178.
Zhu, Y. T., and X. Liao, 2004, Nat. Mater. **3**, 351.